# ABSTRACT


Title of Document: PROGNOSTICS-BASED QUALIFICATION OF WHITE LIGHT-EMITTING DIODES (LEDS)

Moon-Hwan Chang, Doctor of Philosophy (Ph.D.), 2014

Directed By: Professor, Michael G. Pecht,
Department of Mechanical Engineering

Light-emitting diode (LED) applications have expanded from display backlighting in computers and smart phones to more demanding applications including automotive headlights and street lightening. With these new applications, LED manufacturers must ensure that their products meet the performance requirements expected by end users, which in many cases require lifetimes of 10 years or more. The qualification tests traditionally conducted to assess such lifetimes are often as long as 6,000 hours, yet even this length of time does not guarantee that the lifetime requirements will be met.

This research aims to reduce the qualification time by employing anomaly detection and prognostic methods utilizing optical, electrical, and thermal parameters of LEDs. The outcome of this research will be an in-situ monitoring approach that enables parameter sensing, data acquisition, and signal processing to identify the

potential failure modes such as electrical, thermal, and optical degradation during the qualification test. To detect anomalies, a similarity-based-metric test has been developed to identify anomalies without utilizing historical libraries of healthy and unhealthy data. This similarity-based-metric test extracts features from the spectral power distributions using peak analysis, reduces the dimensionality of the features by using principal component analysis, and partitions the data set of principal components into groups using a KNN-kernel density-based clustering technique. A detection algorithm then evaluates the distances from the centroid of each cluster to each test point and detects anomalies when the distance is greater than the threshold. From this analysis, dominant degradation processes associated with the LED die and phosphors in the LED package can be identified. When implemented, the results of this research will enable a short qualification time.

Prognostics of LEDs are developed with spectral power distribution (SPD) prediction for color failure. SPD is deconvoluted with die SPD and phosphor SPD with asymmetric double sigmoidal functions. Future SPD is predicted by using the particle filter algorithm to estimate the propagating parameters of the asymmetric double sigmoidal functions. Diagnostics is enabled by SPD prediction to indicate die degradation, phosphor degradation, or package degradation based on the nature of degradation shape of SPD. SPDs are converted to light output and 1976 CIE color coordinates using colorimetric conversion with color matching functions. Remaining useful life (RUL) is predicted using 7-step SDCM (standard deviation of color matching) threshold (i.e., 0.007 color distance in the CIE 1676 chromaticity coordinates).

To conduct prognostics utilizing historical libraries of healthy and unhealthy data from other devices, this research employs similarity-based statistical measures for a prognostics-based qualification method using optical, electrical, and thermal covariates as health indices. Prognostics is conducted using the similarity-based statistical measure with relevance vector machine regression to capture degradation trends. Historical training data is used to extract features and define failure thresholds. Based on the relevance vector machine regression results, which construct the background health knowledge from historical training units, the similarity weight is used to measure the similarity between each training unit and test unit under the test. The weighted sum is then used to estimate the remaining useful life of the test unit.

# PROGNOSTICS-BASED QUALIFICATION OF WHITE LIGHT-EMITTING DIODES (LEDS)

By

Moonhwan Chang

Dissertation submitted to the Faculty of the Graduate School of the
University of Maryland, College Park, in partial fulfillment
of the requirements for the degree of
Doctor of Philosophy
2014

Advisory Committee:
Professor Michael G. Pecht, Chair
Professor Abhijit Dasgupta
Professor Bongtae Han
Professor Patrick McCluskey
Research Scientist Dr. Diganta Das
Prof. Bilal Ayyub, Dean's Representative

## Dedication

This dissertation is dedicated to my wife, my sons, and my parents, who support me all the time.

# Acknowledgements

First, I would like to express my gratitude and respect to Prof. Michael Pecht for having granted me this opportunity to work on this dissertation topic and challenging me to set a higher standard. I appreciate him for his continuous support towards the progress of this work and taking the time to review and guide me throughout the course of this study.

I would like to especially thank Dr. Diganta Das for his excellent guidance, and support for this study. I am also thankful to Prof. Abhijit Dasgupta, Prof. Patrick McCluskey, Prof. Bongtae Han, and Prof. Bilal Ayyub for their continued interest and efforts involved in reviewing my work. I further extend my thanks to Dr. Michael Azarian, Dr. Chaochao Chen, and Dr. Carlos Morillo for their insightful advice to this work.

I further thank the Prognostics and Health Management (PHM) Consortium in Center for Advanced Life Cycle Engineering (CALCE) for its support. I would like to thank Bhanu Sood and Swapnesh Patel for their guidance and support during conducting the experiments in the laboratories for this thesis. I further extend my thanks to all my friends and colleagues for their support and encouragement. I am thankful to Edwin Sutrisno, Hyunseok Oh, and Arvind Vasan for their advice and encouragement to this work.

Finally, I would like to extend very special thanks to my wife Hyunmee Park for her constant support and encouragement towards my work. I would like to thank my parents for standing by all my decision and constantly encouraging me towards my endeavors.

## Table of Contents

## List of Tables

## List of Figures

# CHAPTER 1 Introduction

This research will enable LED manufacturers to quickly qualify LED prototypes during the development phase under wear-out performance degradation and an unknown failure distribution. This is a benefit because market pressures demand a short qualification testing cycle. A prognostics-based qualification process will evaluate the product reliability in test conditions that accelerate potential failure mechanisms at associated sites, to assess LED degradation, detect anomalies, and estimate the remaining useful life (RUL). By employing the methodology developed in this project, both the qualification test time and costs will be reduced from those in traditional qualification testing allowing LED manufacturers to meet customer requirements based on the intended application and application conditions.

## *1.1 Key Issues*

A major hurdle for getting new LED products to the market quickly is the amount of time it takes to qualify them. Conventional LED qualification processes do not meet the needs of quick qualification. The following key issues and problems with current LED qualification testing will be addressed by our proposed research:

1) Current qualification testing methods based on lumen maintenance (as a failure mode) do not distinguish between failure mechanisms of LEDs since all failures affect light output degradation [1][2]. Therefore, the current product qualification does not provide detailed information on the failure modes, failure mechanisms, and failure sites of LEDs. Chang et al. [1] investigated and grouped thirteen failure mechanisms of LEDs in terms of

three failure sites: semiconductors, interconnects, and package. Each failure mechanism is associated with failure cause, effect on device, and failure mode. It is confirmed that there are multiple types of failure modes beyond the light output degradation in terms of electrical, thermal, and color features such as reverse leakage current, parasitic series resistance, short circuit, open circuit, forward voltage, discoloration of the encapsulant, broadening of spectrum, color coordinates shift, and color temperature shift [1][2]. A new product qualification method is required to consider all of these failure modes which tell the difference among failure mechanisms more clearly.

2) Qualification test time varies depending on the manufacturer, and test results do not offer reliability information about the product when the tests do not include failures. It can take several months to complete operating life tests even when the tests are time-terminated [3]. An accelerated test to reduce the qualification test time is used to predict the lifetime of LEDs by multiplying the light output (i.e., lumen) degradation projection by an acceleration factor, often based on the Arrhenius model [4][5]. However, there is no relationship to relate the time under accelerated test conditions to the time under field conditions with the consideration of actual LED failure mechanisms. Additionally, the extrapolation of LED lifetime based on lumen maintenance under the accelerated test condition is affected by factors such as the number of samples tested, the assumed activation energy, possible failure mechanism shift, and the length of testing [6]-[8].

Current life prediction method does not perform remaining useful life estimation during operation.

3) Major LED manufacturers such as Cree and Nichia evaluate LED failure criteria in terms of light output maintenance, forward voltage shift, and u′v′ shift [9]-[11]. The failure threshold for each parameter varies depending on the manufacturers, applications, and materials. Due to the variability and complexity of these failure thresholds, it is difficult to evaluate and perform product qualification for different products at the same time. The acceptance criteria are usually a binary pass or fail in terms of those parameter thresholds. Manufacturers do not fully analyze the degradation trends and results by utilizing the failure criteria for the qualification tests which require the anomaly detection and the prediction of remaining useful life to reduce the qualification test time.
4) The Illuminating Engineering Society (IES) recommends that LED manufacturers collect color shift data over 6,000 hours of operations [12]; however, a life prediction method in terms of color failure of LEDs has not been developed. Color shift is difficult to extrapolate because of differences in the LED designs, materials, manufacturing processes, optics applied to the LED, and use conditions of LED operation. LED color change has been studied under different current loads [13]-[15]. There is no model that provides detailed information on color degradation.

A new product qualification method is needed that not only reduces the time needed for the qualification process, but also improves life prediction and ensures the reliability of LEDs over their lifetimes.

### *1.2 Purpose of Investigation*

We will investigate and develop a method to reduce LED qualification time by developing prognostic techniques that can be applied to various degradation features, including optical, electrical, and thermal failure precursors, in different types of LEDs due to diverse LED design and material to meet demands of the requirements of specific applications. We will develop an in-situ monitoring system that enables test process, parameter sensing, data acquisition, and signal processing for prognostics-based product qualification method of LEDs. We will develop a qualification method for LEDs by analyzing test data to detect anomalies and predict the remaining useful life of LEDs in a shorter timeframe than is allowed by conventional qualification methods.

### *1.3 Significance*

LEDs are being used in an ever-increasing variety of applications, including television display backlighting, communications, medical equipment, signage, and general illumination [16]–[21]. As the number of LED applications increases, LED manufacturers need to ensure that new products meet the quality and performance expected by commercial end users and that there are reliable savings for utilities. There is a demand on the manufacturers to perform qualification testing quickly. However, the conventional qualification tests are not working. There have been a large number of

LEDs that have passed qualification tests, but have failed in the field. As a result, many companies have incurred costs of these failures. For example, in 2006, it was reported that mounted LED stop lights in the Washington D.C. area had observable lens fading, premature LED dimming, or outright failures due to heat or moisture failings of LEDs or LED circuit boards [22]. LED traffic signal lights have failed in operational control of traffic at intersections in snow-prone areas of the U.S. due to a lack of heat to prevent snow buildup in their fixtures and poor power board quality [23]. Additionally, the failure rate of the 20,000 LED street lamps installed between 2009 and 2011 in Taiwan was about 8.2% as of 2011 [23]. With China's 12th Five-Year Plan (i.e., a new national development program approved by China's National People's Congress for five years from 2011 to 2015) and increasing LED adoption in Europe and the U.S., the LED industry is optimistic about the global LED street lighting market, but the quality and performance of products remain a concern. The best performance of life was 8,000 hours under the condition without adjusting the brightness according to data from the Government-Backed Industry Technology Research Institute [24].

Customers want LED manufacturers to guarantee the lifetime of their LED products. This demand combined with the market gap that will be opening up as incandescent bulbs are phased out, has created the potential for a competitive edge for LED manufacturers who can guarantee the reliability of their products for the widest array of applications, while at the same time getting their products to market the fastest.

## *1.4 Objectives*

The conventional qualification tests used by LED manufacturers often take a long time (more than 6,000 hours) to detect anomalies, and often produce remaining useful life predictions that are at odds with how the LEDs perform in the field. Our prognostics-based qualification method overcomes the addressed key issues by taking into account all failure precursors to detect all possible failure modes in a more accurate and faster manner than the conventional approach. The objectives of this project are as follows:

1) To develop an in-situ monitoring system that enables parameter sensing, data acquisition, and signal processing to collect potential failure modes including electrical and thermal degradation parameters which are readily measurable accompanied with offline-based optical measurements including color features during the qualification testing period.
2) To investigate and formulate a means to reduce qualification time by developing prognostic techniques considering degradation dynamics and unit-to-unit variation that can be applied to various degradation parameters in LEDs, including optical, electrical, and thermal failure precursors.
3) To develop a prognostics-based product qualification method to detect anomalies and predict the remaining useful life (RUL) of LEDs in a shorter timeframe than is allowed by conventional qualification methods, based on a similarity-based-metric test that was developed to identify anomalies without utilizing historical libraries of healthy and unhealthy data for anomaly detection. A detection algorithm evaluates the distances from the

centroid of each cluster to each test point and detects anomalies when the distance is greater than the threshold. To predict RUL of LEDs, prognostics of LEDs are developed with spectral power distribution (SPD) prediction for color failure to indicate potential LED degradation such as the LED die degradation, phosphor degradation, and encapsulant degradation. SPD is deconvoluted with die SPD and phosphor SPD with asymmetric double sigmoidal functions. Future SPD is predicted by using the particle filter algorithm to estimate the propagating parameters of the asymmetric double sigmoidal functions.

4) To develop similarity-based prognostics with Bayesian machine learning techniques to extract features and to define different failure thresholds of each LED. Based on a comparison between the training data and the test data, the anomaly detection and the remaining useful life estimates for the test unit will be determined using electrical and thermal failure precursors by establishing the relationship between light quality and the electrical and thermal parameters.

# CHAPTER 2 Literature Review

Prognostics-based qualification includes two parts: anomaly detection and RUL prediction. Anomaly detection is required for the qualification testing to provide users with an early time to begin remaining useful life (RUL) prediction. This chapter summarizes the studies related to light emitting diodes, qualification test of LEDs, anomaly detection, and prognostics-based RUL prediction of LEDs.

## *2.1 Light Emitting Diodes (LEDs)*

Light emitting diodes (LEDs) are a solid-state lighting source increasingly being used in display backlighting, communications, medical services, signage, and general illumination [16]-[21]. LEDs offer design flexibility, from zero-dimensional lighting (dot-scale lighting) to three-dimensional lighting (color dimming using combinations of colors), with one-dimensional lighting (line-scale lighting) and two-dimensional lighting (local dimming, i.e., area-scale lighting) in between. LEDs have small exterior outline dimensions, often less than 10mm × 10mm. LEDs, when designed properly, offer high energy efficiency that results in lower power consumption (energy savings) with low voltage (generally less than 4 volts) and low current operation (usually less than 700 mA). LEDs can have longer life—up to 50,000 hours—with better thermal management than conventional lighting sources (e.g., fluorescent lamps and incandescent lamps). LEDs provide high performance, such as ultra-high-speed response time (micro-second-level on-off switching), a wider range of controllable color temperatures (4,500K–12,000K), a wider operating temperature range (-20°C–85°C), and no low-temperature startup problems. In addition, LEDs have

better mechanical impact resistance compared to traditional lighting. LEDs are also eco-friendly products with no mercury and low health impact due to low UV radiation. LEDs that have a single color are over ten times more efficient than incandescent lamps. White LEDs are more than twice as efficient as incandescent lamps [18].

LEDs range from a narrow spectral band emitting light of a single color, such as red, yellow, green, or blue, to a wider spectral band light of white with a different distribution of luminous intensity and spectrums and shades depending on color mixing and package design. A recent trend in LEDs to produce white light involves using blue LEDs with phosphors. White light is a mixture of all visible wavelengths, as shown in Figure 1. Along with the prominent blue color (peak wavelength range 455–490nm), there are other wavelengths, including green (515–570nm), yellow (570–600nm), and red (625–720nm) that constitute white light. Every LED color is represented by unique x-y coordinates, as shown in Figure 2. The CIE (Commission Internationale De L'eclairage (International Commission on Illumination)) chromaticity coordinates of x, y, and z are a ratio of the red, green, and blue stimulation of light compared to the total amount of the red, green, and blue stimulation. The sum of the RGB values (x + y + z) is equal to 1. The white area of the chromaticity diagram can be expanded, and boundaries are added to create each color range. The color temperatures and the Planckian locus (black body curve) show how they relate to the chromaticity coordinates [19].

The color temperature of a white light is defined as the temperature of an ideal Planckian black-body radiator that radiates light of comparable hue to that white light source. The color temperature of light is equal to the surface temperature of an ideal

black-body radiator in Kelvin heated by thermal radiation. When the black body radiator is heated to high temperatures, the heated black body emits colors starting at red and progressing through orange, yellow, white, and finally to bluish white. The Planckian locus starts out in the red, then moves through the orange and yellow, and finally enters the white region. The color temperature of a light source is regarded as the temperature of a Planckian black-body radiator that has the same chromaticity coordinates. As the temperature of the black body increases, the chromaticity location moves from the red wavelength range toward the center of the diagram in Figure 2.

LED degradation not only results in reduced light output but also in color changes. LED modules are composed of many LEDs. This means that if some number of LEDs experience color changes, it will be noticed by users. Even if all of the LEDs degrade at the same rate, LED modules need to maintain their initial color, especially for indoor lighting and backlighting applications.

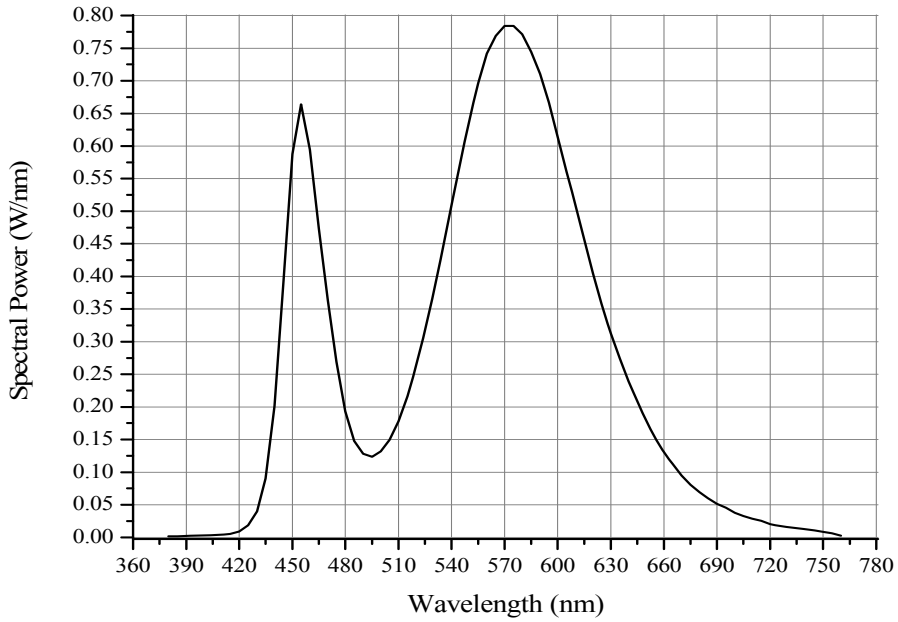


**Figure 1 Spectral power distribution for a white LED.**

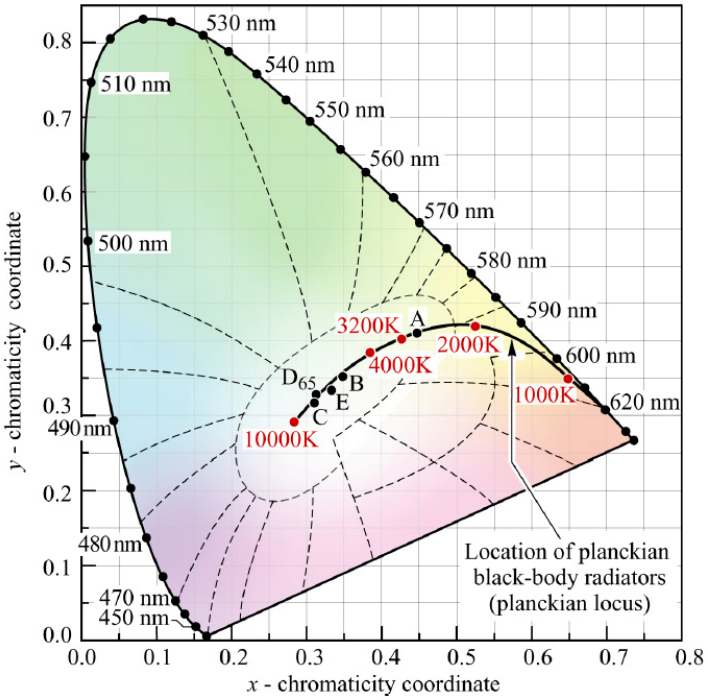


**Figure 2 CIE 1931 Chromaticity Diagram [19].**

LED application areas include LCD backlights, displays, transportation equipment lighting, and general lighting (see Table 1). LEDs are used as a light source for LCD backlights in products such as mobile phones, cameras, portable media players, notebooks, monitors, and TVs. Display applications include LED electronic scoreboards, outdoor billboards, and signage lighting, such as LED strips and lighting bars. Examples of transportation equipment lighting areas are passenger vehicle and train lighting (e.g., meter backlights, tail and brake lights) [25], and ship and airplane lighting (e.g., flight error lighting and searchlights). General lighting applications are divided into indoor lighting (e.g., LED lighting bulbs, desk lighting, and surface lighting) [26][27], outdoor lighting (e.g., decorative lighting, street/bridge lighting, and stadium lighting), and special lighting (e.g., elevator lighting and appliance lighting) [28][29]. The use of LEDs in general lighting has increased, beginning with street

lighting in public areas and moving onto commercial/business lighting and consumer applications.

**Table 1 Application Areas of LEDs**

| Application Area | Application Examples |
|---|---|
| LCD backlight | · Mobile phones<br>· Cameras<br>· Portable media players (PMPs)<br>· Notebooks<br>· Monitors<br>· TVs |
| Displays | · Electric scoreboards<br>· Outdoor billboards<br>· Signage lighting |
| Transportation equipment lighting | · Vehicle/train lighting<br>· Ship/airplane lighting |
| General lighting | · Indoor lighting<br>· Outdoor lighting<br>· Special lighting |

The history of LED development can be divided into three generations, each of which is characterized by distinct advancements in fabrication technology and equipment, development of new phosphor materials, and advancements in heat dissipation packaging technologies. Over time, LEDs have been becoming brighter, and color variance has been becoming more flexible. Light efficiency and light efficacy have also been improving. The first commercialized LED was produced in the late 1960s. This first generation of LEDs lasted from the 1960s until the 1980s. In this period, major application areas were machinery status indicators and alpha-numeric displays. The first commercially successful high-brightness LED (300mcd) was developed by Fairchild in the 1980s. In the second generation, from the 1990s to the present, high-brightness LEDs became popular. The main application areas for the second generation include motion displays, LED flashers, LED back light units (BLUs), mobile phones, automotive LED lighting, and architecture lighting. The third generation is now arriving in the market. These LEDs have been developed for

substantial savings in energy consumption and reduction in environmental pollution. Future LED application areas are expected to include general lighting, lighting communication [30], medical/environmental fields, and critical applications in system controls. Some examples are portable LED projectors, large-size LED backlighting displays, LED general lighting, visible light communication, purifiers, and bio-medical sensors. Moore's Law predicts the doubling of the number of Si transistors in a chip every 18–24 months. Similarly, for LEDs, luminous output (luminous flux, measured in lm) appears to follow Haitz's Law, which states that LED flux per package has doubled every 18–24 months for more than 30 years [17]. This trend in the technological advancement of LEDs is based on industry-driven R&D efforts targeting high-efficiency, low-cost technology solutions that can successfully provide an energy-saving alternative to the recent applications of LEDs.

LED dies are composed of a p-junction, a quantum well (active layer) or multiple quantum wells, and an n-junction. LEDs emit light due to the injection electroluminescence effect in compound semiconductor structures. When a p-n junction is biased in the forward direction, electrons in the n-junction have sufficient energy to move across the boundary layer into the p-junction, and holes are injected from the p-junction across the active layer into the n-junction. The active region of an ideal LED emits one photon for every electron injected. Each charged quantum particle (electron) produces one light quantum particle (photon). Thus, an ideal active region of an LED has a quantum efficiency of unity. The internal quantum efficiency is defined as the number of photons emitted from an active region per second divided by the number of electrons injected into the LED per second. The light extraction efficiency is

defined as the number of photons emitted into free space per second divided by the number of photons emitted from the active region per second [19][31]. Thus, the external quantum efficiency is the ratio between number of photons emitted into free space per second and the number of electrons injected into the LED per second. Higher external quantum efficiency results in higher light output for the same amount of input.

The LED supply chain starts from an LED chip and progresses to an LED package, an LED module, and then to a system. LED production starts from a bare wafer made out of a material such as sapphire, GaN, SiC, Si, or GaAs. Many thin epilayers are grown on the bare wafer. Different colors of LEDs can be made by using different types of epiwafers. The types of epiwafer are InGaN/AlGaN for producing blue, green, and UV-range light; InAlGaP for producing red and yellow light; and AlGaAs for producing red or infrared-range light. The LED chip fabrication process involves attaching electric contact pads on an epiwafer and cutting the epiwafer into LED dies that are then packaged.

LEDs are classified into two types by color output: white LEDs and RGB LEDs. White LED packages can use red/green/blue/orange/yellow phosphors with blue LED chips to produce white light. The phosphors comprise activators mixed with impurities at a proper position on the host lattice. The activators determine the energy level related to the light emission process, thereby determining the color of the light emitted. The color is determined by an energy gap between the ground and excitation states of the activators in a crystal structure. RGB LED packages include red LED packages, green LED packages, blue LED packages, and LED packages with multi-dies in a single package producing white light using a combination of red, green, and blue LED dies.

A cross-sectional side view of white LEDs is shown in Figure 3. An LED package mounted on a printed circuit board is composed of a housing, encapsulant, die, bond wires, die attach, lead frames, metal heat slug, and solder joints. The housing is a body for supporting and protecting the entire structure of an LED device. The housing is usually formed of materials such as polyphthalamide (PPA) or liquid crystal polymer (LCP). The encapsulant positioned over the housing is a resin material for the LED package in the shape of a dome. The typical material types for the resin are epoxy and silicon. The die is a compound semiconductor. The lead frames are used to connect the LED die to an electrical power source. The die attach is used to mechanically and thermally connect the chip to the heat slug. Typical types of die attaches are Ag paste and epoxy paste. Phosphors dispersed in the encapsulant emit white light when they are excited by absorbing a portion of the light from the LED dies.

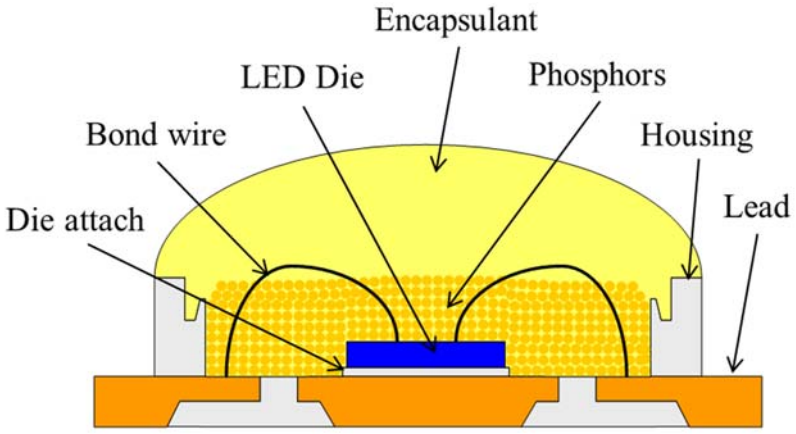


**Figure 3 LED package assembled with printed circuit board (PCB).**

LED types are placed in the following major categories depending on LED electrical power: low power LEDs are under 1W of power (currents typically near 20mA); medium power LEDs (high brightness LEDs) dissipate between 1–3W of

power (currents typically in the 30mA/75mA/150mA range); and high power LEDs (ultra-high-brightness LEDs) have more than 3W of power (currents typically in 350mA/750mA/1000mA range). The LEDs vary because the LED current-voltage curves vary among materials.

The LED industry still faces challenges in attracting widespread consumption. One issue of concern is price, and another is lack of information regarding reliability. The number of LEDs required for the LCD BLU is an area where both of these issues converge. It may take from tens to sometimes thousands of LEDs to produce an LED BLU because the light emission of a single LED covers a limited area. If one single LED fails, the final product is sometimes treated as a failure. For example, the failure of LEDs in an LCD display is critical, even when only a single LED package experiences changes in optical properties [32]. The failure of an LED or LEDs in an LCD display can cause a dark area or rainbow-colored area to appear on the LCD screen.

The LED die is a semiconductor, and the nature of manufacturing LED packages is similar to that of microelectronics. But there are unique functional requirements, materials, and interfaces in LEDs that result in some unique failure modes and mechanisms. The major causes of failures can be divided into die-related, interconnect-related, and package-related failure causes. Die-related failures include severe light output degradation and burned/broken metallization on the die. Interconnect failures of LED packages include electrical overstress-induced bond wire fracture and wire ball bond fatigue, electrical contact metallurgical interdiffusion, and electrostatic discharge, which leads to catastrophic failures of LEDs. Package-related

failure mechanisms include carbonization of the encapsulant, encapsulant yellowing, delamination, lens cracking, phosphor thermal quenching, and solder joint fatigue that result in optical degradation, color change, electrical opens and shorts, and severe discoloration of the encapsulant. In this paper, the focus is on the failure sites, modes, and mechanisms at these three levels.

Cost is another barrier that confronts the LED industry in seeking to expand market share in general lighting. The current cost of LEDs ranges from $0.40 to $4 per package depending on the application. In the recent past, LEDs were often too expensive for most lighting applications. Even though the price of LEDs is decreasing quickly, it is still much higher than the price of conventional lighting sources. However, according to one study, the life cycle cost of an LED lighting system is less than for an incandescent lamp system [33]. The total cost of a lighting system includes the cost of electricity, cost of replacement, and the initial purchase price. Yet since the life cycle savings are not guaranteed at the time of lighting system selection, higher initial costs are still an obstacle to the acceptance of LED lighting. Reducing the manufacturing cost and selling price reduction while maintaining, a high reliability level is key to increasing market share. According to a study by Samsung, the selling price of a white LED lighting system needs to decrease by 50% in order to make LEDs more competitive with fluorescent lamp systems over the next four to five years [33].

### *2.2 LED Reliability*

End-product manufacturers that use LEDs expect the LED industry to guarantee the lifetime of LEDs in their usage conditions. Such lifetime information would allow LED designers to deliver the best combination of purchase price, lighting

performance, and cost of ownership for the life of the end-products. One barrier to the acceptance of LEDs in traditional applications is the relatively sparse information available on their reliability. There are many areas in need of improvement and study regarding LEDs, including the internal quantum efficiency of the active region, light-extraction technology, current-flow design, the minimization of resistive losses, electrostatic discharge stability, increased luminous flux per LED package, and purchase cost [19].

It is rare for an LED to fail completely. LED lifetimes can also vary from three months to as high as 50,000–70,000 hours based on application and construction [3]. LED lifetime is measured by lumen maintenance, which is how the intensity of emitted light tends to diminish over time. The Alliance for Solid-State Illumination Systems and Technologies (ASSIST) defines LED lifetime based on the time to 50% light output degradation (L50: for the display industry approach) or 70% (L70: for the lighting industry approach) light output degradation at room temperature, as shown in Figure 4 [12]. The accelerated temperature life test is used as a substitute for the room temperature operating life test to quickly predict LED lifetime. Prediction of LED lifetime varies with the method of interpreting the results of accelerated testing [4][9][34].

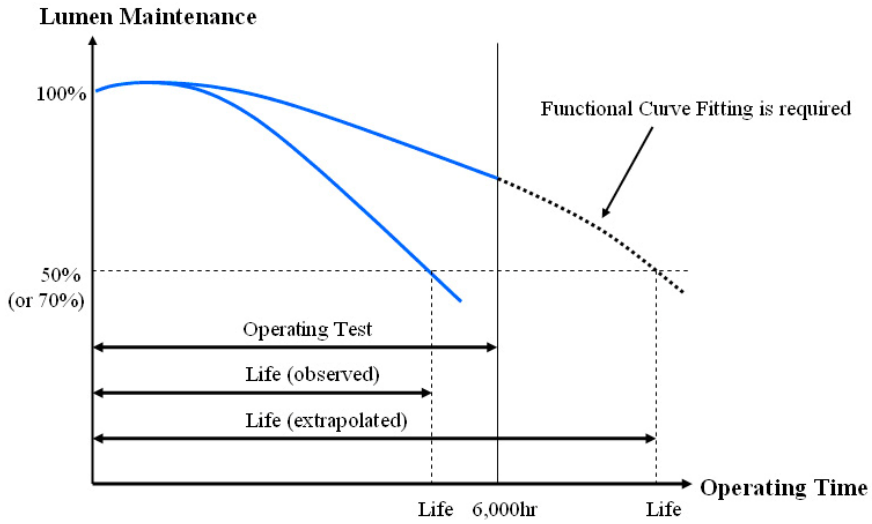


**Figure 4 Lifetime estimation based on LED accelerated life testing.**

LED manufacturers usually perform tests in the product development cycle during the design and development phases. Typical qualification tests of LEDs are categorized into operating life tests and environmental tests by using industrial standards such as JESD, JEDEC or JEITA [9]-[11][36], which have been used by LED manufacturers such as Cree, Samsung, and Nichia. Operating life tests are performed by applying electrical power loads at various operating environment temperatures to LEDs to apply Joule heating to the internal parts of the LEDs. On the other hand, environmental tests are conducted with non-operating life tests. For example, Cree performs the high temperature operating life (HTOL) test with JESD 22 Method A108-C under maximum current in data sheet and 85°C [9]. In some cases, LED manufacturers have independent qualification test conditions different from the industrial standards. Samsung LED performs the HTOL test under high current (than the typical current) and 85°C [10]. Nichia conducts the HTOL test under 100°C and low current (less than the typical current in data sheet) [11][36].

Tests vary among manufacturers. Generally, operating life tests for LEDs include the room temperature test, the high temperature test, the low temperature test, the wet/high temperature test, the temperature humidity cycle test, and the on/off test. Environmental tests of LEDs include the reflow soldering test, the thermal shock test, the temperature cycle test, the moisture resistance cyclic test, the high temperature storage test, the temperature humidity storage test, the low temperature storage test, the vibration test, and the electro-static discharge test. In some cases, combinations of these kinds of loading conditions are used. The acceptance criteria are pass or fail based on lumens, color, and electrical maintenance. Furthermore, when the tests do not include failures, they do not offer any insight on the degradation of LEDs.

Environmental tests are utilized to determine the light output at initial test conditions and final test conditions. Data from other parameters are sometimes collected, such as chromaticity coordinate values (x and y) and reverse current when the lumen measurement is conducted at each data readout time. In many cases, the proper failure criteria of these other parameters are not defined to demonstrate how these collected data are correlated with the data from the light output degradation measurements.

LED system manufacturers are interested in estimating the expected duration of LEDs, since customers want the manufacturers to be able to guarantee a certain level of LED lifetime under usage conditions of the product, and manufacturers want to estimate the life cycle cost of LED systems. To achieve this, manufacturers usually perform accelerated life tests on LEDs at high temperatures while monitoring light output. Modeling of acceleration factors (AF) is generally used to predict the long-term

life of LED packages at specific usage conditions [4][5]. A lifetime estimate is generally made using the Arrhenius model. Activation energy is sensitive to the test load condition, types of materials, and mechanical design of LED packages. The Arrhenius model estimates LED life with uncertainties such as exponential extrapolation of lifetime, assumed activation energy, possible failure mechanism shift between test and usage conditions, and discounting of all other failure causes besides temperature.

One method for predicting the lifetime of LEDs is the use of an accelerated test approach where the estimated lifetime in the accelerated life tests is multiplied by an acceleration factor. The process involves 1) measuring the light output of samples at each test readout time; 2) estimating LED life under the accelerated test conditions (using functional curve fitting of time-dependent degradation under the test conditions) or finding observed lifetime for L50 or L70, as shown in Figure 4; 3) calculating an acceleration factor; and 4) predicting lifetime under the usage conditions by using the acceleration factor multiplied by the lifetime of the test condition, as shown in Equation (1):

$$AF_{temp} = \exp\left[\frac{E_a}{k}\left(\frac{1}{T_u} - \frac{1}{T_a}\right)\right] \qquad (1)$$

where $E_a$ is the activation energy [$eV$], $T_u$ is the junction temperature at usage conditions, $T_a$ is the junction temperature at accelerated conditions, and $k$ is the Boltzmann constant (8.6×10-5 [$eV/K$]).

The optical performance of an LED package is dependent on temperature. The junction temperatures in the active layers (quantum well structures) between the p-n junctions of the chip affect optical characteristics such as color and dominant

wavelength. Direct measurement of the junction temperature is difficult, and the estimation of the junction temperature is derived from the LED case temperature or lead temperature. The luminous efficiency becomes low as the luminous flux emitted from an LED package decreases and the junction temperature increases. The junction temperature is dependent on the operating conditions (the forward current and the forward voltage) and operating environment. Light output measurement does not isolate the failure mechanisms of LEDs, because all failures affect light degradation. This current method of life testing (L50 or L70) may provide a basis for comparing the life expectancy of different LEDs, but it does not provide detailed information on the failure modes, failure mechanisms, and failure sites of LEDs. This method also does not help in remaining useful life estimation during operation.

Each LED lighting system manufacturer may use additional tests based on empirical development histories, applying previous product information to product development. Simple functional plotting in test conditions can be affected by the value of the activation energy of the Arrhenius model. This empirical curve plotting sometimes results in unclear data trending of LED lifetime even in the test conditions, since the functional curve fitting is very sensitive in terms of the number of samples and test duration [6]-[8]. There is a need to develop a more advanced life qualification tool that is able to predict the lifetime of a lighting system during the design, development, and early production phases using analytical tools, simulation, and prototype testing [37]-[44]. These techniques must be properly utilized in order to achieve improved reliability, increased power capability, and physical miniaturization [45]-[49].

Today's ever-diminishing product development cycle time requires rapid and cost-effective reliability analysis and testing of LEDs. If conducted early in the development phase, reliability analysis and accelerated life testing can enable early introduction of mature products with robust design margins. The construction of LEDs is somewhat similar to microelectronics, but there are functional requirements, materials, and interfaces in LEDs that make their failure modes and mechanisms unique.

When a high current is applied to LEDs, there is increased light output. The problem is that light output can change as a result of operating conditions, temperature in particular. Light output decreases with a temperature rise in LEDs, since quantum efficiency decreases at higher temperatures, which contributes to more non-radiation recombination events in LEDs [50]. A temperature increase is also related to forward a voltage decrease in the I-V curve due to a decrease in the bandgap energy of the active region of LEDs and also due to a decrease in series resistance occurring at high temperatures. The resistance decrease is due to higher acceptor activation occurring at elevated temperatures as well as the resulting higher conductivity of the p-type layer and active layers. In addition to the quantum efficiency drop, the color of the LEDs also changes. In particular, phosphor-converted LEDs with blue InGaN and yellow phosphors experience light output degradation, which causes shifts of blue peak wavelength toward longer wavelengths and shifts of the peak energy of the phosphors to lower wavelengths when the temperature of the LEDs increases. The shifts of the blue peak wavelength toward longer wavelengths having lower energy are due to the junction temperature dependence of energy gap shrinkage. The peak energy shifts of

the phosphors are due to phosphor thermal quenching. To sum up, many important reliability-related features of LEDs are a function of temperature.

High power LEDs' long-term stability and lifetime are typically judged on the basis of measured light output. The measured light output mostly depends on the junction temperature. Hence, the reliability of light output measurements is determined by the temperature stability of the light output measurement setup and by the accuracy of the temperature measurement. Prediction of the junction temperature is complicated, and there are associated uncertainties, as it is junction temperature is measured in an indirect way by measuring the temperatures of reference points on leads or metal heat slugs and utilizing them to estimate the junction temperature.

Thermal stressing of LEDs directly or indirectly by high junction temperature affects internal efficiency, maximum light output, reliability, peak wavelength, and spectral wavelength [51]. When a drive current is applied to an LED, the LED junction produces heat, and heat then flows through the junction to the outside of the junction. An accurate method of measuring junction temperature is required to make sure that critical high temperatures beyond the absolute maximum ratings are avoided.

Extensive research on failure mechanisms of LEDs has been conducted as shown in Table 2 [1][52]. The overall reliability of LED packages is related to interconnect failures, semiconductor failures, and package failures. Interconnect failures are responsible for broken bond wires and lifted balls, electrical metallurgical interdiffusion, and electrostatic discharge [53][54]. LED semiconductor failures are manifested as die cracking, defect and dislocation generation and movement, dopant diffusion, and electromigration [1][52][54]. Package failures involve mechanical

interaction with LED chips, die adhesives, heat slugs, lead frames, and encapsulants. The failure mechanisms responsible for package failures include carbonization of the encapsulant, delamination, encapsulant yellowing, phosphor thermal quenching, and lens degradation. These result in optical degradation, color change, electrical opens/shorts, and severe discoloration of the encapsulant. Many of these failures are related to thermal stress as well as electrical stress and hygromechanical stress. Thermal stress affects die cracking, wire ball bond fatigue, delamination, lens cracking, encapsulant yellowing, electrical contact metallurgical interdiffusion, and phosphor thermal quenching. The failure modes of LEDs relate to light output and optical characteristics. These modes differentiate LEDs from the failure modes of other electronic parts where the failures are generally related to electrical parameter degradation.

If the reliability analysis and accelerated testing are not conducted correctly, unexpected field failures will still occur and the test will become a waste of time and money. Because of the acceptance of different standards, conditions, durations, and failure criteria, product certification methodologies need to change from standards-based reliability certification to an approach based on an understanding of failure mechanisms and the end-user conditions. The use of standards-based qualification without consideration of actual LED failure mechanisms results in testing without value, since there is no relationship provided to relate time under accelerated test conditions to time under field conditions.

PoF-based accelerated stress testing was also reviewed briefly. This involves the use of PoF models to qualify the acceleration factors between the expected life

cycle stress profile and the accelerated test profile so that the test can be optimized for minimum time and cost. Further research can be devoted to designing a better test (possibly by using more effective combinations of multiple types of stresses) and providing recommendations about the optimal test conditions that will address the life cycle failure risks at minimum time and cost.

**Table 2 Failure Sites, Causes, Effects, Modes, and Mechanisms of LEDs.**

| Failure Site | Failure Cause | Effect on Device | Failure Mode | Failure Mechanism |
|---|---|---|---|---|
| Semiconductor (Die) | High Current–Induced Joule Heating | Thermomechanical Stress | Lumen Degradation, Increase in Reverse Leakage Current, Increase in Parasitic Series Resistance | Defect and Dislocation Generation and Movement |
| | High Current–Induced Joule Heating | Thermomechanical Stress | Lumen Degradation | Die Cracking |
| | High Ambient Temperature | | | |
| | Poor Sawing and Grinding Process | | | |
| | Poor Fabrication Process of p-n Junction | Thermal Stress | Lumen Degradation, Increase in Series Resistance and/or Forward Current | Dopant Diffusion |
| | High Current–Induced Joule Heating | | | |
| | High Ambient Temperature | | | |
| | High Drive Current or High Current Density | Electrical Overstress | No Light, Short Circuit | Electromigration |
| Interconnects (Bond Wire, Ball, and Attachment) | High Drive Current/ High Peak Transient Current | Electrical Overstress | No Light, Open Circuit | Electrical Overstress-Induced Bond Wire Fracture |
| | Thermal Cycling Induced Deformation | Thermomechanical Stress | No Light, Open Circuit | Wire Ball Bond Fatigue |
| | Mismatch in Material Properties (e.g., CTEs, Young's Modulus) | | | |
| | Moisture Ingress | Hygro-mechanical Stress | | |
| | High Drive Current or High Pulsed / Transient Current | Electrical Overstress | Lumen Degradation, Increase in Parasitic Series Resistance, Short Circuit | Electrical Contact Metallurgical Interdiffusion |
| | High Temperature | Thermal Stress | | |
| | Poor Material Properties (e.g., poor thermal conductivity of substrate) | Thermal Resistance Increase | No Light, Open Circuit | Electrostatic Discharge |
| | High Voltage (Reverse Biased Pulse) | Electrical Overstress | | |
| Package (Encapsulant, Lens, Lead Frame, and Case) | High Current–Induced Joule Heating | Electrical Overstress | Lumen Degradation | Carbonization of the Encapsulant |
| | High Ambient Temperature | | | |

| Failure Site | Failure Cause | Effect on Device | Failure Mode | Failure Mechanism |
|---|---|---|---|---|
| | Mismatch in Material Properties (CTEs and CMEs) | Thermomechanical Stress | Lumen Degradation | Delamination |
| | Interface Contamination | | | |
| | Moisture Ingress | Hygro-mechanical Stress | | |
| | Prolonged Exposure to UV | Photodegradation | Lumen Degradation, Color Change, Discoloration of the Encapsulant | Encapsulant Yellowing |
| | High Drive Current Induced Joule Heating | Thermal Stress | | |
| | High Ambient Temperature | | | |
| | Presence of Phosphor | | | |
| | High Ambient Temperature | Thermomechanical Stress | Lumen Degradation | Lens Cracking |
| | Poor Thermal Design | | | |
| | Moisture Ingress | Hygro-mechanical Stress | | |
| | High Current–Induced Joule Heating | Thermal Stress | Lumen Degradation, Broadening of Spectrum (Color Change) | Phosphor Thermal Quenching |
| | High Ambient Temperature | | | |
| | Mismatch in Material Properties / Thermal Cycling Induced High Temperature Gradient | Mechanical Stress | Lumen Degradation, Forward Voltage Increase | Solder Joint Fatigue |
| | | Cyclic Creep and Stress Relaxation | | |
| | | Fracture of Brittle Intermetallic Compounds | | |

## *2.3 Anomaly Detection of LEDs*

LED lifetime is defined by the general lighting industry as the time to reach 70% light output [12] and 0.007 color shift [55] on the CIE (Commission Internationale De L'eclairage) 1976 chromaticity diagram. The Illuminating Engineering Society (IES) recommends that LED manufacturers collect color data from LEDs over 6,000 hours of operation while collecting light output data [12]. The U.S. Department of Energy (DOE) also published the "Energy Star® Program Requirements: Product Specification for Luminaires" with the Environmental Protection Agency (EPA) regarding LED color failure [56]. This document describes color shift using the 7-step SDCM (standard deviation of color matching) in product qualification tests, where the change in chromaticity over the first 6,000 hours of LEDs should be within 0.007 on the CIE 1976 chromaticity diagram.

The performance of LEDs is evaluated during qualification tests, where the performance of the product consists of quality (which includes function) and reliability, and the requirements are set during product design. The qualification testing method for color failure utilizes the 0.007 color shift without identifying LED die degradation or LED phosphor degradation within the LED package that degraded. However, if qualification testing could identify the main parts in an LED that degrade, such as the die, phosphors, or encapsulant, then the product design, such as geometric dimensions and material properties, can be optimized to meet the specified targets for products.

### *2.3.1 Overview of Anomaly Detection of LEDs*

A life prediction method based on the color failure of LEDs has not yet been developed. It is difficult to extrapolate color change because of the differences in the design, materials, manufacturing processes, and optics applied to LEDs and in their use conditions. LED color change has been studied under different current loads [13]- [15], but there is no model that provides detailed information on color degradation. Therefore, an anomaly detection technique is needed for qualification testing to obtain the exact time to predict the remaining useful life of the products so that accurate prognostics-based qualification can be achieved without waiting 6,000 hours and without increasing the prediction error.

Prognostics and health management (PHM) is a methodology for detecting anomalies and predicting the remaining useful life of products. PHM is an enabling discipline consisting of technologies and methods to assess the reliability of a product in its actual life cycle conditions to determine the advent of failure and mitigate system risk [57]-[59]. However, very little research has been conducted on anomaly detection

in LEDs. Sutharssan et al. [60] conducted real-time monitoring and detected anomalies with Mahalanobis distance (MD) and Euclidean distance (ED) using applied voltage and three (current, light, temperature) sensor voltages. The thresholds were identified as the point where the light output started to decrease continuously for each of the seven LEDs, and they took the minimum values for detection thresholds of MD and ED. Avenel [61] developed a method to identify at least one faulty LED in a string of LEDs using voltage responses. Fan et al. studied the initial anomaly detection work for chromaticity shift of high power white LEDs using the MD approach [62]. However, there has been little reported work on anomaly detection in LEDs utilizing color degradation to provide more detailed information than simply chromaticity shift. Color degradation is a critical issue for some application areas of LEDs, such as museum lighting or decorative lighting, as one of the benefits of LEDs is that they can produce a wide range of colors from 4,500K to 12,000K [1]. If an LED product cannot maintain its initial color properties, this means that the product will lose its advantage over traditional lighting sources such as fluorescent lamps or incandescent bulbs.

### *2.3.2 Clustering Techniques – Exploratory Data Analysis*

PHM involves analyzing and categorizing multivariate data. This can be carried out using two different approaches. Clustering belongs to division of data into groups based on similarities in proximity measures. On the other hand, Classification is affiliated with division of data into groups based on prior labeling (defined by training data).

Exploratory data analysis (EDA) is an approach/philosophy for data analysis that employs a variety of techniques (mostly graphical) to maximize insight into a data

set, to uncover underlying structure, to extract important variables, to detect outliers and anomalies, to test underlying assumptions, to develop parsimonious models, and to determine optimal factor settings. EDA approach is precisely not a set of techniques, but an attitude/ philosophy about how a data analysis should be carried out.

EDA is not identical to statistical graphics although the two terms are used almost interchangeably. Statistical graphics is a collection of techniques- all graphical based and all focusing on one data characterization aspect. EDA encompasses a larger venue. EDA is an approach to data analysis that postpones the usual assumptions about what kind of model the data follow with the more direct approach of allowing the data itself to reveal its underlying structure and model. EDA is not a mere collection of techniques. EDA is a philosophy as to how we dissect a data set, what we look for, how we look, and how we interpret. EDA is a philosophy heavily uses the collection of techniques that we call statistical graphics, but it is not identical to statistical graphics.

John W. Tukey (1977) was one of the first statisticians to provide a detailed description of EDA. He defined it as "detective work – numerical detective work – or counting detective work – or graphical detective work. It is mostly a philosophy of data analysis where the researcher examines the data without any pre-conceived ideas in order to discover what the data can tell him about the phenomena being studied. Tukey contrasts this with confirmatory data analysis (CDA), an area of data analysis that is mostly concerned with statistical hypothesis testing, confidence intervals, and estimation. Tukey stated that confirmatory data analysis is judicial or quasi-judicial in character. CDA methods typically involve the process of making inferences about or estimates of some population characteristics and then trying to evaluate the precision

associated with the results. EDA and CDA should not be used separately from each other, but rather they should be used in a complementary way. The analyst explores the data looking for patterns and structure that leads to hypotheses and models.

Tukey thought EDA at a time when computers were not widely available and the data sets tended to be somewhat small, especially by today's standards. So, Tukey developed methods that could be accomplished using pencil and paper, such as the familiar box-and-whisker plots (also known as boxplots) and the stem-and-leaf. He also included discussions of data transformation, smoothing, slicing, and others. Since today is a time when computers are widely available, researchers go beyond what Tukey used in EDA and present computationally intensive methods for pattern discovery and statistical visualization.

Tukey, expanding on his ideas of how EDA and CDA analysis fit together, presented a typical straight-line methodology for CDA. Its steps follow: (1) sate the equation(s) to be investigated; (2) design an experiment to address the questions; (3) collect data according to the design experiment; (4) perform a statistical analysis of the data; and (5) produce an answer. The procedure is core of the usual confirmatory process. To perform EDA, Tukey revised the first two steps as follows: (1) start with some idea; and (2) iterate between asking a question and creating a design.

Some of the ideas of EDA and their importance to teaching statistics were discussed by Chatfield [1985]. He called the topic initial data analysis or IDA. While Chatfield agrees with the EDA emphasis on starting with the noninferential approach in data analysis, he also discussed the need for looking at how the data were collected, what are the objectives of the analysis, and the use of EDA/IDA as part of an integrated

approach to statistical inference. Hoaglin [1982] provided a summary of EDA in the Encyclopedia of Statistical Sciences. He describes EDA as the "flexible searching for clues and evidence" and confirmatory data analysis as "evaluating the available evidence." In his summary, he stated that EDA are composed of four themes: resistance, residuals, re-expression and display.

Resistant data analysis pertains to those methods where an arbitrary change in a data point or small subset of the data yields a small change in the result. A related idea is robustness, which has to do with how sensitive an analysis is to departures from the assumptions of an underlying probabilistic model. Residuals are what we have left over after a summary or fitted model has been subtracted out. This was read such as Residual = data – fit.

Residuals should be looked at carefully for lack of fit, heteroscedasticity (nonconstant variance), nonadditivity, and other interesting characteristics of the data. Re-expression has to do with the transformation of the data to some other scale that might make the variance constant, might yield symmetric residuals, could linearize the data or add some other effect. The goal of re-expression for EDA is to facilitate the search for structure, patterns, or other information.

Finally, the displays used most often by early practitioners of EDA included the stem-and-leaf plots and boxplots. The use of scientific and statistical visualization is fundamental to EDA, because often the only way to discover patterns, structure or to generate hypotheses is by visual transformations of the data. Given the increased capabilities of computing and data storage, where massive amounts of data are

collected and stored simply because we can do so and not because of some designed experiment, questions are often generated after the data have been collected.

Clustering is the process of partitioning a set of data (or objects) into sets of meaningful sub-classes called clusters. A cluster is a collection of data (or objects) that are "similar" (based on some proximity measures) to one another and thus can be treated collectively as a group. Clustering applications include pattern recognition, spatial data analysis, and image processing.

Clustering techniques can be broadly categorized into five approaches [63][64]. Hierarchical algorithms construct a hierarchical decomposition of the set of data. Partitioning-based algorithms construct partitions in data and evaluates them by some criterion. Density-based algorithms are based on connectivity and density functions. Grid-based algorithms are based on multiple level granularity structure. Model-based algorithms are hypothesized and fit to each cluster.

Clustering is used for the exploration of inter-relationships among a collection of patterns, by organizing them into homogeneous clusters [63][64]. Clustering does not use priori labeling of some patterns to use in categorizing others and inferring the cluster structure of the whole data. Kotsiantis et al. introduced intra-connectivity and inter-connectivity to explain the concept of clustering [63]. Intra-connectivity is a measure of the density of connections between the instances of a single cluster. The authors stated that a good clustering arrangement needs a high intra-connectivity since the instances grouped within the same cluster are highly dependent on each other. Inter-connectivity is a measure of the connectivity between distinct clusters. It is

required for the inter-connectivity that a low degree of inter-connectivity is better because it tells that individual clusters are largely independent of each other.

There is a question with regard to clustering techniques in that the interpretation of the clusters is difficult. In addition to this problem, the techniques can get a wrong decision assigning the data to clusters even if there were no clusters in the data. So it is necessary to analyze if the data set exhibits a clustering tendency when the cluster structure is investigated based on inferences. In real application, there are noises (i.e., errors) in the collected data set due to missing values or inaccurate measurement. So a strategy needs to be selected for handling missing attribute values. We need pre-processing techniques. Also basic question is that what specific learning algorithm is suitable for the data set. Jain et al. discussed that learning algorithms based on the type of data and the nature of the problem were still remained an open and fundamental problems [65].

Kotsiantis et al. [63] studied that many factors such as effective similarity measures, criterion functions, algorithms, and initial conditions plays an important role to develop fine-tuned clustering technique for a given clustering problem. The authors also argued that no clustering method can properly handle all kinds of cluster structures in terms of shape, size, and density. So depending on the data structure from collected data, different techniques can be selected to obtain best results from clustering techniques.

It is common to delete noisy values by a preprocessing step. Small clusters are often eliminated because they frequently represent groups of outliers (i.e., instances with noise). The missing value problems occurred due to some occasional sensor

failures. One way to cope with this problem is to throw away the incomplete attribute vectors. Another way to deal with this is taking median value of that attributes across all training instances.

Also two small clusters close together can be merged. Alternatively large clusters can be split into smaller clusters. The authors used outlier detection term as anomaly detection [63]. The authors explained that outlier detection is to find small groups of data objects that are exceptional when compared with rest large amount of data. Outlier mining has been used in the areas of telecommunication, financial fraud detection, and data cleaning. The anomalies are usually interesting for helping the decision makers to make profit or improve the service quality.

Usually, from statistical point of view, instances with many irrelevant input attributes provide little information. So, in practical applications, it is required to choose attributes providing information to a proper learning algorithm. Different algorithms have been developed for this purpose. For example, this can be accomplished by discarding attributes that show little variation or that are highly correlated with other attributes [66].

Hierarchical clustering (HC) algorithms organize data into a hierarchical structure according to some proximity measure (e.g. Euclidian distance or Manhattan distance). The results of HC are usually depicted by a binary tree or dendrogram. An example of typical dendrogram is shown in Figure 5. Hierarchical clustering methods are categorized into agglomerative (bottom-up) and divisive (top-down) shown in Figure 6. Agglomerative clustering starts with one-point (singleton) clusters and recursively merges two or more most appropriate clusters. Divisive clustering starts

with one cluster of all data points and recursively splits the most appropriate cluster. In both approaches, the process continues until a stopping criterion (frequently, the requested number ('k') of clusters) is achieved.

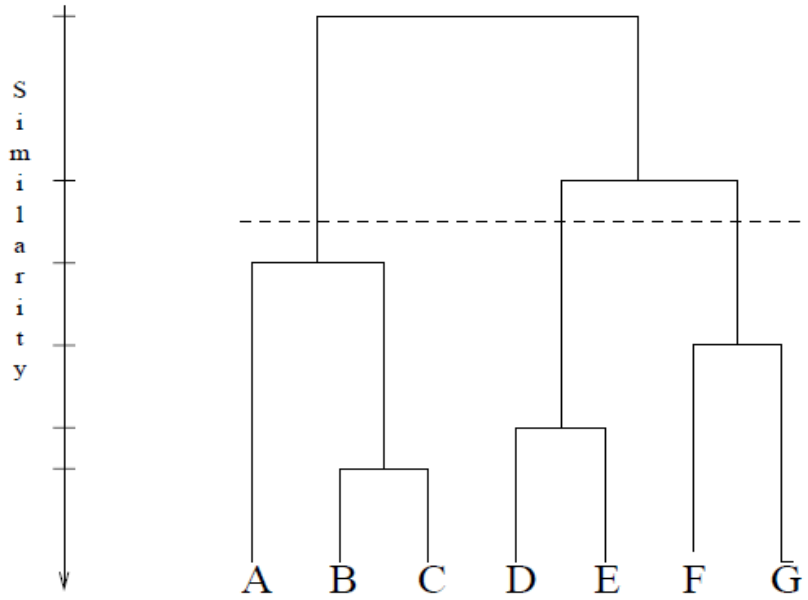


**Figure 5 Typical dendrogram.**

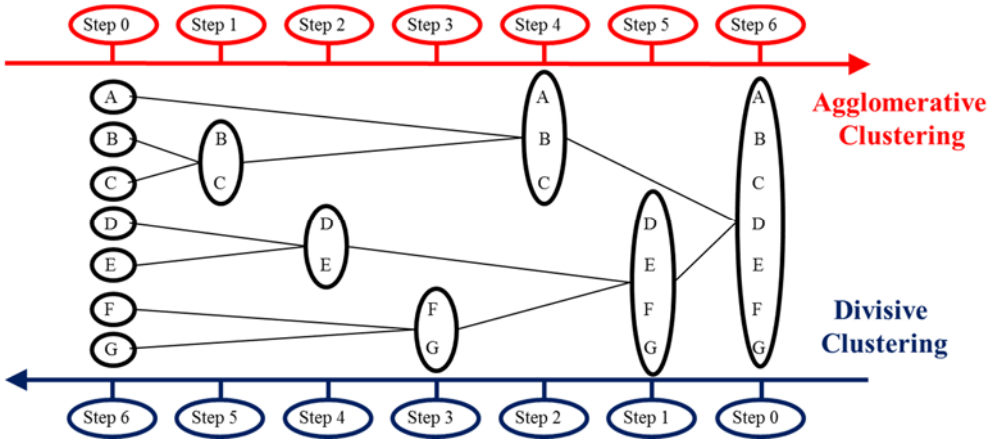


**Figure 6 Schematic for agglomerative clustering and divisive clustering.**

However, it is known that both agglomerative and divisive clusterings have limitation in a sense that adjustment of clustering is not available once the splitting or merging decision is made [63]. Advantages of the hierarchical clustering techniques are: they do not require deciding the number of clusters in advance; they compute a

complete hierarchy of clusters; good result visualizations are possible to see the clusters; and a "flat" partition can be derived via a cut through the dendrogram shown in Figure 5.

Hierarchical clustering techniques utilize criteria to determine "which clusters should be joined (for agglomerative clustering) or split (for divisive clustering)" locally at each step. For agglomerative hierarchical techniques, the criterion is typically to merge the "closest" pair of clusters, where "close" is defined by a specified measure of cluster proximity. There are three definitions of the closeness between two clusters including single-link, complete-link, and average-link. The single-link similarity between two clusters is the similarity between the two most similar instances, one of which appears in each cluster. Single-link is suitable for dealing with non-elliptical shapes, but it is sensitive to noise and anomalies. The complete-link similarity is the similarity between the two most different instances, one from each cluster. Complete-link is less sensitive to noise and outliers, but can break large clusters, and has trouble with convex shapes. The average-link similarity is a compromise between two clusters. Known hierarchical techniques on clustering are BIRCH, CURE, and CHAMELEON.

Partitioning-based clusterings typically partition the data set into a desired number (such as k) of clusters using a specific criterion [67]. Representative partitioning techniques are centroid clustering and medoids clustering. The centroid algorithms identify each cluster by using the center of the gravity of the instances. The medoids algorithms represent each cluster by means of the instances closest to the center of the gravity.

K-means clustering is one of the most well-known centroid algorithms. K-means clustering partitions the data set into k subsets such that all points in a given subset are closest to the same center. Brief flowchart for k-means clustering is shown in Figure 7. It needs to choose the number of clusters at the beginning of the operation.

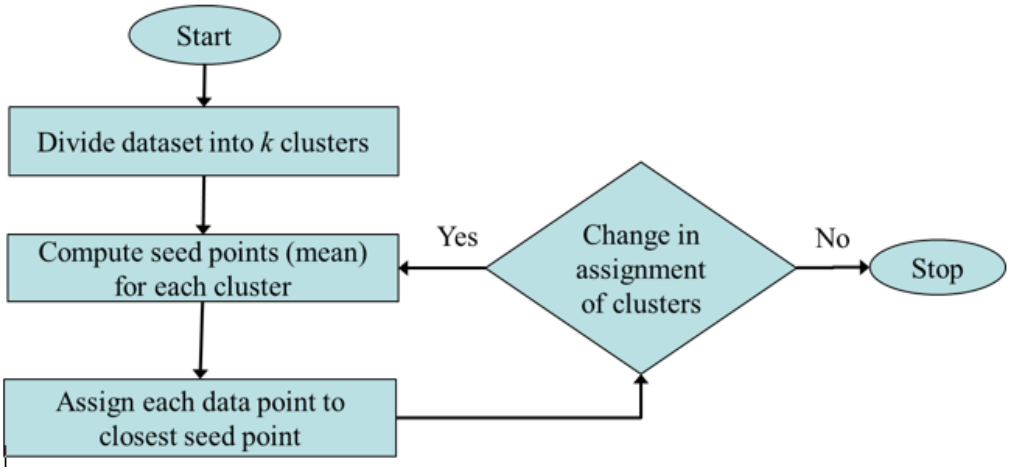


**Figure 7 Flowchart for K-means clustering.**

The number k needs to be selected before we conduct the k-means clustering technique. In detail K-means clustering randomly initiates to select k of the instances to represent the same clusters. Based on the selected k instances, the whole data set is split into k sub-clusters assigned to their closer centers. K-means then computes the new centers by taking average of all data points in each sub-cluster. The operation is continuously repeated until there is no change in the center of the gravity as shown in Figure 8. Even though optimum k-values need to be selected until the most suitable value is found unless k can be known ahead of computation, it was discussed [63][64] that a way of finding a distance measure working good with all types of data determines the effectiveness of this method.

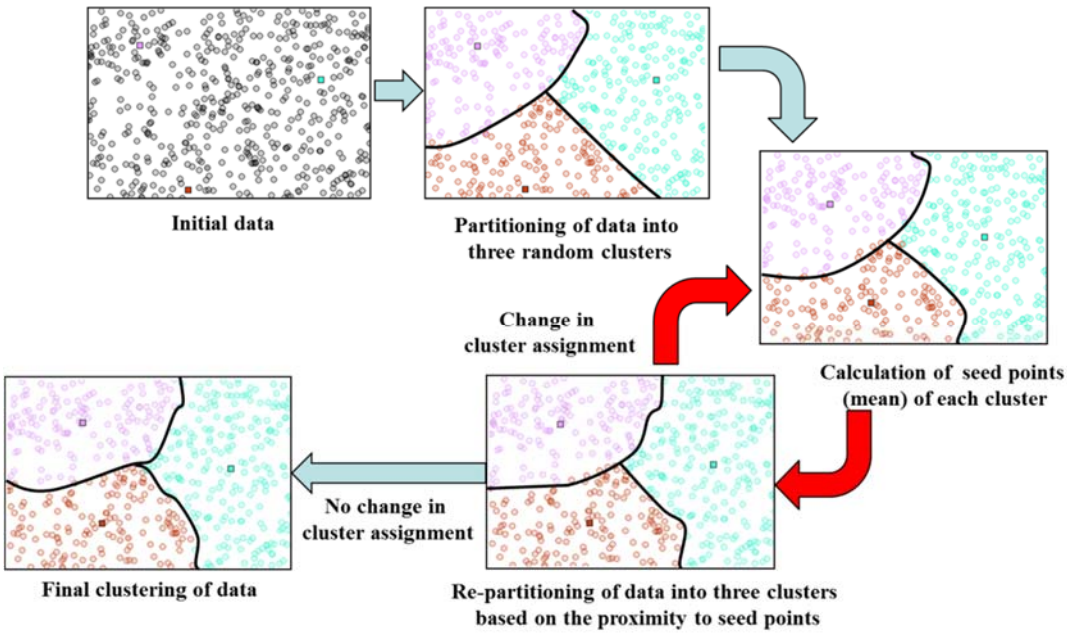


**Figure 8 Schematics of k-means clustering.**

The k-means clustering has the following characteristics: It is efficient in processing large data set; It often terminates at a local optimum; The clusters have spherical shapes; and It is sensitive to noise. The k-modes algorithm is a partitioning algorithm and uses the simple matching coefficient measure to deal with categorical attributes [68]. The k-prototypes algorithm advanced k-means and k-modes algorithms by clustering instances designed by mixed attributes [68]. Another drawback of k-means clustering is that the computations are complex causing more money and another problem is overfitting. The speed of the simulation is out of focus in this study so this disadvantage will be considered as negligible.

Finding clusters in data especially like LED spectral data becomes an issue when clusters are dealing with different sizes, densities, and shapes. Also it is challenging to find clusters in data when the data contains large amount of noise and outliers. Many of these issues will be severer when the data is composed of high

dimensionality such as time series data or text data. In many cases, clustering techniques have issues related to how to handle to noise and outliers, how to determine the number of clusters, and how to find clusters with different sizes, shapes, and densities [69].

Density-based clustering algorithms try to find clusters based on density of data points in a region. In other words, density-based algorithms define a cluster to be a region in the data space that exceeds a given density threshold. An advantage of the density-based clustering over the partition-based and hierarchical algorithms is in identifying clusters of arbitrary shapes. K-means clustering as a representative method for the partition-based clustering is good for spherical shapes of the data set. The key idea is that neighborhood of a given radius for each instance of a cluster has to contain at least a minimum number of instances [63].

In early stage of developing density-based clustering technique, one of the most well-known techniques is DBSCAN (density-based spatial clustering of applications with noise) [69][70]. DBSCAN separated data points into three classes: core points, border points, and noise points [69][70]. Core points are the points that are at the interior of a cluster. A point is regarded as the interior point if there are enough points in its neighborhood. Board point is a point that is not a core point, i.e., there are not enough points in its neighborhood, but it falls within the neighborhood of a core point [63]. Noise point is any point that is not a core point or a board point.

In DBSCAN, the density associated with a point is obtained by counting the number of points in a region of specified radius around the point. Points with a density above a specified threshold are classified as core points, while noise points are defined

as non-core points that do not have a core points within the specified radius [69]. The noise points are discarded, while clusters are formed around the core points. If two core points are neighbors of each other, then their clusters are joined [69].

The concept of the density is described in Figure 9. This figure shows what density means. The density is related to how to the points are packed together to form clusters. It is not related to probability densities. Although DBSCAN is good for finding clusters of arbitrary shapes, it is not suitable to form clusters including different densities [69].

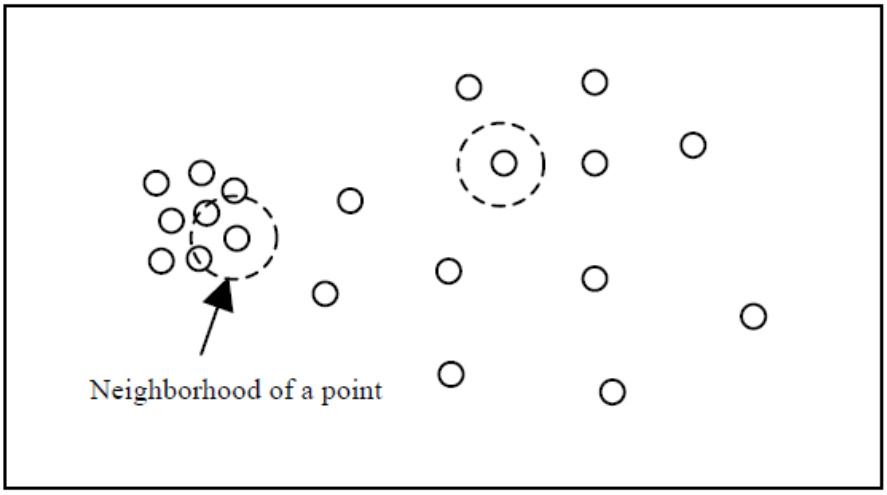


**Figure 9 Density-based neighborhoods [69].**

CURE (Clustering Using Representatives) algorithm was later introduced after DBSCAN. The better thing than DBCAN was that the representative points were used to find non-globular clusters. However, there were still many types of globular shapes that CURE could not handle [69]. Similar approach was introduced as Chameleon algorithm. All three algorithms (i.e., DBSCAN, CURE, and Chameleon) have in common with determining clusters of different shapes and sizes based on points or small subsets of points and then finding clusters around them.

In summary, the main differences between these three algorithms are following: DBSCAN do not consider noise points to form clusters. CURE eliminated noise points by periodically eliminating small groups of points that are not growing fast. Chameleon does not eliminate points, but it does eliminate most of the influence of noise points on the clustering process by building the similarity graph for the nearest neighbor list [69].

Other density-based clustering techniques were developed such as the incremental DBSCAN, GBDSCAN (generalized density-based algorithm DBSCAN), PDBSCAN (parallel version of DBSCAN), DBSCLASD (Distribution Based Clustering of Large Spatial Data Sets), DENCURE, and OPTICS [63].

Grid-based clustering algorithms first quantize the clustering space into a finite number of cells (hyper-rectangles) and then perform the required operations on the quantized space [63]. Cells containing more than certain number of points are treated as dense and the dense cells are connected to form the clusters. Some of the grid-based clustering algorithms are STING (Statistical Information Grid-based method), WaveCluster, and CLIQUE (Clustering in QUEst).

STING divides the spatial area into several levels of rectangular cells in order to form a hierarchical structure. The cells in a high level are composed from the cells in the lower level. STING generates a hierarchical structure of the grid cells to represent the clustering information at different levels [63]. Flaws of STING algorithm is that the performance mainly relies on the granularity of the lowest level of the grid structure; and the resulting clusters are all bounded horizontally or vertically, but not diagonally.

CLIQUE is another grid-based clustering that starts by finding dense areas in one-dimensional spaces for each attribute [71]. CLIQUE generates a set of

two-dimensional cells that can be dense by looking at dense one-dimensional cells. CLIQUE generated a possible set of k-dimensional cells by searching dense (k-1) dimensional cells [63][71].

Clustering groups objects characterized by the values of a set of variables into separate groups (clusters), based on their similarities [63][72]. In other words, clustering of multispectral data groups objects with respect to a distance, or equivalently, a similarity measure [73]. However, the successful application of clustering on multivariate data sets depends on the understanding the data set and a good choice of the clustering algorithm.

When clustering techniques are considered for the multivariate data, the main things considered are listed with feature dimension, noise, overlapping clusters, number of clusters, unequal cluster density, and unequal cluster size [72]. The improvement of data collection equipment can cause a large number of variables. This increases feature dimension.

Many data sets include noise or outliers because of limited sensor sensitivity, statistical variation, or signal interference. This can lead to a wrong solution. In many cases, clusters are overlapping in the feature domain; even though two objects may belong to different clusters, they may have features that are similar. Then, if a clustering algorithm uses only feature information, it will not have a good result [72].

Number of clusters has to be determined from the data. This results in the accuracy of the anomaly detection with the clustering technique. The unequal cluster density in the feature space is the number of objects contained in a unit of the data space.

If the data set includes many different densities, it makes the cluster algorithm difficult to group the data set into clusters.

Density-based clustering technique utilizes a local cluster criterion such that clusters are determined with regions in data space where the objects are dense, and clusters are recognized from another one by low-density regions [73]. It was known that a small cluster can be important to analyze the data but it can be often not found since the larger clusters determine the clustering result [72]. In some cases, clustering techniques often identify the low density regions as the noise. And also, the high dimensionality of multivariate data sets is another issue when dealing with density-based clustering techniques.

One of the solutions for the high dimensionality problems is utilizing k-nearest-neighbor (KNN) density estimation technique. Instead of defining threshold to local density function, low-density regions, and valleys, KNN separate clusters by calculating number of shared neighbors. If the number of shared neighbors of two adjacent objects is below a threshold (i.e., number of objects), then it is regarded that there is a gap, a valley, in between [73].

### *2.4 Prognostics-based RUL prediction of LEDs*

A light-emitting diode (LED) is a solid state light source that emits light by electroluminescence, where light is generated by the flow of electrons applied to a semiconductor device die [1]. LEDs are being used in an ever-increasing variety of applications, including television display backlighting, communications, medical equipment, signage, and general illumination [1][16]-[18]. For many of these LED applications, LED manufacturers need to ensure that their products meet the quality

and performance expectations of end users and their targeted applications. However, one bottleneck is that typical qualification tests performed by manufacturers are time-consuming and often not informative. As per industry normative (IESNA) standards, it takes at least 6,000 hours (i.e., eight months) to complete qualification test and 10,000 hours are preferred for prediction [12][76].

The Alliance for Solid-State Illumination Systems and Technologies (ASSIST) defines LED lifetime as the time to 50% light output (for the display industry) or 70% (for the lighting industry) at room temperature [12][76]. LED lifetimes can vary from 2,000 hours to as high as 70,000 hours based on the particular application and construction [1]. LED lifetime is measured by lumen maintenance, which describes how the light output degrades over time. Qualification life testing can be used to predict LED lifetime based on lumen maintenance. For example, based on data from a test run for 6,000 hours, the time to 50% or 70% light output can be extrapolated, creating a remaining useful life prediction under qualification conditions that can, in turn, be used for estimating life in field conditions.

There is no unified standard for qualification testing in the LED industry. Each LED manufacturer decides which tests and conditions to use to qualify new products. Typical qualification tests include operating life tests and environmental tests based on semiconductor-based industrial standards published by organizations such as JESD, JEDEC, or JEITA [9]-[11] as well as the IESNA standards suggesting the guideline under operating life tests. CIE (the international commission on Illumination) provides standards, technical reports, and recommendations [77].

The failure mechanisms of LEDs are related to multiple health indicators, such as color, electrical, and thermal properties, as well as light output [1]. These health indicators can be divided into two categories: optical health indicators (e.g., light and color parameters) and thermal and electrical health indicators. An LED is regarded as failed when an optical health indicator crosses a predetermined failure threshold. For example, according to industry practices and standards, degradation of light output (lumens) to 70% of the original light output is considered a failure [3][4]. However, there is no specific guideline for failure criteria based on thermal and electrical health indicators.

The existing methods that predict the lifetimes of LEDs are based on light output degradation [1][13][78]-[86]. The most common models are exponential models [4][13][78]-[82]. Other models include inverse power models [83][84] and the kinetic (theoretical) model for die-defect generation and movement [85]. Fan et al. [86] utilized a data-driven extrapolating degradation path model for the prediction of light output degradation. Sutharssan et al. [60] performed prognostics using Euclidean distance (ED) and Mahalanobis distance (MD). They estimated the RUL by trending the ED and MD curves over time. All of these methods require specific mathematical model for the prediction. If the degradation path of an LED is different from the model, the prediction cannot capture the degradation dynamics of each LED.

Bürmen et al. [15][87] developed a method for predicting color coordinates x and y (in the 1931 chromaticity coordinates) by constant offset moving of the known coordinate value in the reference current as a function of the normalized light output degradation rate. If the entire test data on the current devices at specific current load did

not exist, this method cannot be used for predict the color failure. Only tested current device at different current load can be predicted for the color failure. Although LED manufacturers are required to collect data on color shift over 6,000 hours of operation [12], there is no accepted way to use these data to extrapolate color shift. Therefore, more research is needed on the life prediction of color failure for LEDs.

Electrical degradation has been studied under different current loads [88]-[93]. It has been reported that the reverse (leakage) current (which cannot be measured in-situ) and the forward series resistance at different current loads (which cannot be obtained under single current loads) increases after aging tests [88]-[93]. It has been argued that electrical changes are relatively small in the operation region of I-V characteristics, and therefore electrical degradation has not been frequently studied. Thermal degradation has been used to predict the lifetime of LEDs based on the degradation criterion of a reduction to 70% of light output [4][78]-[82]. Junction temperature and thermal resistance are not directly measurable parameters, but Keppens et al. studied that junction temperature can be correlated with the electrical power and radiant flux as a function of forward current and thermal resistance [94]. The failure thresholds of the in-situ health indices based on the characteristics of optical health indicators (such as 30% reduction of the light output) have not been addressed.

### *2.5 Thesis Scope*

At first, a method for conducting anomaly detection on the color failure of LEDs is presented. Then, prognostics-based RUL prediction of LEDs are presented with two different approaches. First approach is made when the historical data from other devices tested is not available. Second approach is made based on the assumption

such that the historical data from other devices previously developed and tested for qualification test.

# CHAPTER 3 Anomaly Detection of Light Emitting Diodes Using the Similarity-Based-Metric Test

This chapter presents a method for conducting anomaly detection on the color failure of LEDs. Features were extracted by analyzing the data of spectral power distributions exhibiting multiple peaks, which are defined as the power per unit area per unit wavelength of a radiant exitance (*section 3.1*). The features were reduced by principal component analysis (*section 3.2*). Then the principal components were partitioned into clusters (*section 3.3*). Anomalies were detected when the similarity distance was greater than the pre-determined thresholds (*section 3.4*). Discussion and conclusions are given in *section 3.5* and *3.6*.

## *3.1 Feature Extraction*

Anomaly detection was performed by following the steps described in Figure 10 and Figure 11. The approach in Figure 10 uses the entire spectral power distributions (SPDs) for anomaly detection. The approach in Figure 11 utilizes each specific peak in the SPDs, such as die peak and phosphor peak. Individual anomaly detection with each peak component (i.e., die and phosphor) in the SPDs is conducted to identify the die and the phosphor degradation or to determine whether the die or phosphors degrade faster depending on the failure mechanisms of the LEDs. The die peak and phosphor peak were separated based on the wavelength range (in this case

study, 380nm to 495nm for the die peak and 495nm to 745nm for the phosphor peak) in the SPD.

The full detection scheme is described as follows. Twelve features (e.g., peak area, FWHM (full width at half maximum), and peak centroid) were extracted from each die and phosphor peak, as discussed in this section. Then, the features from all of the component peaks (i.e., using the entire SPD) in Figure 10 and the features from each separate peak in Figure 11 were reduced to three principal components to reduce dimensionality (see *section 3.2*).

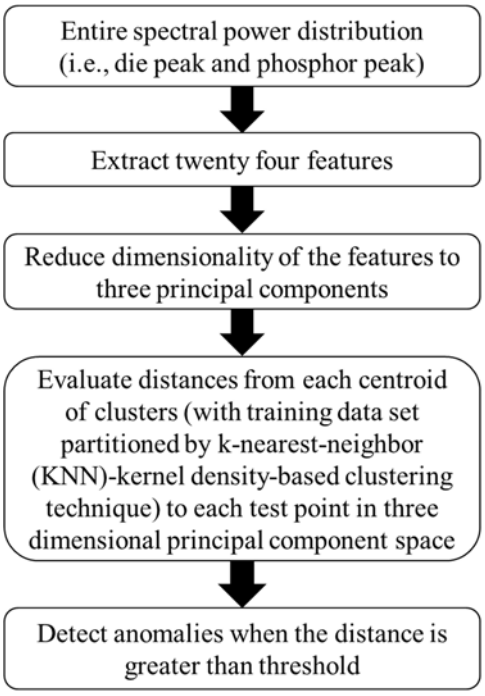


**Figure 10 Anomaly detection scheme with the similarity-based-metric test over the entire spectral power distribution.**

Each data set (the entire SPD, die peak, and phosphor peak) was partitioned into clusters using a KNN-kernel density-based clustering technique (see *section 3.3*). The similarity-based-metric test was developed to evaluate the distance from each centroid in each individual cluster to the test data points to conduct anomaly detection (see

*section 3.4*). If the distance was greater than the pre-determined threshold, an anomaly was detected. Otherwise, the algorithm continued to measure the distance between the centroids and the test data points in three-dimensional PC space. This section covers feature extraction by analyzing the SPDs.

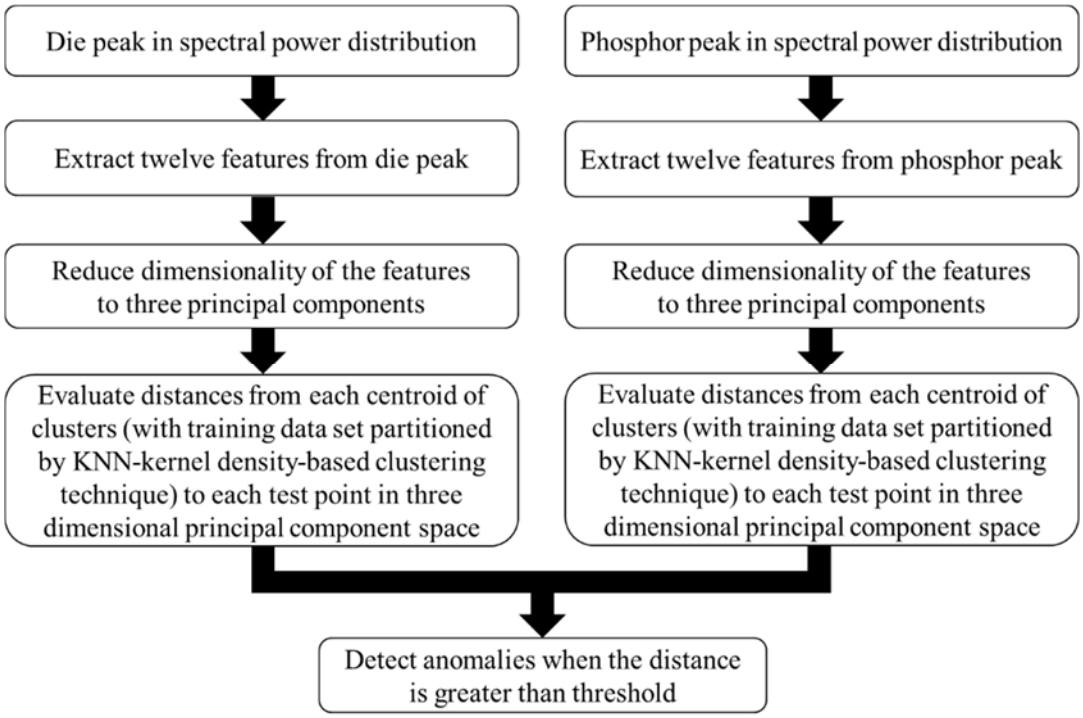


**Figure 11 Anomaly detection scheme with similarity-based-metric test identifying parts that degraded mainly in the LED package.**

Qualification tests of LEDs measure the degradation of certain variables (such as light output and color parameters) without identifying the specific components within the LED that degraded. Light and color output are evaluated from the spectral power distribution (SPD) of LEDs. An example of an SPD for a phosphor-converted white LED is shown in Figure 12. The SPD is composed of two parts: a peak from the LED die (i.e., the left peak) and a peak from the phosphors (i.e., the right peak). Depending on product design, application, cost, and material properties, the number of

peak components can be different. LED phosphors are embedded inside a resin that surrounds the LED die. The phosphors convert some portion of the short wavelength light from the LED into long wavelength light, and the LED light combined with the down-converted light produces the desired white light [95]. The two peaks in the SPD show the effects of die degradation, phosphor degradation, and package degradation. These types of degradation will be discussed in *section 3.2*.

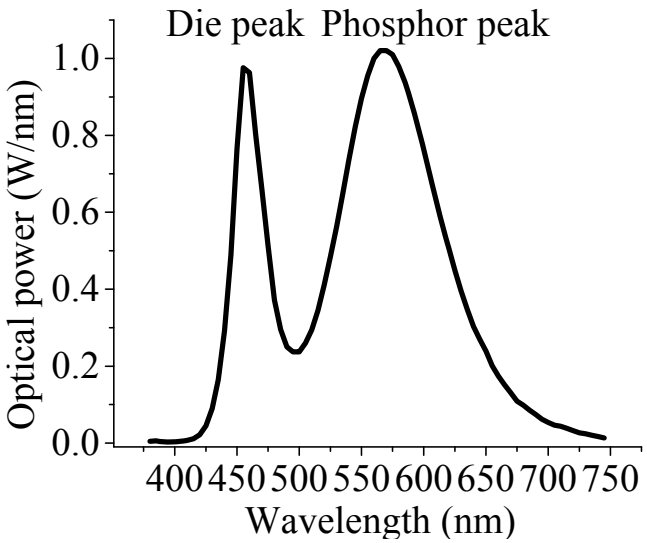


**Figure 12 SPD of white LED with LED die peak and phosphor peak [21].**

Data from an aging test was used to develop and validate the anomaly detection process (Appendix A: Test Results). The test samples in this study were 3W InGaN white LEDs. Sixteen LED samples were mounted on an aluminum metal core printed circuit board (MCPCB). The test setup is shown in Figure 13. The test condition was a 350mA constant current and a chamber temperature of 40ºC recommended by its manufacturer and the IES-LM-80-08 standard. The junction temperature was expected to stay below the absolute maximum rating junction temperature of 135ºC [95][96].

The SPDs of all of 16 LEDs were measured after every 22.5 hours of exposure to this condition.

The failure criterion was a 7-step SDCM (discussed in the introduction) for color shift. The times to color failure data are plotted with a 3-parameter Weibull in Figure 14. The shape parameter was 1.2, the scale parameter was 91.3, and the location parameter was 1859.6. The time to failure (TTF) range for color failure was 1,891 hours to 2,206 hours. The mean time to color failure was 1,945.5 hours (referred to as the unadjusted plot) in Figure 14.

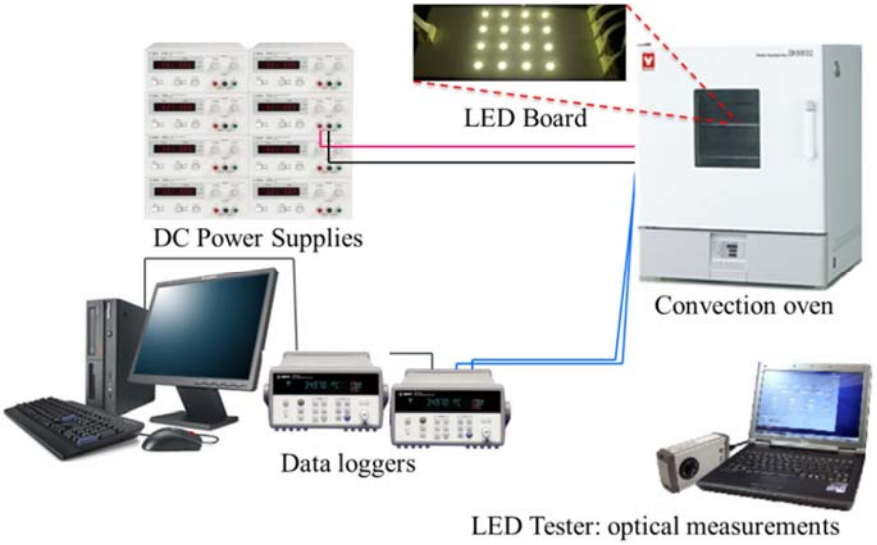


**Figure 13 Data collection of LEDs [20][21].**

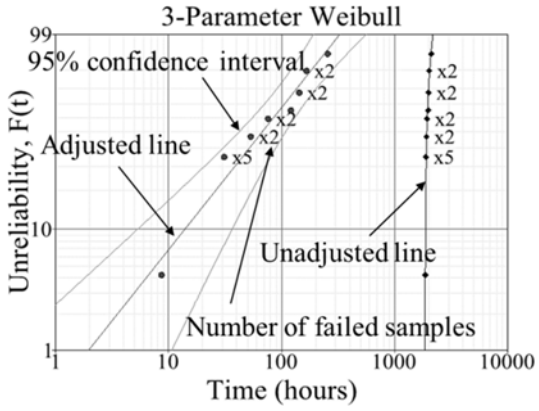


**Figure 14 Color failure result (7-step SDCM).**

Features were extracted from both the LED die peak and the phosphor peak, as shown in Figure 15. The LED die peak was the wavelength range between 380nm and 495nm, and the phosphor peak was the wavelength range between 495nm and 745nm. Twelve features were extracted from each peak. The features were peak area (denoted as v1), average of the peak (v2), peak centroid (v3), peak height (v4), root mean square (RMS) (v5), crest factor (v6), standard deviation (v7), skewness (v8), kurtosis (v9), full width at half maximum (FWHM) (v10), peak wavelength (v11), and left half width (v12). SPD was defined by a function *f(x)* in the range of wavelength *x* of *a* and *b* (i.e., $a<x<b$), as shown in Figure 16. All features are described in equations (1) through (12) in mathematical terms.

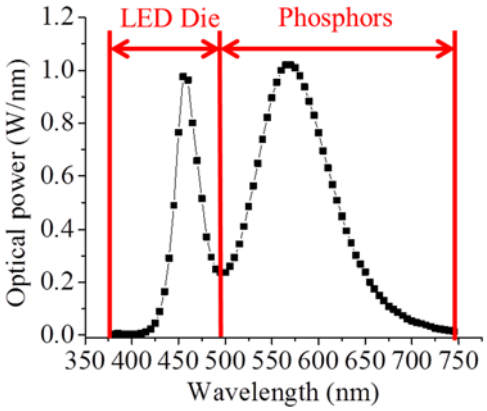


**Figure 15 Feature extraction from SPD.**

$$v1 = \int_a^b f(x)dx \tag{1}$$

$$v2 = \frac{1}{b-a}\int_a^b f(x)dx \tag{2}$$

$$v3 = \frac{\int_a^b xf(x)dx}{\int_a^b f(x)dx} \tag{3}$$

$$v4 = h \tag{4}$$

$$v5 = RMS_x = \sqrt{\frac{1}{b-a}\int_a^b f(x)^2dx} \tag{5}$$

$$v6 = \frac{h}{RMS_x} \tag{6}$$

$$v7 = \sqrt{\left[\frac{1}{b-a}\int_a^b f(x)^2 dx\right]^2 - \left[\frac{1}{b-a}\int_a^b f(x)dx\right]^2} \tag{7}$$

$$v8 = \frac{\frac{1}{N}\sum_{i=1}^{N}(f(x_i) - v2)^3}{(\frac{1}{N}\sum_{i=1}^{N}(f(x_i) - v2)^2)^{3/2}} \tag{8}$$

$$v9 = \frac{\frac{1}{N}\sum_{i=1}^{N}(f(x_i) - v2)^4}{(\frac{1}{N}\sum_{i=1}^{N}(f(x_i) - v2)^2)^2} - 3 \tag{9}$$

$$v10 = x_2 - x_1 \tag{10}$$

$$v11 = peak\ wavelength \tag{11}$$

$$12 = v11 - x1 \tag{12}$$

where $x_1$, $x_2$, v4, v10, and v11 are shown in Figure 16, and $N$ is the number of data points in the SPD by optical measurements.

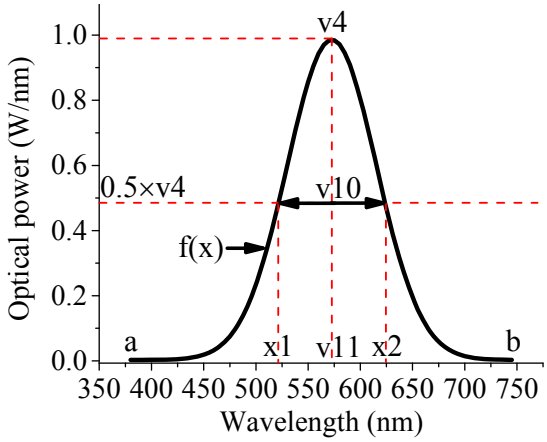


**Figure 16 Description of features in the SPD.**

### *3.2 Dimensionality Reduction Using Principal Components Analysis*

Principal component analysis, an exploratory data analysis technique, was used to transform the 24 extracted features (twelve from the die peak and twelve from the phosphor peak for each SPD) into principal components. A different number of training data points (i.e., the initial test data points) can be applied to detect anomalies,

where a larger number of training data points reduces the error of anomaly detection because more training data points include more information on the actual degradation trend of LEDs. To investigate detection accuracy based on the number of training data points, anomaly detection using the entire SPD, with die and phosphor peaks together, was conducted with four different training data sets: 10 data points, 20 data points, 30 data points, and 40 data points from each LED. For each LED, 123 data points were collected.

**The data points that were not used in the data set were used for testing (i.e., anomaly detection). Examples of training data sets utilizing the entire SPD are described in Table 3. In addition to detection with the entire SPD, anomaly detection was conducted for each peak with 30 data points and 40 data points from each LED, as shown in**

Table 4. Each training data set was used to evaluate the loading matrix and variances for the principal component analysis. The principal component scores for the test data points were obtained by multiplying the loading matrix and the feature vectors.

**Table 3 Sample size factor inference for training data sets with the entire SPD.**

| Training data set (i.e., initial data points) with 16 LEDs | | 160 data points (10 × 16) | 320 data points (20 × 16) | 480 data points (30 × 16) | 640 data points (40 × 16) |
|---|---|---|---|---|---|
| Total number of data points for each LED (123EA) | No. of training data points | 10 | 20 | 30 | 40 |
| | No. of data points for anomaly detection | 113 | 103 | 93 | 83 |

**Table 4 Sample size factor inference for training data sets with each peak.**

| Training data set (i.e., initial data points) with 16 LEDs | | Die peak | Phosphor peak | Die peak | Phosphor peak |
|---|---|---|---|---|---|
| | | 480 data points (30 × 16) | 480 data points (30 × 16) | 640 data points (40 × 16) | 640 data points (40 × 16) |
| Total number of data points for each LED (123EA) | No. of training data points | 30 | 30 | 40 | 40 |
| | No. of data points for anomaly detection | 93 | 93 | 83 | 83 |

The Scree test was used to determine the number of principal components for dimensionality reduction. The Scree test plots the principal components in the x-axis and their corresponding Eigenvalues (i.e., variances of principal components) in the y-axis. All of the points along the level part of the line, including the transition point, are dropped, and three points are counted along the precipitously dropping part of the line. The twelve features for the die peak and the phosphor peak were reduced to three principal components using the Scree test results, as shown in Figure 17 and Figure 18, respectively.

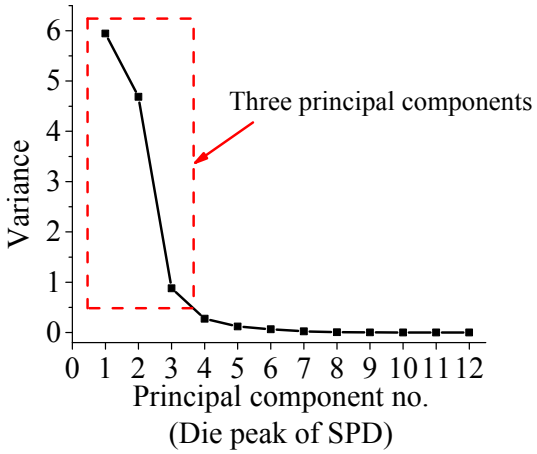


**Figure 17 Scree test results for the die peak using 480 data points (i.e., 30 data points from each LED).**

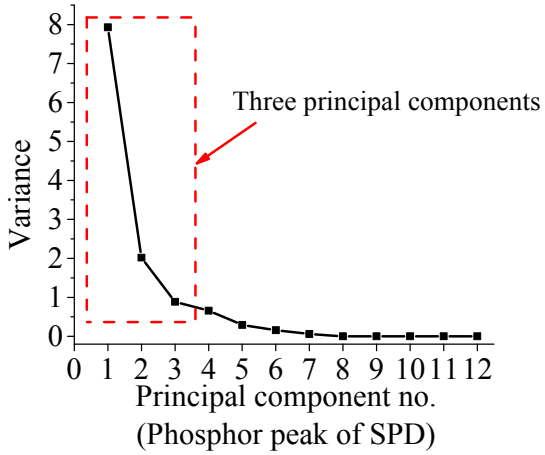


**Figure 18 Scree test results for the phosphor peak using 480 data points (i.e., 30 data points from each LED).**

### *3.3 KNN-Kernel Density-Based Clustering*

Analysis and categorization of multivariate data can be carried out either by clustering (which divides data into groups based on similarities in proximity measures) or classification (which divides data into groups based on prior labeling of data as healthy or unhealthy). Clustering is the process of partitioning a set of data (or objects) into sets of meaningful sub-classes called clusters. A cluster is a collection of data (or objects) that are similar (based on proximity measures) to one another, and thus can be treated collectively as a group [63][64]. It is difficult to define clusters and to determine the number of clusters in data when clusters have different sizes, densities, and shapes [65][69]. Also, it is challenging to find clusters in data when the data contain a large amount of noise and outliers, particularly with higher dimensional data.

Density-based clustering algorithms define clusters based on the density of data points in a region. In other words, density-based algorithms define a cluster as a region in the data space that exceeds a given density threshold. One advantage of

density-based clustering is that it can identify clusters of arbitrary shapes. Density-based clustering techniques utilize a local cluster criterion, such that clusters are determined with regions in the data space where the objects are dense, and clusters are distinguished from one another by low-density regions [73]. A cluster with a small number of data points (i.e., a low density region) can often not be found with density-based clustering [72]. In some cases, clustering techniques identify the low density regions as noise.

One of the solutions for this high dimensionality problem is to use the k-nearest neighbor (KNN) density estimation technique. KNN-density estimation was developed by Lofsgaarden and Quesenberry (1965) and then advanced by Terrell and Scott (1992) [29]. Instead of defining the threshold to the local density function, low-density regions, and valleys, KNN separates clusters by calculating the number of shared neighbors. If the number of shared neighbors of two adjacent objects is below a threshold (i.e., a number of objects), then there is a gap, or valley, in between the two objects [73]. For anomaly detection in this paper, clusters were partitioned with a KNN-kernel density-based clustering technique. The KNN-kernel density-based clustering method is based on a combination of nonparametric KNN and kernel density estimation methods [73]. The KNN-kernel-density estimation technique makes it possible to model clusters of different densities in high dimensional data sets.

A nonparametric kernel density method can be used to estimate an unknown probability density function of a data set. If we have an N × d dimensional data set, the multivariate kernel density estimated at the object x with kernel K is defined as [74]:

$$\hat{f}(x) = \frac{1}{NV}\sum_{i=1}^{N} K((x - x_i)./H) \tag{13}$$

where $N$ is total number of data set, $V$ is volume (hyper-rectangles), $K$ is multivariate kernel function defined by the product of univariate kernels, and $H$ is a scale vector $H=[h_1 \ldots h_d]$ in $d$-dimensional space. In many cases, a triangular or Gaussian kernel function is used. It is known that KNN-density was developed by Lofsgaarden and Quesenberry (1965) and then advanced by Terrell and Scott (1992) [56]. The KNN-kernel technique enables density estimate smooth by using kernel function; and KNN approach enables an adaptive kernel width, a border kernel in low-density regions and a narrower kernel in high-density regions.

To understand the algorithm flow of the KNN-kernel density-based clustering, we need to understand mathematical derivation of classification rule (i.e., way to assign objects (i.e., data) to clusters) based on KNN-kernel density estimates [13][56]. The common way of classification rule is based on Bayes' decision rule:

$$p(x|\omega_i)p(\omega_i) > p(x|\omega_j)p(\omega_j), \quad \forall j \neq i \tag{14}$$

where p(x | ωi ) is the class-conditional density function at x of each class ωi and p(ωi ) is the prior probability function. The class-conditional density function for the nonparametric KNN-kernel density-based clustering technique is such that

$$\hat{p}(x|\omega_i) = \frac{1}{n_i V_x} \sum_{x_j \in \omega_i} K((x - x_j)./H_x) \tag{15}$$

where $n_i$ is the size of cluster $\omega_i$, and $\sum_i n_i = N$. So equation (14) can be modified by using equation (15) as:

$$\frac{1}{n_i V_x}\left(\sum_{x_l \in \omega_i} K((x - x_l)./H_x)\right)p(\omega_i) > \frac{1}{n_j V_x}\left(\sum_{x_l \in \omega_j} K((x - x_l)./H_x)\right)p(\omega_j), \quad \forall j \neq i \tag{16}$$

If the prior probability functions of $p(\omega_i)$ and $p(\omega_j)$ are simplified as $n_i/N$ and $n_j/N$, respectively, we obtain Bayes' decision rule for KNN-kernel density-based clustering:

$$\sum_{x_l \in \omega_i} K((x - x_l)./H_x) > \sum_{x_l \in \omega_j} K((x - x_l)./H_x), \qquad \forall j \neq i \tag{17}$$

The algorithm of KNN-kernel density-based clustering follows the steps shown in Figure 19. The first step is to input data with N single clusters. A KNN table (N×k) is then formed, which lists the k[th] nearest neighbor distances for each of the N datasets. Cluster memberships are assigned using the class condition shown in equation (5), and the cluster memberships are recalculated if the cluster memberships change in order to maximize the total class conditional density of the point xi being assigned to cluster c as:

$$D = \sum_{i=1}^{N} \hat{p}\,(x_i|c) \tag{18}$$

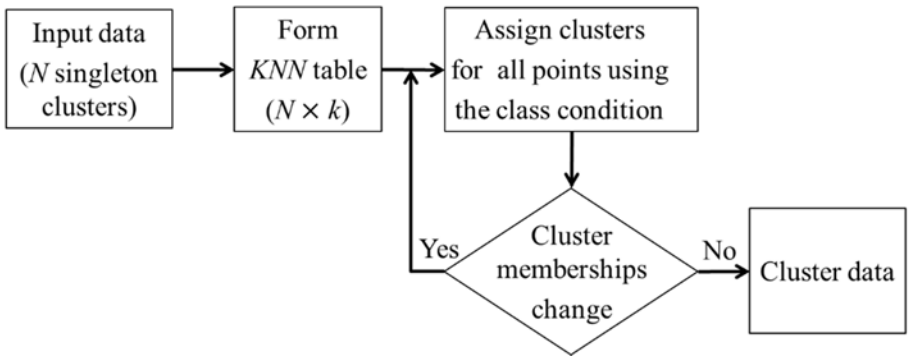


**Figure 19 KNN-kernel density-based clustering.**

The KNN-kernel density-based algorithm adjusts and selects all parameters and conditions except for the user-defined parameter, k, which is the number of neighborhood points. The number of clusters decreases with a larger k. In this study, the optimal number for k was selected by trying multiple values of k and picking the one that captured the features of the dataset with 3D graphical exploratory data analysis. The optimal numbers for k for 160, 320, 480, and 640 training data points with the entire SPD were 12, 19, 22, and 28, respectively. The number of partitioned clusters from the four training data sets was 9 for a data set with 160 training data points, 10 for

a dataset with 320 training data points, 8 for a dataset with 480 training data points, and 14 for a dataset with 640 training data points. The results show that having more training data results in better cluster formation.

To identify the degradation components in the LED package, the optimal numbers for k were 60 (for 480 training data points) and 68 (for 640 training data points) using the triangular kernel function for both the die peak and the phosphor peak. In addition to the 3D graphical exploratory data analysis, an approach was used with a plot similar to the Scree test to determine the correct number of clusters in the data set. The "elbow" in the plot (along the sharply declining part of the line) was considered based on "within-cluster sum of squares" to choose the number of clusters.

The within-cluster sum of squares (WCSS) was defined for given a set of observations ($x_1, x_2, \ldots, x_n$), where each observation is a d-dimensional real vector. The KNN-kernel density-based clustering aims to partition the n observations into k sets ($k \leq n$) of clusters $C = \{C_1, C_2, \cdots, C_k\}$ with the centroid $v_j$ in cluster $C_j$ [98][99].

$$WCSS = \sum_{i=1}^{k} \sum_{x_j \in C_j} \|\boldsymbol{x}_j - \boldsymbol{v}_j\|^2 \tag{19}$$

Two training data sets (one for die peak and the other for phosphor peak) were partitioned with 7 clusters by the algorithm for a data set with 480 training data points, as shown in Figure 20 and Figure 21. Elbows were observed in the 3rd and 7th clusters shown in Figure 20 and in the 2nd and 7th clusters shown in Figure 21. Due to multiple bins (i.e., classification) of LEDs based on optical properties (such as light output and color) in the specification sheet, the degradation paths and patterns of LEDs were grouped in 7 clusters rather than in 2 or 3 clusters.

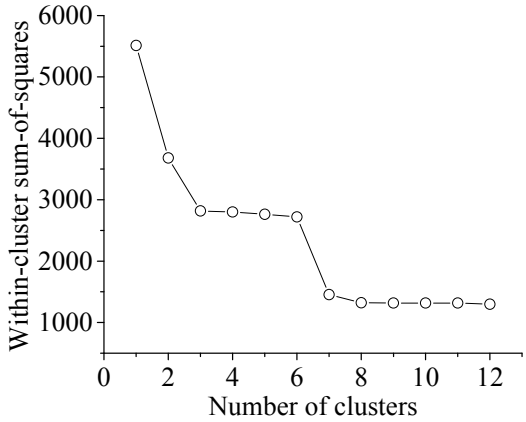


**Figure 20 WCSS for die peak training data with 480 data points.**

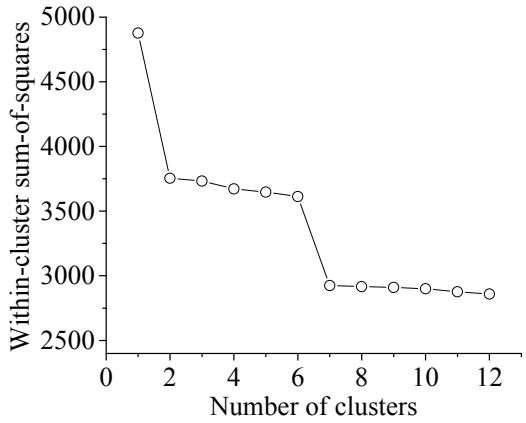


**Figure 21 WCSS for phosphor peak training data with 480 data points.**

Trials have been made for anomaly detection with three clusters for die peak training data and two clusters for phosphor peak training data with 480 data points. The detection results missed the anomalies. Seven clusters were utilized for both die peak and phosphor peak training data, as shown in Figure 22 and Figure 23. With the same algorithm, two training data sets with 640 training data points were partitioned with 8 clusters.

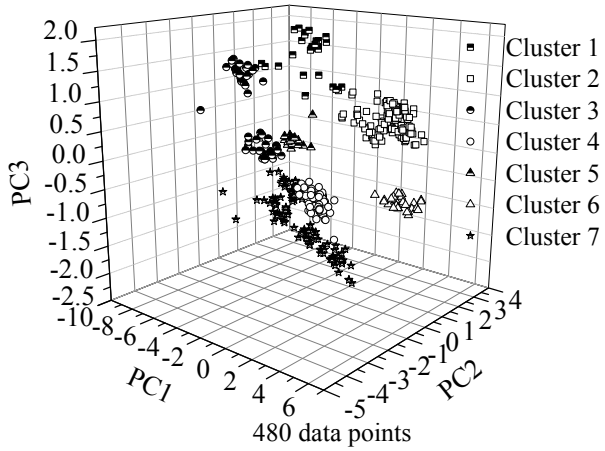


**Figure 22 KNN-kernel density-based clustering for die peak training data with 480 data points.**

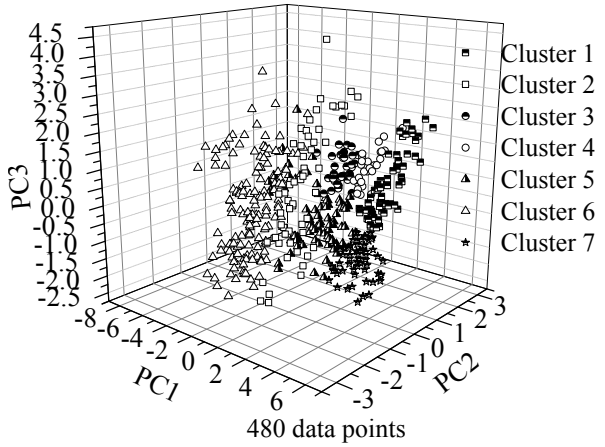


**Figure 23 KNN-kernel density-based clustering for phosphor peak training data with 480 data points.**

*3.4 Anomaly Detection Results with Similarity-Based-Metric Test*

After partitioning the training data into clusters using the KNN-kernel density-based clustering technique, the similarity-based-metric test (depicted in Figure 24) was conducted to detect anomalies in color change. When the training data were partitioned with m clusters, each centroid ($V_j$) from each cluster was evaluated. Then, the distance ($D$) between one data point and each cluster was evaluated with the Euclidian distance from the data point to the centroid. The distance from each cluster was evaluated and compared with a pre-determined threshold. The detection threshold

($T_j$) for anomaly detection was the threshold of the cluster with the shortest distance ($D_j$) from the threshold (i.e., maximum $T_j$ - $D_j$ distance). This procedure was repeated for the next test data point if the distance ($D_j$) was smaller than the detection threshold ($T_j$). If the distance ($D_j$) was greater than the detection threshold ($T_j$), then the algorithm detected an anomaly.

The mean radius ($R(C_j)$) is the average distance from member points in the cluster to the centroid of each cluster. In other words, the mean radius ($R(C_j)$) is a measure of the tightness of the cluster around the centroid. Given m-dimensional data vectors $\boldsymbol{v_i}$ in a cluster $C_j=\{\boldsymbol{v_i} \mid j=1,2,\ldots,m\}$, the centroid $\boldsymbol{v_j}$ and mean radius ($R(C_j)$) are evaluated as [100][101]:

$$\boldsymbol{v_j} = \frac{\sum_{i=1}^{m} \boldsymbol{v_i}}{m} \tag{20}$$

$$R(C_j) = \sqrt{\frac{\sum_{i=1}^{m} (\boldsymbol{v_i} - \boldsymbol{v_j})^2}{m}} \tag{21}$$

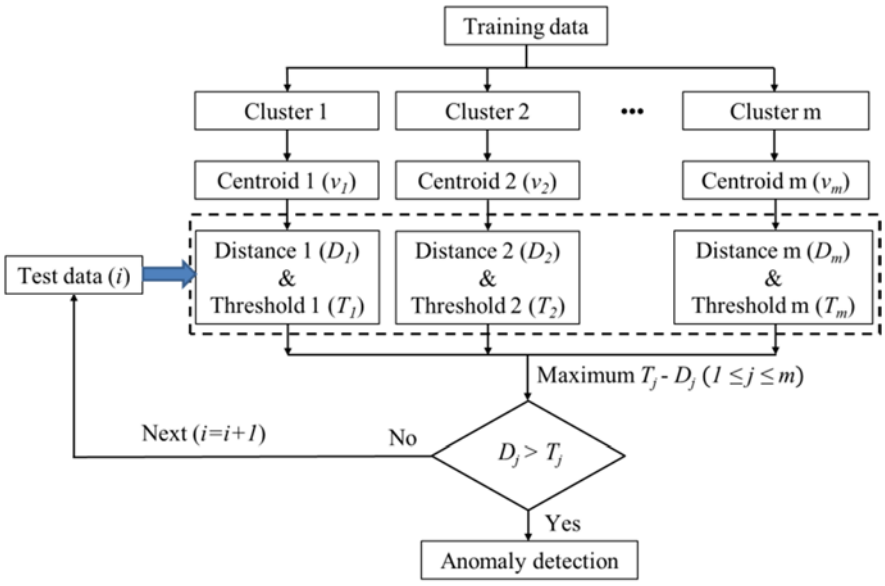


**Figure 24 Similarity-based-metric test for anomaly detection.**

If the data form a spherical shape, the detection threshold ($T_j$) is ideally the mean radius ($R(C_j)$) of the closest cluster. The data shown in Figure 22 and Figure 23 are not spherical, but elliptical. The elliptical shape has regions of clusters wider than the mean radius ($R(C_j)$) and regions of clusters narrower than the mean radius ($R(C_j)$). So, adjustment of the detection threshold determines the accuracy of the detection. If the cluster shapes are not spherical, then the threshold is in a range between the minimum distance from the centroid (i.e., the distance between the closest member point and the centroid) and the maximum distance from the centroid (i.e., the distance between the farthest member point and the centroid) in the cluster. The threshold changes the sensitivity of the anomaly detection. In other words, the fault detection rate increases if the detection threshold ($T_j$) is close to the minimum distance from the centroid in the cluster, whereas the missed alarm rate increases if the detection threshold ($T_j$) is close to the maximum distance from the centroid in the cluster. To improve the accuracy of anomaly detection, the distributions of points in a cluster are considered to define a new threshold for each cluster. In this study, a detection threshold metric was developed as:

$$Detection\ threshold\ (T) = mean\ radius\ (r) + \frac{standard\ deviation\ (\sigma)}{dimensional\ factor\ (d)} \qquad (22)$$

where the standard deviation (σ) is the standard deviation of all distances of member points from the centroid in the cluster, and the dimensional factor (d) is the number of dimensions of the data space. In this study, the dimensional factor (d) was 3, because data analysis was conducted in three dimensional principal component space, as shown in Figure 10 and Figure 11. This metric minimizes the error from the cluster shape and the data distribution of the cluster.

Using the entire SPD, including both the die peak and the phosphor peak, 160 training data points were used to detect anomalies, with thresholds of both the mean radius in equation (21) and the developed detection threshold in equation (22). The centroids of the clusters were evaluated using equation (20) for the ten clusters. Data were collected for 123 days in total, with 113 days for anomaly detection after the initial data points and 10 days to create the clusters. When a new data point was collected during the accelerated test, the closest cluster was found by evaluating the distance ($D_j$) of the data point from the each centroid ($C_j$). Anomalies were detected when $D_j$ was greater than $T_j$, as described in Figure 24.

Data points from LED 15 are used here to illustrate this detection scheme. Detailed distance plots were constructed for the entire data collection period from cluster 1 to cluster 8 for LED 15 utilizing the developed detection thresholds. Cluster 1 and cluster 2 gave false alarms, with an alarm at 11 days immediately after starting the detection algorithm, as shown in Figure 25 and Figure 26, respectively.

An anomaly was detected at day 72 from cluster 8, as seen in Figure 27. The anomaly was detected in cluster 8 because the maximum $T_j$ - $D_j$ distance came from cluster 8. The actual time to failure for LED 15 was day 88. The distance plots of cluster 3, cluster 4, and cluster 5 are similar to cluster 1, as shown in Figure 25, while the distance plots of cluster 6, cluster 7, and cluster 9 are similar to cluster 2, as shown in Figure 26.

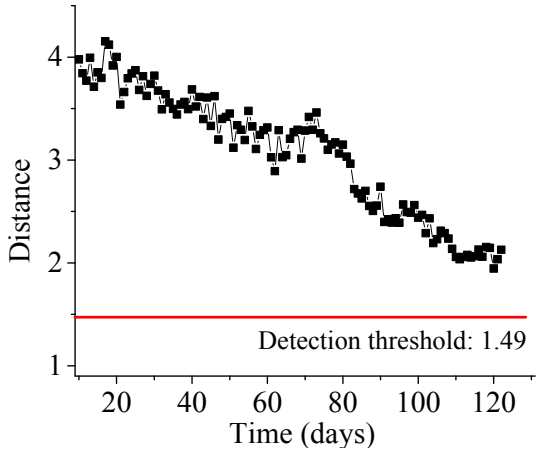


**Figure 25 Distance measure of cluster 1 from LED15.**

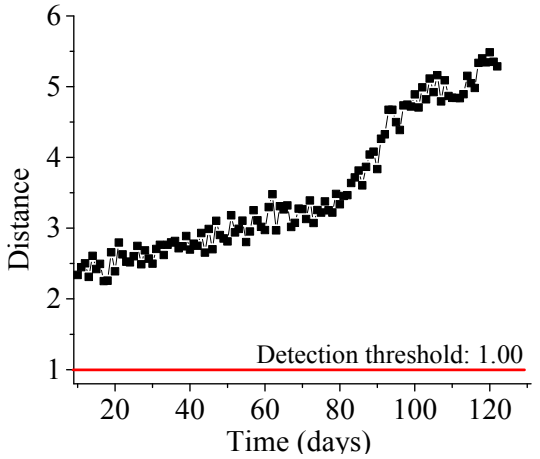


**Figure 26 Distance measure of cluster 2 from LED15.**

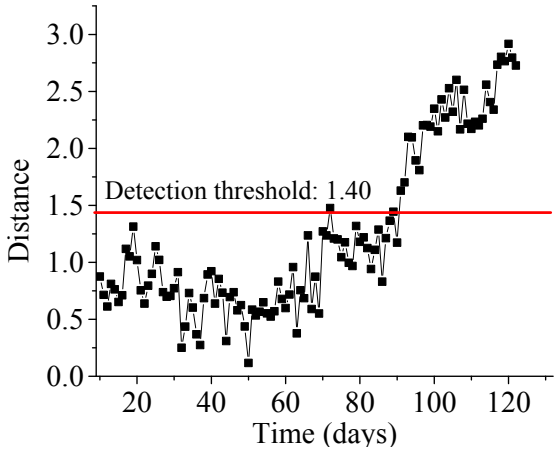


**Figure 27 Distance measure of cluster 8 from LED15.**

Application of the developed detection threshold improved the anomaly detection rate from 25% (4 out of the 16 LEDs) with the mean radius metric to 50% (8 out of the 16 LEDs) for the case with 160 training data points, as shown in Table 5. A false alarm was defined to occur when anomalies were detected immediately after beginning the algorithm (within 5% of the ratio of the detection time divided by the actual time to failure). Detection results with 320, 480, and 640 training data points were also improved using the detection threshold in equation (9). Table 5 summarizes the anomaly detection results for LEDs based on the similarity-based-metric test. As the number of training data points increases, the anomaly detection rate increases. Anomalies were successfully detected in 81.25% of LEDs using 14 clusters with 640 training data points, as shown in Figure 28. The algorithm missed an alarm for LED 14, where the anomaly was detected at day 88 but the actual time to failure was day 84 (Figure 28).

The detection rate increases with the number of training data points. The initial data points have variation caused by the short-term aging effect of the color degradation parameters. When the number of training data points increases, the short-term aging effect is decreased and the accuracy increases. The detection results showed that the similarity-based-metric test can provide advance warning of failures.

**Table 5 Summary of anomaly detection results using similarity-based-metric test.**

| | 160 training data points (9 clusters) | | Results with 320 training data points (10 clusters) | Results with 480 training data points (8 clusters) | Results with 640 training data points (14 clusters) |
|---|---|---|---|---|---|
| | Mean radius (eq.(8)) | New detection threshold (eq.(9)) | | | |
| Missed alarm | 0% (0/16) | 0% (0/16) | 6.25% (1/16) | 0% (0/16) | 6.25% (1/16) |
| False alarm | 75% (12/16) | 50% (8/16) | 43.75% (7/16) | 31.25% (5/16) | 12.50% (2/16) |
| Anomaly detection | 25% (4/16) | 50% (8/16) | 50% (8/16) | 68.75% (11/16) | 81.25% (13/16) |

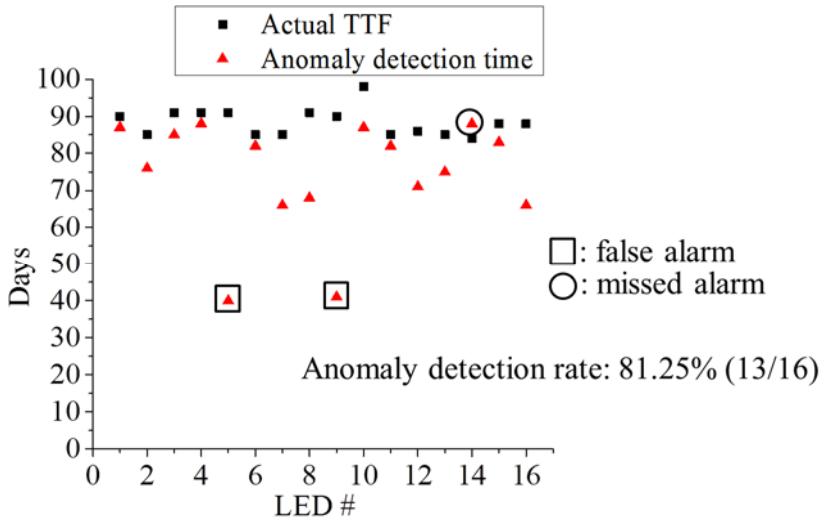


**Figure 28 Anomaly detection results with 640 training data points using the entire SPD.**

An advanced technique that does not necessarily wait until the signature of the anomalies is close to the time to failure, as shown in Figure 28, is required for fast qualification of LEDs. Each peak component in the SPD, specifically die SPD and phosphor SPD, were independently utilized for anomaly detection to identify the die and the phosphor degradation or determine whether the die or phosphors degrade faster depending on the failure mechanisms of LEDs.

As a case study, the training data set with 480 data points (i.e., 30 data points from each of the 16 LEDs) was partitioned into 7 clusters, as shown in Figure 22 for the die peak and Figure 23 for the phosphor peak, and 93 data points from each LED were used for anomaly detection. LED 3 is used here to illustrate the detection scheme. First, the centroids of the clusters were evaluated using equation (19) for seven clusters. Then, the developed threshold ($T_j$) of each cluster from the die peak and phosphor peak were calculated.

The distances from the centroids of the clusters to the new data points of LED 3 were evaluated for the entire data collection period. The $T_j - D_j$ distances over time were greatest at cluster 4 for the die peak and cluster 2 for the phosphor peak. An anomaly was detected at day 59 from cluster 4 for the die peak, as seen in Figure 29. An anomaly was detected at day 83 from cluster 2 for the phosphor peak, as shown in Figure 30. The actual TTF for LED 3 was day 91. All of the anomaly detection results for die peak and phosphor peak are included in Appendix B. Smoothing can improve the anomaly detection results, as shown in Appendix B. In further, anomaly detection results under the condition of 200mA drive current and chamber temperature 90°C are shown in Appendix C.

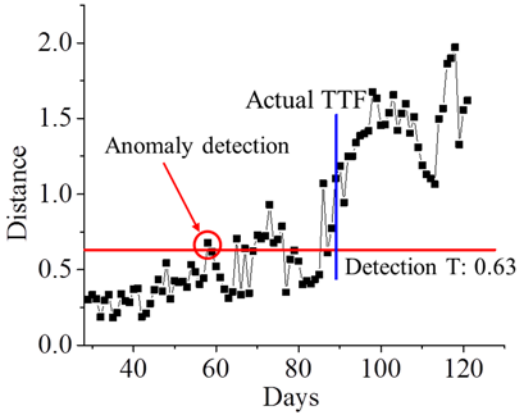


**Figure 29 Distance measure of cluster 4 from LED 3 for die peak.**

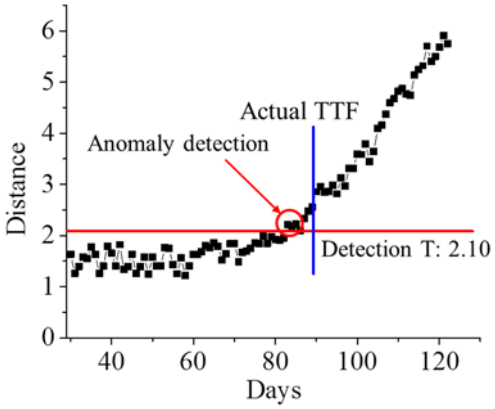


**Figure 30 Distance measure of cluster 2 from LED 3 for phosphor peak.**

Figure 31 summarizes the anomaly detection results for all LEDs based on the similarity-based-metric test using 480 data points. The results showed that die degradation is an earlier sign of color failure of LEDs than phosphor degradation. Therefore, die degradation initiates color failure of LEDs. As a result, future package designs must consider how to strengthen LED die performance. The die and phosphor degradation can be directly explained by SPD changes over time during the aging test. The SPDs for LED 3 at day 0, the anomaly detection times for die and phosphor peaks and the actual TTF are shown in Figure 32. The phosphor peak degraded together with the die peak. This type of peak change is due to die degradation. All LEDs degraded in a manner similar to the result in Figure 32. In Figure 31, most of the anomalies from the die peaks were detected in less than 1,000 hours. This shows that this test can reduce the time needed for predicting the remaining useful life of LEDs during qualification tests. The starting point for early anomaly detection is the earliest time at which users can begin to predict the remaining useful life of LEDs.

For all LEDs, the die peak increased from day 0 until the detection times (i.e., day 59 and day 83), and then decreased to the initial day 0 value at the actual TTF. On the other hand, the phosphor peaks decreased from day 0 until the actual TTF time. The amount of die degradation was relatively less (i.e., 0.066) than the amount of change from phosphor degradation (i.e., 0.143), but the die degradation detected the anomalies earlier than the phosphor degradation. As seen in Figure 33, using the same algorithm, which used 640 data points, the anomalies were first detected from the die degradation and later from the phosphor degradation. The anomalies were detected at about 1,200 hours in the die peak data. The detection time for both the die and phosphor peaks

increased due to the larger amount of training data (640 data points vs. 480 data points), and therefore provided more information about the degradation trends.

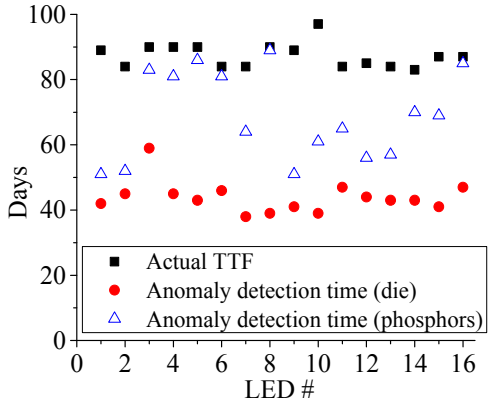


**Figure 31 Anomaly detection using 480 data points (i.e., 30 data points from each LED).**

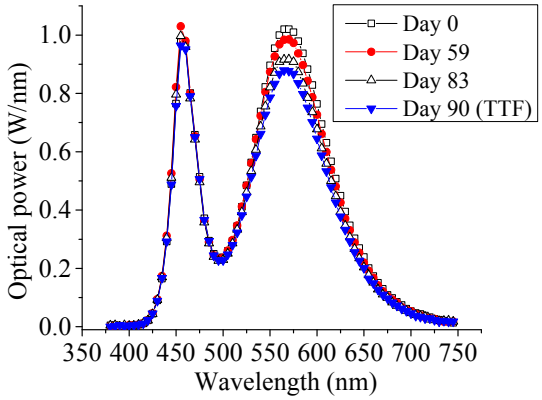


**Figure 32 SPD changes at different detection times for LED 3.**

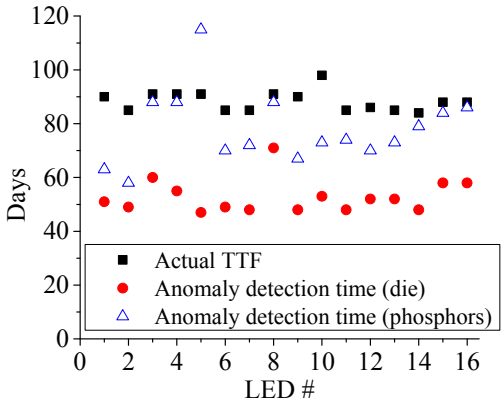


**Figure 33 Anomaly detection using 640 data points (i.e., 40 data points from each LED).**

### *3.5 Discussion*

The similarity-based-metric test for LED anomaly detection presented in this chapter extracted features from the spectral power distribution, reduced the dimensionality of the features by using principal component analysis, and grouped the data set into clusters using the KNN-kernel density-based clustering technique. Then, the distances from each centroid of cluster to each test point were measured. The algorithm detected anomalies when the distance was larger than the pre-determined threshold.

The similarity-based-metric test can significantly decrease the amount of time needed for LED qualification by using prognostic techniques. This anomaly detection method will provide users with an earlier time to begin remaining useful life prediction than LED qualification tests, such as those based on the IES LM-80-08 standard and the U.S. DOE Standard, "Energy Star® Program Requirements: Product Specification for Luminaires," which require at least 6,000 hours of test time. The similarity-based-metric test presented in this paper can potentially decrease the amount of time needed for qualification testing to about 1,000 hours.

This is the first study to use the spectral power distribution (SPD) for anomaly detection in qualification tests. The similarity-based-metric test utilizes features from the SPDs as leading indicators. SPD, which denotes the radiant power at each wavelength per wavelength interval in the visible spectrum, can be used to obtain degradation information for LEDs. The SPD of the tested LEDs includes two parts: a peak from the LED die and a peak from the phosphors. LED phosphors are embedded inside a resin that surrounds the LED die. The blue light emitted from the die excites

the phosphors, which then emit yellow light; the blue light and yellow light combine to emit white light. Previous research driven by the industrial standards utilized u′v′ color shift in the CIE 1976 chromaticity diagram to explain color change of LEDs. Color shift can be used for identifying color change; however, it cannot explain the internal phenomena through which the each optical contributor mixes its independent light into white light.

## *3.6 Conclusions*

The similarity-based-metric test was developed to diagnose degradation in the die and phosphors inside LEDs by using the KNN-kernel density-based technique clustering the data with independent optical components in the spectral power distributions and measuring the distance from the centroid. The underlying assumption is that die degradation reduces the phosphor peak as well as the LED die peak. As the amount of photons extracted from the LED die is reduced, the amount of phosphor light converted from the short wavelength (i.e., the LED die peak) is also reduced. When phosphors are only degraded by phosphor thermal quenching, the phosphor peak will be reduced and the LED die peak will not change shape, since the LED die emits light as a normal condition independent of phosphor degradation.

This anomaly detection method does not require historical data. It integrates the advantages of anomaly detection under wearout performance degradation and is suitable for the qualification of new products. LED manufacturers can use the similarity-based-metric test to increase the quality of their LED products by detecting anomalies early on and fixing potential problems. Combined with an RUL prediction method, this process will help to make product development, design improvement, and

qualification better and could reduce qualification testing time. This could enhance the competitiveness of LED manufacturers that employ this qualification method by enabling them to quickly identify bad batches or designs during tests. As LED lighting is a growing field, the similarity-based-metric test will enable new technologies to be assessed and improved more rapidly. This will assist in the development of this important field.

# CHAPTER 4 Prognostics of LEDs Using Spectral Power Distribution (SPD) Prediction for Color Failure

The increase in the use of LEDs leads to the need for more information regarding failure and usable life estimates for manufacturers to produce higher quality LEDs for consumers, particularly those consumer requiring specific chromaticity in their applications [1][4]. Many modern methods for testing LEDs use accelerated methods to establish an expected lifespan however they fail to identify failure modes as they as generally based on a failure criteria such as a percentage loss of luminous power as in [1][4].

One type of white LED is the Phosphor-based LED. The LED produces light via the die which emits a blue light around 450-480nm. The phosphor coating of the LED absorbs some of this light and emits it with maximum intensity at approximately 600nm, a yellow color. Together these emissions produce a white light [18][102].

## *4.1 SPD and Degradation of LEDs*

The spectral power distribution plots the power of electromagnetic radiation as a function of wavelength [103] as in Figure 12. By observing the full spectral

distribution the behavior of the die, phosphor, and silicon encapsulation can be modeled and predicted over significant periods of time. As the LED die degrades with time, the both peaks of the curve degrade, see Figure 34. As expected decreased light emission from the die decreases the peak associated with the die.

Similarly, as less light is emitted from the die, less light may be absorbed and emitted by the phosphor, thus decreasing the associated phosphor peak proportionally. Associated with phosphor degradation in an LED is a decrease in the emissive power of the phosphor peak, see Figure 35. As the die has not degraded, any decrease in its optical power will be negligible and the die peak will appear as it did initially. Another site for degradation is in the silicon encapsulation as with extended time and use the encapsulation may begin to yellow shown in Figure 36. Such degradation causes decrease spectral power of the die [102][104]; however it has little effect on the yellow phosphor peak.

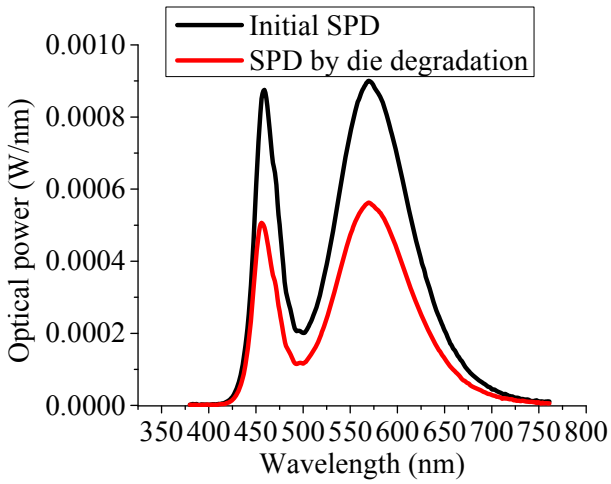


**Figure 34 LED die degradation.**

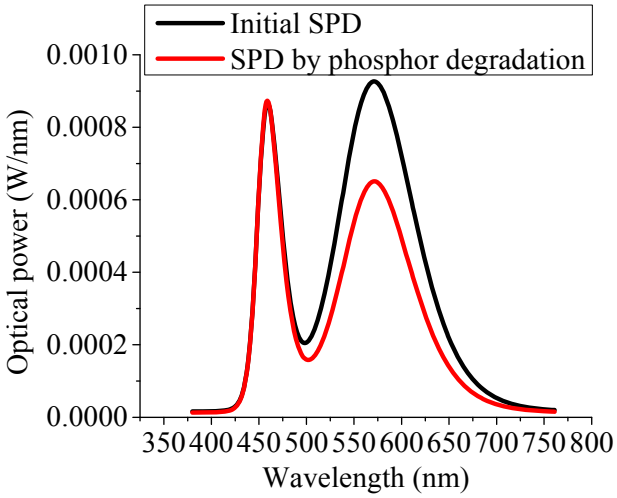


**Figure 35 Phosphor degradation.**

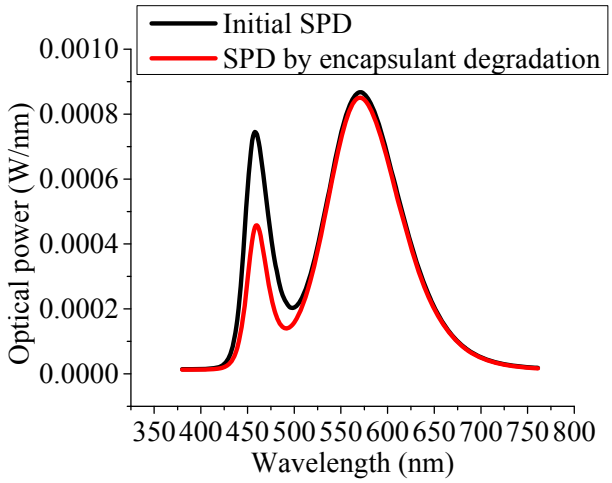


**Figure 36 Encapsulant degradation.**

In addition to the SPD of the LEDs the color position was observed. Trichromatic theory suggests that, due to the physiology of the human eye, all colors in the visible spectrum can be defined by a combination of the colors any three primary colors [106]. Primary colors are any set of three colors in which any one of the colors cannot be produced by the other two. In the field of optics a common selection of primary colors is the red, green, blue color scale. Every color has three chromaticity coordinates which define the amount of each primary color needed to produce the expected color.

Graphical depictions of all colors as a relationship of a combination of chromaticity coordinates manifest themselves in color spaces, see Figure 2. In a color space the spectral colors exist on a line that bounds the color space through the curved portion on the top and sides. The bottom bound does not exist in the spectrum and is created with linear combinations of red and blue [106]. Traditionally color spaces are normalized and governed by a relationship such as $r + g + b = 1$. In such cases only two coordinates are needed to define a color.

Given that a color can be defined by a pair of coordinates, color spaces are traditionally shown in two dimensions, see Figure 2. A complication in creating all colors in the visible spectrum using a combination of red, green, and blue arises in that creating some wavelengths a negative amount of red must be added [106][107]. In fact, there is no set of real primary colors which can match all of colors in the visible spectrum without requiring a negative amount of one of the primary colors. Such a phenomena bears little physical meaning, therefore in 1931 a new model was proposed which linearly transformed the coordinates so that each of the coordinates x, y, and z have positive values.

The complication for the CIE 1931 Color Space is that equal Euclidean distances within the color space do not necessarily imply equal differences in color perception [108]. The human eye is able to distinguish between blues and violets to a higher degree than greens and yellows, as observed by MacAdam [109]. A goal in colorimetry has long been to create a uniform color space (UCS) in which equal Euclidean distances in chromaticity correspond to equal distances in perception of colors. While no such color space has been created to date, a nonlinear transform was

proposed and accepted by the International Commission on Illumination (CIE) in 1976 which creates a more linear relationship with between distance and color perception. Chromaticity coordinates, u′ and v′ define the position of the light in the CIE 1976 Color Space. The chromaticity coordinates of the LEDs were recorded as they aged, allowing for explicit observation of the change of the LED color.

### *4.2 SPD Modeling*

Steps of prognostics of LED color failure using SPD prediction are shown in Figure 37. SPD is modeled with asymmetric double sigmoidal functions. SPD is predicted by using the particle filter algorithm to estimate the propagating parameters of the asymmetric double sigmoidal functions. Color distance is calculated from SPD. Finally RUL is estimated by using 7-step-SDCM (standard deviation of color matching) threshold (i.e., 0.007 color shift in CIE 1976 coordinates).

Data from an aging test was used to develop the RUL prediction process. The test samples in this study were 3W InGaN white LEDs. Sixteen LED samples were mounted on an aluminum metal core printed circuit board (MCPCB). The test condition was a 200mA constant current and a chamber temperature of 90ºC recommended by its manufacturer and the IES-LM-80-08 standard. The junction temperature was expected to stay below the absolute maximum rating junction temperature of 133ºC [95][96]. The SPDs of all of 16 LEDs were measured after every 22.5 hours of exposure to this condition. The time to failure range of color failure of the 16 LEDs based on 0.007 u′v′ color shift was between 345 hours and 874 hours as shown in Figure 38.

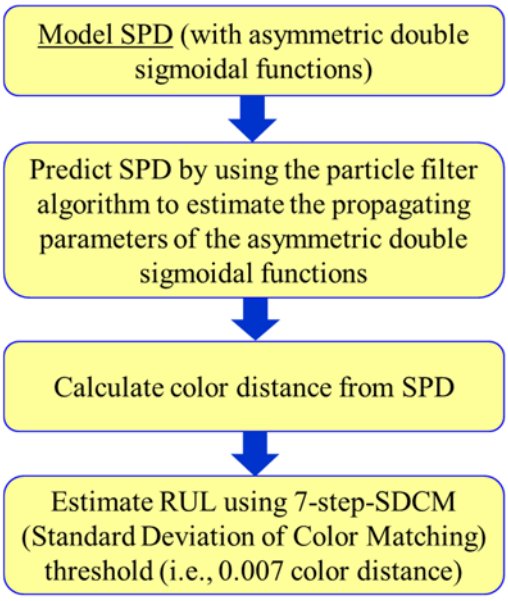


**Figure 37 Approach for prognostics of LED color failure using SPD prediction.**

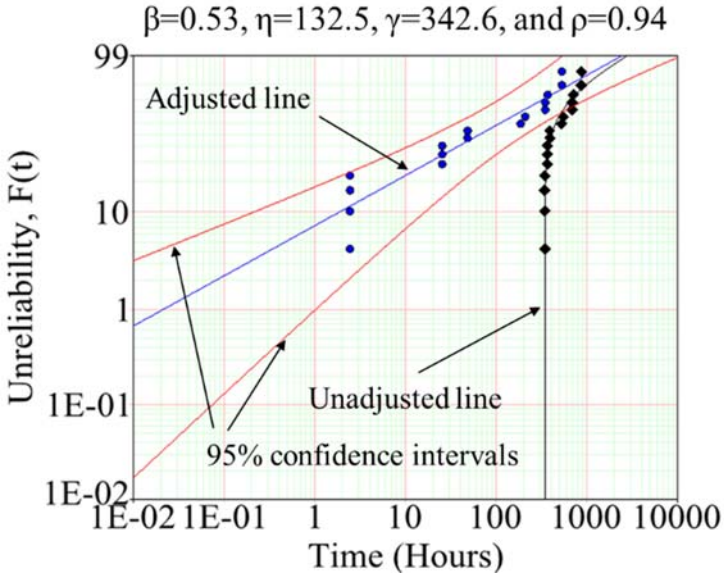


**Figure 38 Aging test results.**

SPD was mathematically modeled with deconvolution by using two asymmetric double sigmoidal functions as shown in Figure 39. For each SPD (for die SPD and phosphor SPD) in Figure 39, there are six parameters composing the asymmetric double sigmoidal function. Six parameters are offset ($y_0$), center max ($x_c$), amplitude (A), width$_1$ ($w_1$), width$_2$ ($w_2$), and width$_3$ ($w_3$).

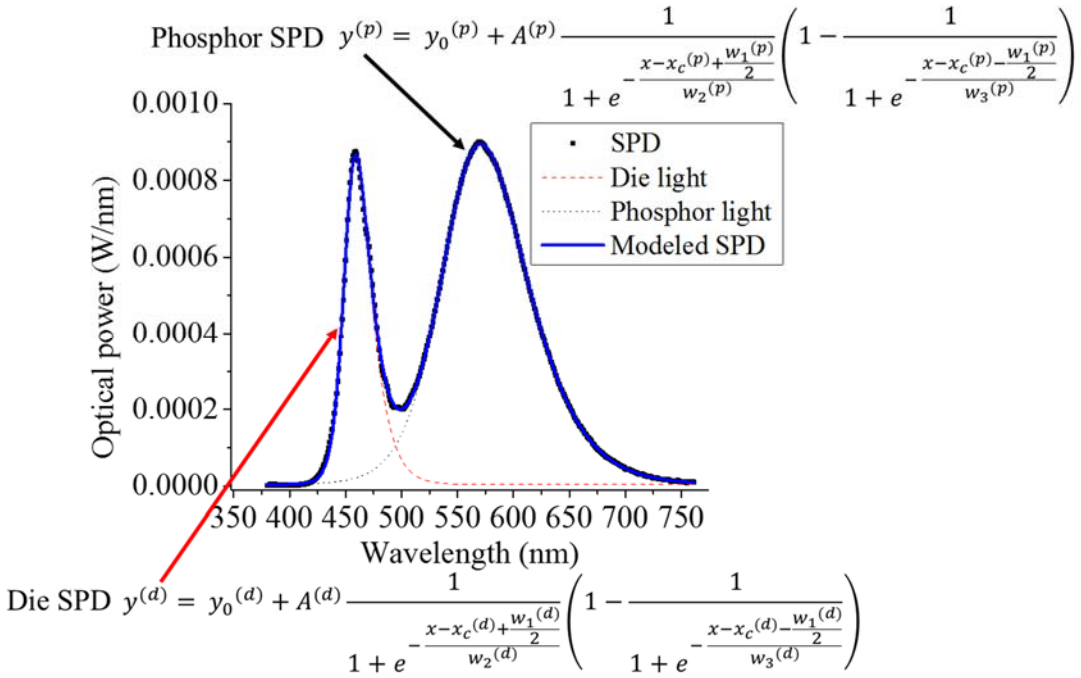


**Figure 39 SPD model with deconvolution using two asymmetric double sigmoidal functions.**

### *4.3 SPD Prediction Results*

Average smoothing was used to mitigate the effect of fluctuations in the test data to identify the proper fitting model for each parameter of both die SPD and phosphor SPD as shown in Figure 40 and Figure 41. The smoothed parameters of the asymmetric double sigmoidal function were fitted using a 2nd order Fourier series model, which is a finite linear combination of trigonometric functions of sin($nt$) and cos($nt$) with n natural numbers, and a double exponential function model, which is a linear summation of two exponential functions.

$$F(t) = a_0 + a_1\cos(nt) + b_1\sin(nt) + a_2\cos(2nt) + b_2\sin(2nt) \quad (23)$$

where f is a parameter of the asymmetric double sigmoidal function and t is time. $a_0$, $a_1$, $b_1$, $a_2$, $b_2$, and n are the parameters of the Fourier series model.

$$F(t) = a \times \exp(bt) + b \times \exp(dt) \quad (24)$$

where f is a parameter of the asymmetric double sigmoidal function and t is time. a, b, c, and d are the parameters of the double exponential model.

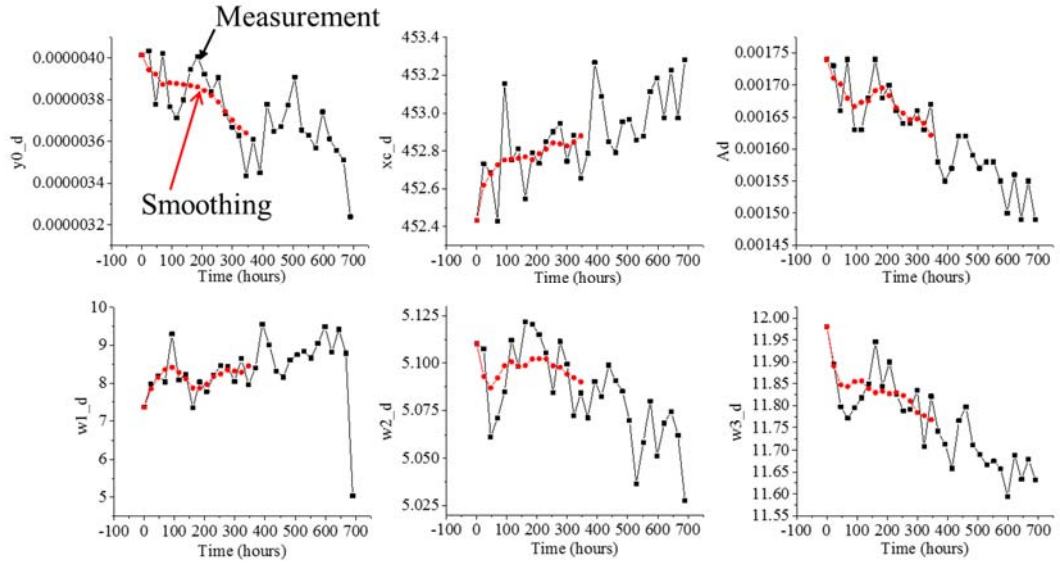


**Figure 40 Parameter trending of asymmetric double sigmoidal function for die SPD.**

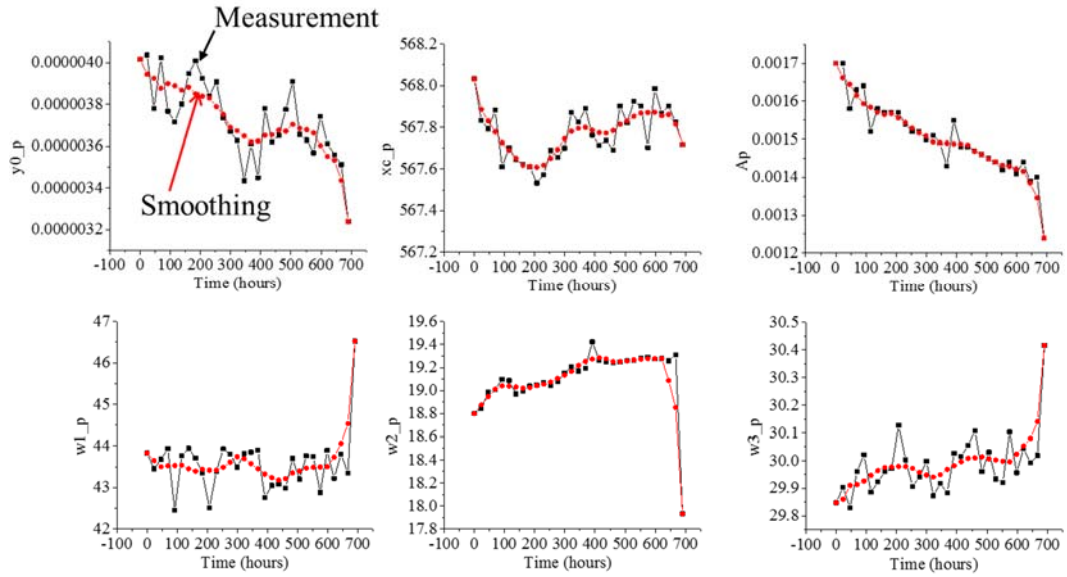


**Figure 41 Parameter trending of asymmetric double sigmoidal function for phosphor SPD.**

SPD prediction was performed by using the particle filter algorithm (as shown in Figure 42) to propagate 12 parameters in two asymmetric double sigmoidal functions. For prediction, 2nd order Fourier series, 5th order polynomial equation, an

double exponential equation were applied to predict 12 parameters. 2nd order Fourier series and 5th order polynomial model show test result for the SPD prediction. The curve-fit result after projecting the curve into further time instant could not track the parameter trending in future. In particle filter algorithm, state space model tacks data up to time to start prediction. After that, it recursively fit the state space model function based on the recent particle distribution, so it weight more on recent data. This fact makes the particle filter should be better than just simple curve fitting projection because curve-fitting gave equal weight to recent and old data, while old data contain very little degradation information.

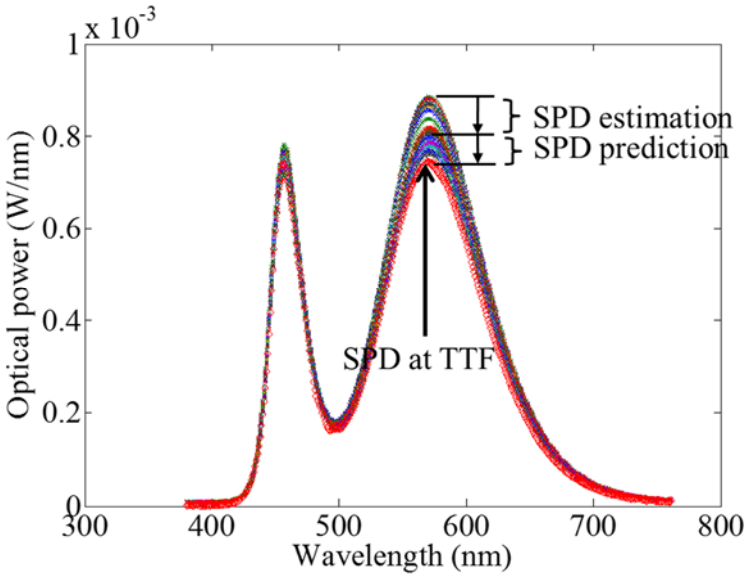


**Figure 42 Prediction of SPD.**

Figure 43 shows SPD prediction of all LEDs indicating potential LED degradation. Phosphor degradation can be identified from SPD change over time for most of LEDs as previously explained in Figure 35. SPD change over time for LED 13, LED 14, and LED 16 indicated die degradation. SPD prediction was successfully performed for all LEDs. Verification will be given based on color failure time prediction by using the SPD prediction results.

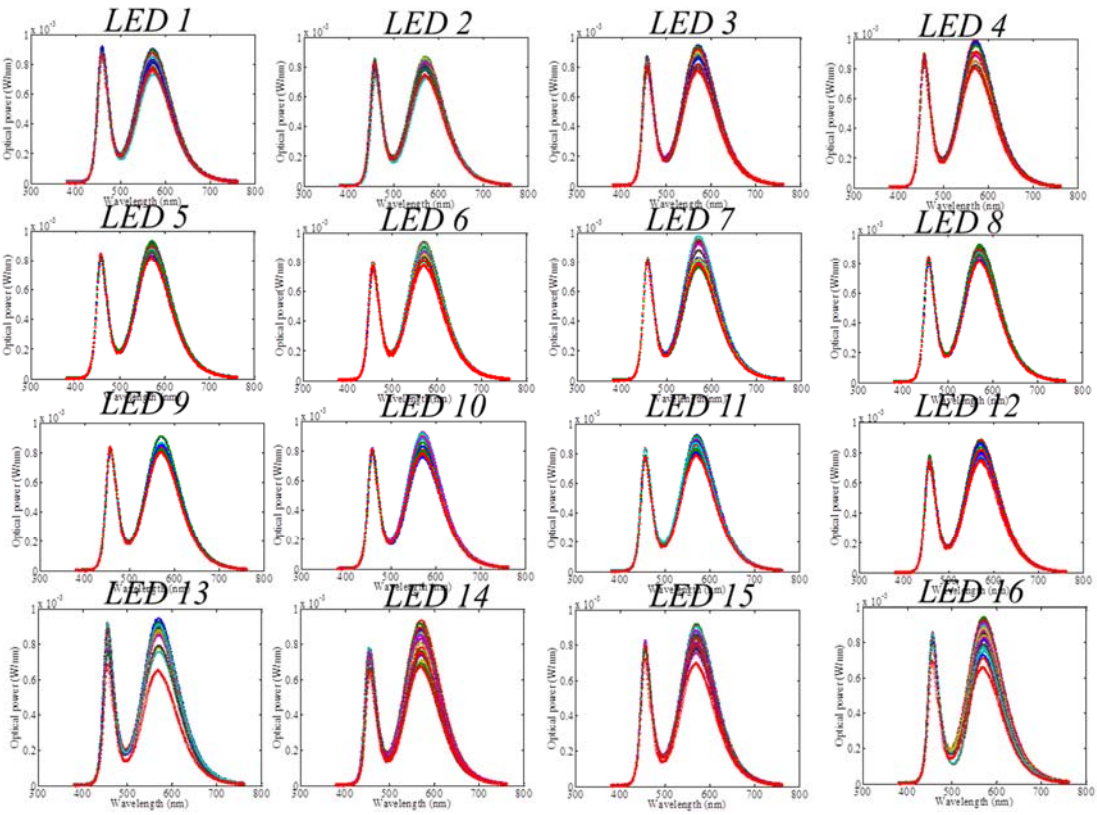


**Figure 43 SPD prediction to indicate potential LED degradation.**

### *4.4 Discussion*

To predict LED color failure by using prognostics, SPD must converted to photometric units, which define light output and color degradation. LED RUL based on color degradation is estimated by using SPD prediction. Radiometric SPD can be converted to photometric unit by using color matching functions as shown in Figure 44. For color shift prediction, SPD modeling over time is needed. And then the predicted SPD is multiplied to the color matching function. Tristimulus values (X, Y, and Z) are obtained. X, Y, and Z are converted to u′ and v′ coordinates to project color change in the color space. u′v′ distance is estimated by the results of SPD prediction. RUL is

predicted by the time when the estimated when the estimated u′v′ distance crosses the failure threshold as shown in Figure 45.

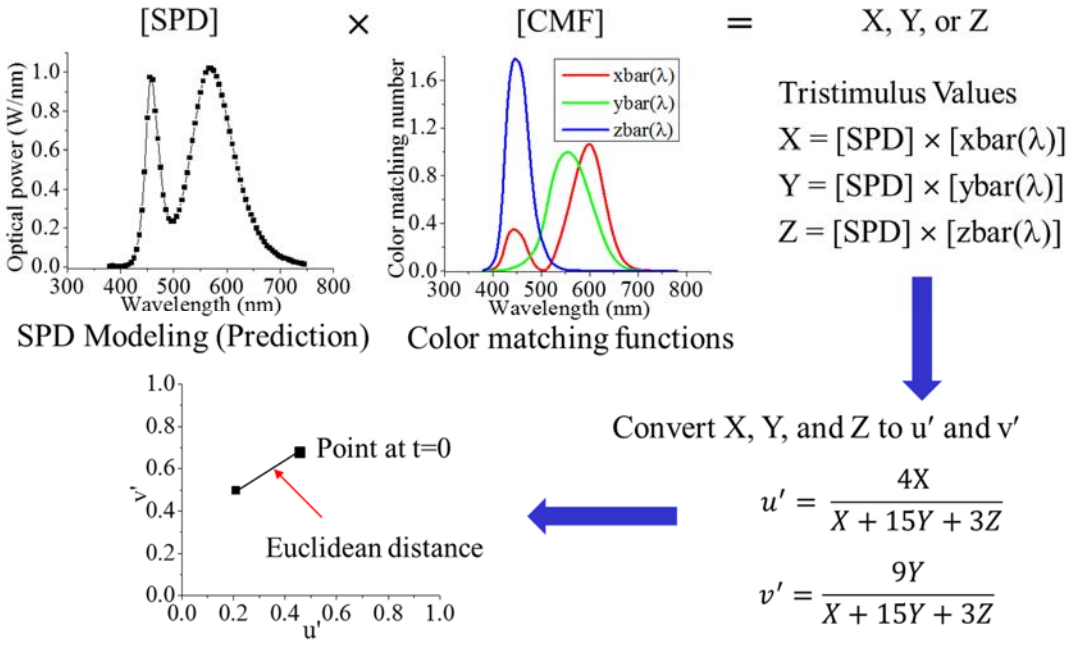


**Figure 44 Procedure for prognostics of LED color failure.**

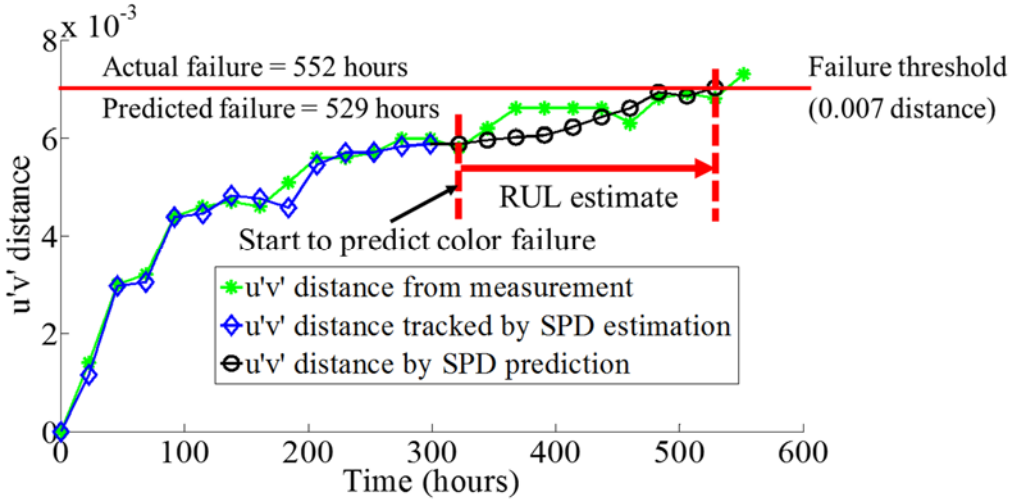


**Figure 45 Color failure prediction.**

Table 6 and Table 7 show the prediction error (%) for all LEDs based on available data length to estimate RUL of each LED. The prediction error for color failure of LEDs shows that the prediction can be made with less time when prediction

can be made. For example, at 40% lifetime data, maximum error was -17.4 % at LED 12. However, with 90% lifetime data, maximum error for the prediction was 8.7% at LED 12. More available test data can help to increase the accuracy of the prediction.

**Table 6 Prediction error (%) for LED1 to LED8.**

| Lifetime when prediction is made (% lifetime) | 40% | 50% | 60% | 70% | 80% | 90% |
|---|---|---|---|---|---|---|
| LED 1 | -4.2% | -20.8% | -16.7% | 8.3% | 4.2% | 8.3% |
| LED 2 | -11.8% | -11.8% | -11.8% | 0% | 12.5% | 0% |
| LED 3 | -6.3% | 6.3% | 6.3% | 6.3% | 12.5% | 0% |
| LED 4 | 12.5% | -12.5% | 12.5% | 6.3% | -6.3% | 6.3% |
| LED 5 | -9.7% | -9.7% | 3.2% | 3.2% | 3.2% | 0% |
| LED 6 | -12.5% | 6.3% | 0% | 0% | 6.3% | 0% |
| LED 7 | -13.3% | -6.7% | 0% | 6.7% | 0% | 0% |
| LED 8 | -13.3% | 6.7% | 0% | 6.7% | 6.7% | 0% |

$$\text{Prediction error (\%)} = \frac{(t_{True} - t_{Prediction})}{t_{True}} \times 100$$

($t_{True}$: actual failure time, $t_{Prediction}$: predicted failure time)

**Table 7 Prediction error (%) for LED9 to LED16.**

| Lifetime when prediction is made (% lifetime) | 40% | 50% | 60% | 70% | 80% | 90% |
|---|---|---|---|---|---|---|
| LED 9 | 0% | -6.7% | 6.7% | -6.7% | 0% | 0% |
| LED 10 | 6.7% | 8.7% | 6.7% | 6.7% | 0% | 0% |
| LED 11 | -11.8% | -17.6% | -5.9% | 11.8% | 0% | 0% |
| LED 12 | -17.4% | 16.3% | 26.1% | 4.3% | 21.7% | 8.7% |
| LED 13 | -5.3% | 15.8% | 0% | -2.6% | -13.2% | 0% |
| LED 14 | -10% | -13.3% | 6.7% | 10% | 3.3% | 0% |
| LED 15 | -10% | -6.7% | 10% | -3.3% | -6.7% | -3.3% |
| LED 16 | -11.5% | 2.6% | -7.9% | 13.2% | 2.6% | 2.6% |

$$\text{Prediction error (\%)} = \frac{(t_{True} - t_{Prediction})}{t_{True}} \times 100$$

($t_{True}$: actual failure time, $t_{Prediction}$: predicted failure time)

## *4.5 Conclusions*

In this study, diagnostic technique was developed through SPD prediction deconvoluted with minimum number of curves using asymmetric double sigmoidal functions which separate SPD into component levels of the LED package. Prognostics technique for color failure of LEDs was developed by predicting SPDs over time. This technique enables to improve reliability and design by identifying failure sites with regard to LED die, LED phosphor, and LED encapsulant in product qualification. Manufacturers' performance and reliability testing of LED products with time has generally been limited to discrete qualifications such as color distance and light output intensity. While these traits allow for prediction of usable lifetime, they fail to identify the failure site of the LED.

The failure site can be identified with the Spectral Power Distribution (SPD) as either the degradation of the die, phosphor, or silicon encapsulation. By modeling the SPD data with an asymmetric double sigmoidal function the shape of the SPD over time can potentially be predicted using techniques such as particle filter technique. This would allow for a prediction of the remaining useful life using Standard Deviation of Color Matching (SDCM) thresholds such as chromaticity color distance change. With better diagnostic and prognostic information, improvements can be made by LED manufacturers ensuring the performance and reliability of LEDs for consumers.

# CHAPTER 5 Prognostics of LEDs Using the Similarity-Based Statistical Measures with Relevance Vector Machine Regression

This chapter presents the prediction of the RUL of LEDs by utilizing similarity-based statistical measure with relevance vector machine regression in terms of optical and in-situ health indices representing LED failures. A method is presented for determining the health index set of LEDs by mapping multiple uncorrelated health indicators. The RUL of LEDs is predicted in order to capture degradation dynamics and resolve prediction uncertainties using a health index.

LED prognostics by similarity-based statistical measure with RVM regression is composed of two processes: a learning process and a prediction process. A schematic diagram of LED prognostics is depicted in Figure 46. Once time to failure data set is collected as the training data from multiple sensors or optical measurement equipment, a data feature is extracted using a one-dimensional health index to map multiple health indicators. Sparse Bayesian machine learning using relevance vector machine (RVM) captures the degradation dynamics from the health index set of LEDs. RVM enables health knowledge to be constructed from all training units. After the health knowledge using TTF data is developed, this information is utilized to predict the remaining useful life (RUL) of test units. Features from the test data that are relevant to the degradation dynamics are extracted, and similarity-based statistical measures for the test units are conducted for RUL prediction to resolve prediction uncertainties, such as unit-to-unit variations.

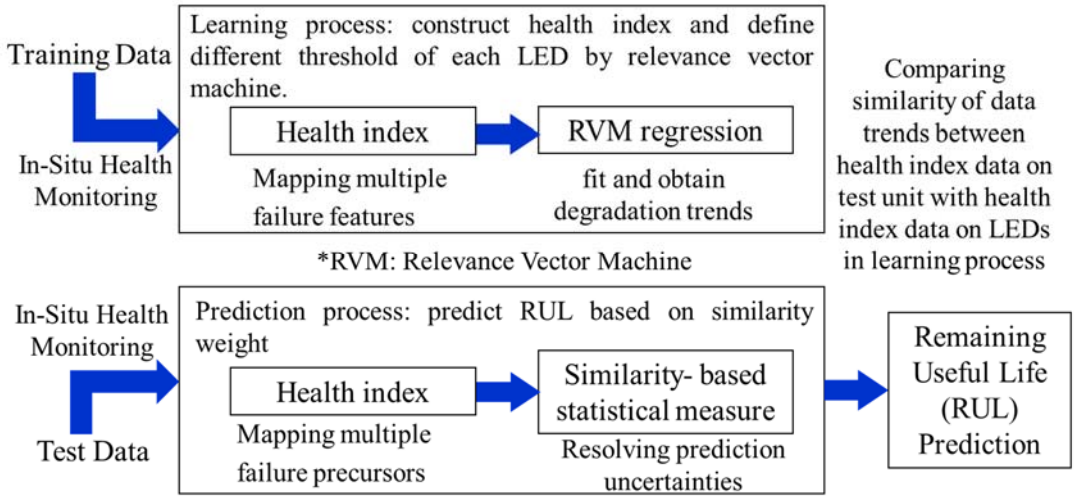


**Figure 46 Approach for LED prognostics using statistical measure with RVM regression.**

*5.1 Learning Process: RVM Regression*

In supervised Bayesian machine learning, there is a set of training input vectors, $\{x_n\}_{n=1}^{N}$, along with corresponding targets (i.e., real values), $\{t_n\}_{n=1}^{N}$. The underlying functional mapping can be determined from these input-target pairs. In Bayesian machine learning, a distribution over the parameters in **w** is inferred, rather than learning comprising the optimization of the quality measure of the input-target pairs. Linear models can be achieved by a parameterized function y(**x**; **w**) with a linearly weighted sum of M fixed basis functions $\phi_m(\boldsymbol{x})$ [110]:

$$\mathrm{P}(\boldsymbol{t}|\boldsymbol{x}) = \mathrm{y}(\mathbf{x};\ \mathbf{w}) = \sum_{m=1}^{M} \omega_m\, \phi_m(x) \qquad (25)$$

where $\mathbf{w} = (\omega_1, \omega_2, \ldots, \omega_M)$ is a vector of adjustable model parameters.

One approach to supervised learning using flexible (i.e., multi-parameter) linear kernel methods is the support vector machine (SVM) [111]. SVM makes predictions based on a function of the form:

$$y(\boldsymbol{x}; \boldsymbol{w}) = \sum_{n=1}^{N} \omega_n K(\boldsymbol{x}, \boldsymbol{x}_n) + \omega_0 \qquad (26)$$

where $K(\boldsymbol{x}, \boldsymbol{x}_n)$ is a kernel function and $\{\omega_n\}$ are the model weights.

SVM avoids over-fitting and results in a sparse model dependent only on a subset of kernel functions [112]. Despite its success, there are disadvantages to the SVM learning methodology [113][114]; for example, its predictions are not probabilistic. In regression, the SVM outputs a point estimate. Additionally, SVM requires an increasing number of kernel functions. The number of kernel functions grows steeply with the size of the training data set. Finally, SVM also requires a cross-validation procedure.

A relevance vector machine (RVM) is a probabilistic sparse kernel model utilizing the same data-dependent kernel basis as SVM [110][113]-[115]. However, RVM utilizes fewer kernel functions than SVM. RVM is capable of generalization performance comparable to an equivalent SVM. RVM performance includes adopting a fully probabilistic framework and introducing a prior (distribution) over the model weights governed by a set of hyperparameters whose most probable values are used to estimate the posterior distributions by iterative re-estimation from the data [113][114]. Sparsity is obtained by posterior distributions of many of the weights which are sharply peaked around zero (i.e., relevance vectors means the remaining non-zero weight training vectors). RVM computes the predictive distribution based on the posterior distribution over the weights with maximizing hyperparameters.

Given a data set of input-target pairs $\{x_n, t_n\}_{n=1}^{N}$, we follow the standard formation (($t_n = y(\boldsymbol{x_n}; \boldsymbol{w}) + \epsilon_n$, where process noise $\epsilon_n \sim N(0|\sigma^2)$) and assume that p($t_n|\boldsymbol{x}$) is Gaussian $N(t_n|y(\boldsymbol{x}_n), \sigma^2)$. The mean of this distribution for a given x is modeled by y($x$), as defined for SVM. The likelihood of the complete dataset can then be written as [110]:

$$(\boldsymbol{t}|\boldsymbol{x},\ \boldsymbol{w},\ \sigma^2) = \prod_{n=1}^{N} p(t_n|x_n, \boldsymbol{w}, \sigma^2) = \prod_{n=1}^{N} (2\pi\sigma^2)^{-1/2} exp\left|-\frac{\{t_n - y(x_n;\boldsymbol{w})\}^2}{2\sigma^2}\right| \quad (27)$$

The maximum-likelihood estimate, identical to the 'least-squares' solution, for $\boldsymbol{w}$ is the value $\boldsymbol{w}$ that maximizes$p(\boldsymbol{t}|\boldsymbol{w},\ \sigma^2)$. Least squares (i.e., maximum likelihood) estimation also results in overfitting. To control the model complexity, instead of the regularization of weight penalty $E_w(\boldsymbol{w})$, we now define a prior distribution which expresses our 'degree of belief' over the values that $\boldsymbol{w}$ might take $p(\boldsymbol{w}|\boldsymbol{\alpha}) = \prod_{n=0}^{N} N(\omega_n|0,\ \alpha_n{}^{-1})$. This choice of a zero-mean Gaussian prior expresses a preference for smoother models by declaring smaller weights to be a priori more probable. The maximum-likelihood estimations of $\boldsymbol{w}$ and $\sigma^2$ generally lead to overfitting, so we encode a preference for smoother functions by defining prior over the weights [110][113]:

$$p(\boldsymbol{w}|\boldsymbol{\alpha}) = \prod_{n=0}^{N} N(\omega_n|0,\ \alpha_n{}^{-1}) \quad (28)$$

where α is a vector of *N+1* hyperparameters.

This introduction of an individual hyperparameter for every weight is the key feature of the RVM model, and is responsible for its sparsity properties. The prior $(\mathbf{w}|\boldsymbol{\alpha})$ is nevertheless still Gaussian; it could not be sparsity. So, for full Bayesian consistency we should now define hyperpriors over all $\alpha_m$.

To complete "hierarchical prior", we define hyperpriors over $\boldsymbol{\alpha}$ as well as over the noise variance $\sigma^2$:

$$p(\boldsymbol{\alpha}) = \prod_{n=0}^{N} Gamma\ (\alpha_n|a_n, b_n) \quad (29)$$

$$p(\sigma^2) = Gamma\ (\sigma^2|c,\ d) \quad (30)$$

where $Gamma\ (\alpha|a,b) = \Gamma(a)^{-1} b^a \alpha^{a-1} e^{-b\alpha}$ with $\Gamma(a) = \int_0^\infty t^{a-1} e^{-t} dt$

The weight hierarchical prior p(**ω**) is obtained by:

$$p(\boldsymbol{\omega}) = \int p(\boldsymbol{\omega}|\boldsymbol{\alpha})p(\boldsymbol{\alpha})\, d\boldsymbol{\alpha} \quad (31)$$

Initially, to set these hierarchical priors to a flat Gamma distribution, we fix a, b, c, and d values as small values: e.g., a=b=c=d=0. The combination of the prior over $\alpha_m$ controlling the prior over $w_m$ gives us what is often referred to as a hierarchical prior. $p(\boldsymbol{\omega})$ is not a Gaussian prior, but a Student-t distribution.

The posterior distribution for sparse Bayesian learning is:

$$p(\boldsymbol{w},\ \boldsymbol{\alpha},\ \sigma 2|\boldsymbol{t}) \equiv p(\boldsymbol{w}|\boldsymbol{t},\boldsymbol{\alpha},\sigma^2)p(\boldsymbol{\alpha},\ \sigma^2|\boldsymbol{t}) \quad (32)$$

The weight posterior distribution $p(\boldsymbol{w}|\boldsymbol{t},\boldsymbol{\alpha},\sigma^2)$ is obtained by:

$$p(\boldsymbol{w}|\boldsymbol{t},\boldsymbol{\alpha},\sigma^2) = (2\pi)^{-(N+1)/2}|\Sigma|^{-1/2}\exp\{-\frac{1}{2}(\boldsymbol{w}-\boldsymbol{\mu})^T\Sigma^{-1}(\boldsymbol{w}-\boldsymbol{\mu})\} \quad (33)$$

where the posterior covariance and mean are respectively:

$$\Sigma\ =\ (\sigma^{-2}\boldsymbol{\Phi}^T\boldsymbol{\Phi} + \boldsymbol{A})^{-1} \text{ with } \boldsymbol{A} = diag(\alpha_0, \alpha_1,\ \ldots, \alpha_N) \quad (34)$$

$$\mu\ =\ \sigma^{-2}\Sigma\Phi^T t \quad (35)$$

So, instead of learning a single value for **w**, we have inferred a distribution over all possible values. In effect, we have updated our prior "belief" in the parameter values in light of the information provided by the data **t**, with a higher posterior probability assigned to values which are both probable under the prior and which explain the data. The posterior having observed ($t_1$,..,$t_k$) as the 'prior' for the remaining data ($t_{k+1}$,…,$t_N$) and the equivalent result in seeing all the data at once.

The hyperparameter posterior $p(\boldsymbol{\alpha},\ \sigma^2|\boldsymbol{t})$ adopts an approximation at its most-probable values of $\boldsymbol{\alpha}_{MP}$ and $\sigma^2{}_{MP}$. Therefore, relevance vector "learning"

becomes the search for the hyperparameter posterior mode (i.e., the maximization of $p(\boldsymbol{\alpha}, \sigma^2|\boldsymbol{t}) \propto p(\boldsymbol{t}|\boldsymbol{\alpha}, \sigma^2)$ with respect to $\boldsymbol{\alpha}$ and $\sigma^2$).

$$p(\boldsymbol{t}|\boldsymbol{\alpha}, \sigma^2) = (2\pi)^{-N/2}|\sigma^2\boldsymbol{I} + \boldsymbol{\Phi}\boldsymbol{A}^{-1}\boldsymbol{\Phi}^T|^{-1/2}\exp\{\frac{1}{2}\boldsymbol{t}^T(\sigma^2\boldsymbol{I} + \boldsymbol{\Phi}\boldsymbol{A}^{-1}\boldsymbol{\Phi}^T)^{-1}\boldsymbol{t}\} \quad (36)$$

The values of $\boldsymbol{\alpha}$ and $\sigma^2$ that maximize $p(\boldsymbol{t}|\boldsymbol{\alpha}, \sigma^2)$ cannot be obtained in closed form, so we optimize $p(\boldsymbol{t}|\boldsymbol{\alpha}, \sigma^2)$ via gradient-based prediction (i.e., iterative re-estimation). Initially, setting $\alpha$ and $\sigma^2$ to zero and rearranging are performed by the re-estimation formulae:

$$\alpha_i^{new} = \frac{\gamma_i}{\mu_i^2} \quad (37)$$

$$(\sigma^2)^{new} = \frac{||\boldsymbol{t}-\boldsymbol{\Phi}\boldsymbol{\mu}||^2}{N-\Sigma_i\gamma_i} \quad (38)$$

where $\gamma_i = 1 - \alpha_i\Sigma_{ii}$ and $\Sigma_{ii}$ is the i[th] diagonal element of the posterior weight covariance computed with the current $\boldsymbol{\alpha}$ and $\sigma^2$. The prediction learning algorithm then initializes all $\{\alpha_i\}$ and $\sigma^2$ ; computes the weight posterior sufficient statistics $\boldsymbol{\mu}$ and $\Sigma$; computes all $\{\gamma_i\}$ and then re-estimates $\{\alpha_i\}$ (and $\sigma^2$ if desired); repeats from 2 until convergence; deletes the weights for optimal $\alpha_i = \infty$, since this implies $\mu_i = 0$; and makes predictions for new data via the predictive distribution computed with the converged $\boldsymbol{\alpha}_{MP}$ and ${\sigma^2}_{MP}$:

$$P(t_*|\boldsymbol{t}) = \int p(t_*|\boldsymbol{w}, {\sigma^2}_{MP})\, p(\boldsymbol{w}|\boldsymbol{t}, \boldsymbol{\alpha}_{MP}, {\sigma^2}_{MP})d\boldsymbol{w} \quad (39)$$

This equation is computable and Gaussian [110][113][114]. The predictive mean of $P(t_*|\boldsymbol{t})$ is the model function evaluated with the posterior mean weights. The predictive variance comprises the estimated noise on the data and the uncertainty in the prediction of the weights.

*5.2 Prediction Process: Remaining Useful Life Estimates Based on Similarity-based Statistical Measures*

The prediction process predicts the RULs for new test units by employing a set of RVM regression curves built into the learning process of the training units. The prediction process involves RUL calculation based on each training unit and RUL calculation of the test unit with the linearly weighted sum of RULs from the training units [115]-[117]. The RUL for a test unit is defined as a similarity-based statistical measure such that the RUL prediction of a test unit is a linear interpolation in terms of the projected RULs (i.e., $\widehat{L_t}s$) of K training units.

$$RUL = \frac{1}{W}\sum_{i=1}^{K}(W_i\widehat{L_i}) \quad (40)$$

where $w = \sum_{i=1}^{K} W_i$.

Similarity weight is evaluated with:

$$W_i = \left[\sum_{m=1}^{N}(y_i(x_m) - y_{p_i}(x_m))^2\right]^{-1} \quad (41)$$

where $W_i$ is the similarity weight of the ith training unit, $w$ is the total weight of K training units, $y_i(x_m)$ is a real test point under the test at a certain time instance $x_m$, and $y_{p_i}(x_m)$ is the prediction result at the time instance $x_m$.

The summation in equation (41) is designated for the sum of the squared error between the true value and the predicted value at each point. The similarity weight enhances the accuracy of the RUL prediction, as can be seen in the example in Figure 47 where a larger weight is given to a training unit with a higher similarity to the test unit. If the test part appears similar to a certain training part, then the weight for that

training data is higher. This prediction process can utilize any training data set which was conducted for all devices. This means that all historical data set can be used for prediction mathematically. Uncertainty caused by modeling state space equation which shows the degradation path model is reduced based on utilization of all training samples.

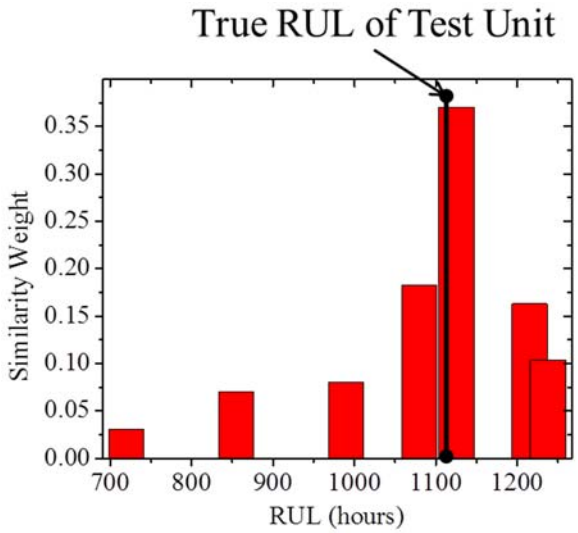


**Figure 47 RUL prediction based on weight measure.**

*5.3 Experimental Procedures and Results*

An overview of the test setup is shown in Figure 48. The LED board was placed in a forced convection oven temperature chamber and each LED was tested under 350mA constant current and a data logger (Agilent 34970A) monitoring the electrical and thermal measurements. A photometric instrument (BTS 256 LED tester (Gigahertz-Optik)) was utilized to collect the optical health indicators.

Three-watt high power InGaN LEDs with maximum absolute junction temperature ratings of 135˚C were mounted on an aluminum metal core printed circuit board (MCPCB). An MCPCB consists of a base layer (aluminum), a dielectric layer (FR-4 layer), and a circuit layer (Cu trace layer) for higher heat dissipation than the

FR-4 board. Thermocouple wires were attached to the anode side of the lead for the tested LEDs.

The test conditions were a 350mA drive current and an ambient temperature of 40°C. The average junction temperature was estimated to be 132.6°C [118]. The junction temperature of LEDs was directly estimated from the correlation between junction temperature and the forward voltage for long-term aging tests of high power LEDs [118]. There were 16 LED samples (designated as LED 1 to LED 16) mounted on the MCPCB. The measurement interval for the electrical parameters (input constant current and output forward voltage) and thermal parameters (ambient temperature and lead temperature) was every five minutes; and the measurement interval for the optical parameters (light output, correlated color temperature, color rendering index, and u′v′ distance) was every 22.5 hours.

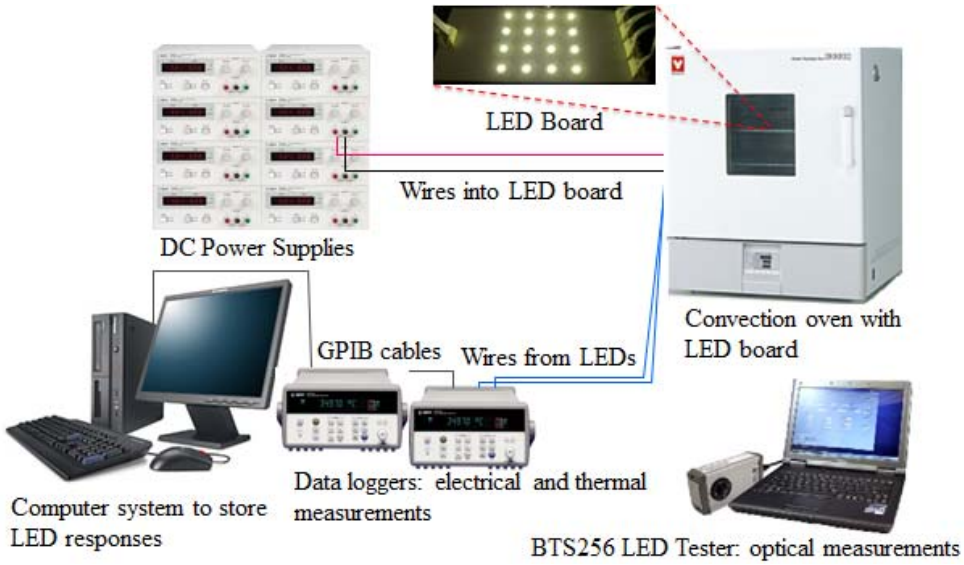


**Figure 48 Overview of LED test setup.**

Color failures were observed ahead of light output failures. The average time of 16 LEDs for the light output to decrease from 100% to 70% is shown in Figure 49 with the standard deviation (i.e., the horizontal bar). The average time for each color

distance to increase from 0.001 to 0.007 is shown in Figure 50 with the standard deviation. The standard deviation of the time to reach each step of color distance in Figure 50 is 4 times larger in maximum than the standard deviation of the time to reach each percent step of light output in Figure 49. The time step to reach each color distance from 0.001 to 0.007 and each percent of light output from 100% to 70% did not match with a linear relationship because the degradation dynamics were exponentially decrease and increase in Figure 49 and Figure 50.

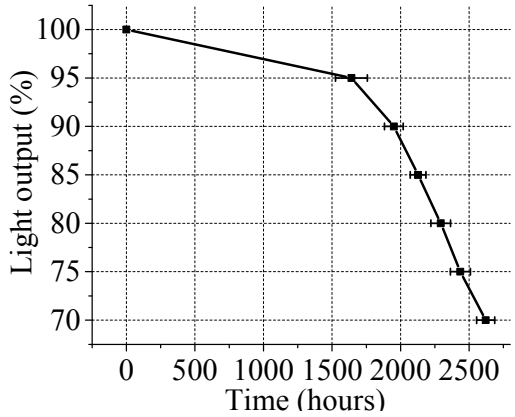


**Figure 49 Average time for the percent of light output to decrease from 100% to 70%, with standard deviations.**

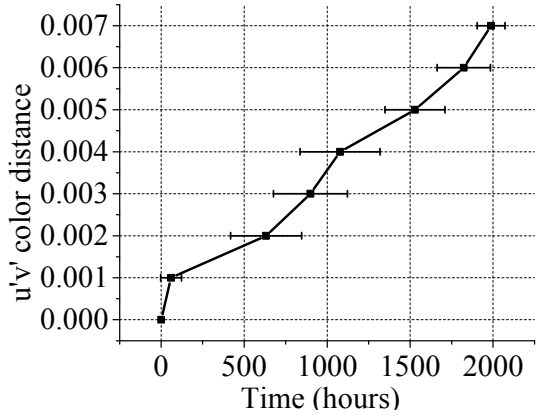


**Figure 50 Average time for the u'v' distance to increase from 0.001 to 0.007, with standard deviations.**

The time to failure (TTF) range of color failure based on 7-step-standard deviation of color matching from MacAdam ellipses (7 standard deviations from the initial color state, i.e., a u′v′ distance of 0.007) was between 1,891 hours and 2,206 hours, as shown in Figure 51. MacAdam ellipses are described as having ‘step’, which means standard deviations [77]. The TTF range of L70 (i.e., 30% degradation of light output) was between 2,251 hours and 2,633 hours, as shown in Figure 52. The mean time to failure (MTTF) for the color shift was 1,945.5 hours, and the light output degraded by 10% at an average time of 1,951 hours. The unreliability in Figure 51 and Figure 52 is the probability that a device will not perform its intended function for a given interval of time under specified operating conditions.

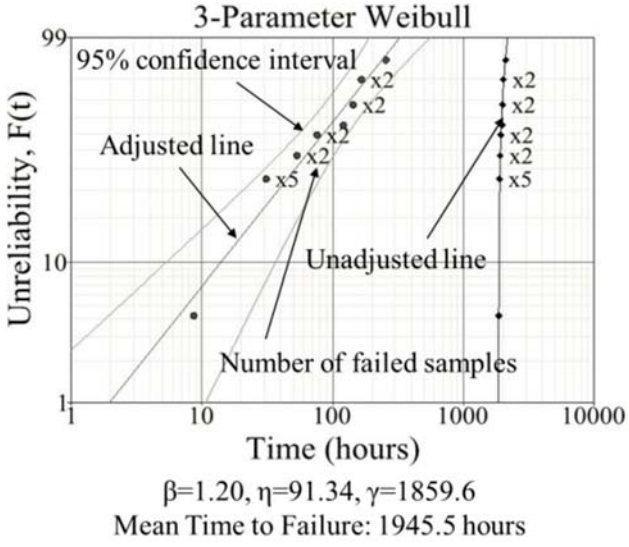


**Figure 51 Result of color failure.**

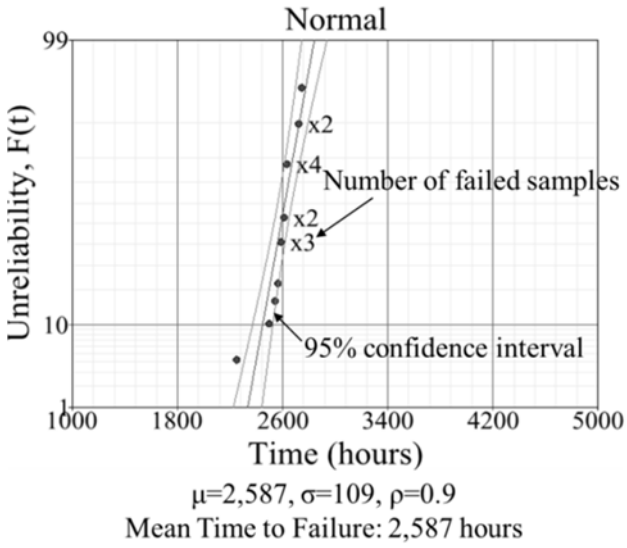


**Figure 52 Result of light output failure.**

### *5.4 RUL Prediction Results*

Prediction was performed with optical health indices and in-situ health indices. Optical health indices include information on light and color health indicators. In-situ health indices include information on electrical and thermal health indicators of LEDs. The prediction results with optical and in-situ health indices are compared in this section. Further, the results are compared with previously published research on LED prognostics in [60].

#### *5.4.1 RUL Prediction in Terms of Optical Health Indicators*

LED prognostics includes a feature extraction by one-dimensional health index, a learning process using RVM regression, and a prediction process utilizing similarity-based statistical measure. A one-dimensional optical health index was generated using Mahalanobis distance (MD). MD is the square distance between observed vector and the mean vector of a population as shown equation (42) [119][120]. Four optical health indicators (luminous flux, correlated color temperature,

color rendering index, and u′v′ distance) for each LED were used to construct the health indices.

$$MD_i = \frac{1}{p} Z_i C^{-1} {Z_i}^T \quad (42)$$

where i = 1,…,n where i is ith row in data matrix, k = 1,…,p where p is number of parameters in column of data matrix, Zi = ith vector of Zix, T = transpose of the vector, C-1 = inverse of the correlation matrix of standardized values, and $Z_{iX} = \frac{(x_i - \bar{x})}{\sigma_X}$ is mean centered standardized values of xik. The data set (including failure data) for each LED was constructed based on L70 failure criterion. Figure 53 shows how to extract features from the four optical health indicators.

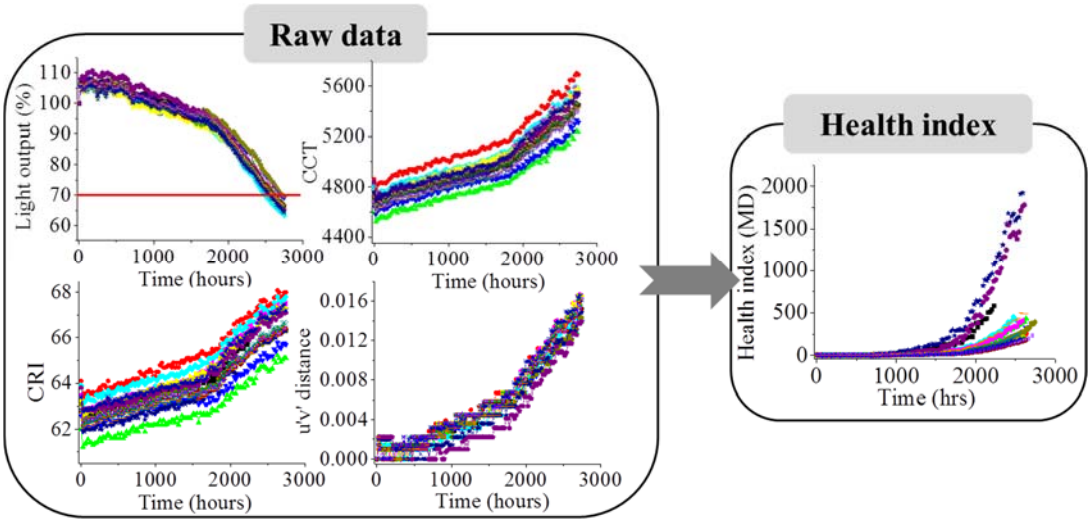


**Figure 53 Feature extraction: Optical health index.**

Ten of the 16 sample LEDs were used to perform RVM learning to construct the background health knowledge, as shown in Figure 54. The prediction process used the similarity-based statistical measure, as shown in Figure 55. RUL was calculated using equation (41) and equation (43). The true RUL was 1,215 hours, and the similarity-based statistical measure predicted a RUL of 1,201 hours.

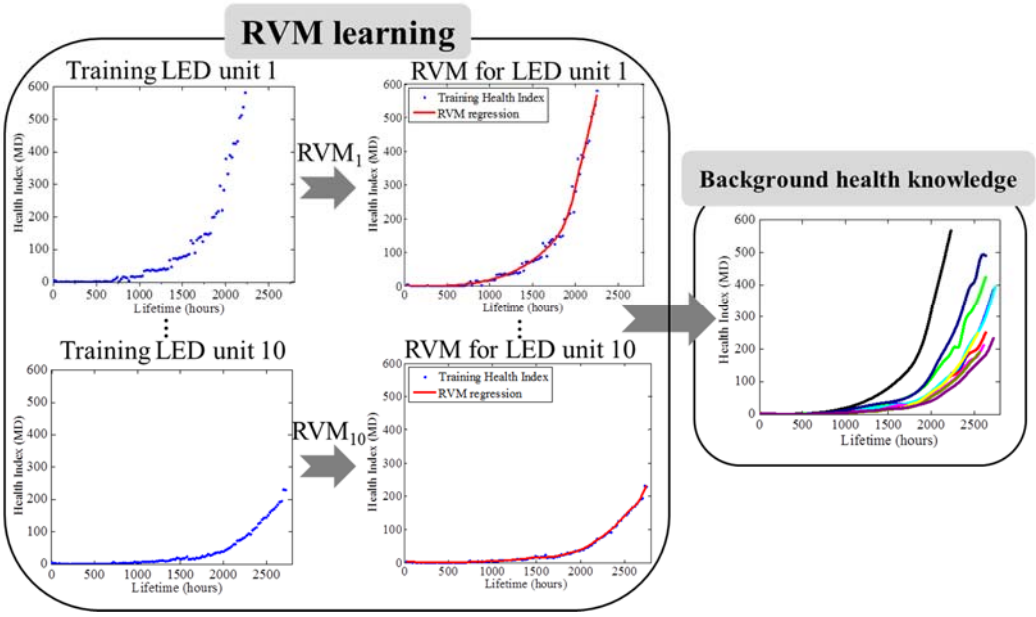


**Figure 54 Learning process: RVM learning for optical health indices.**

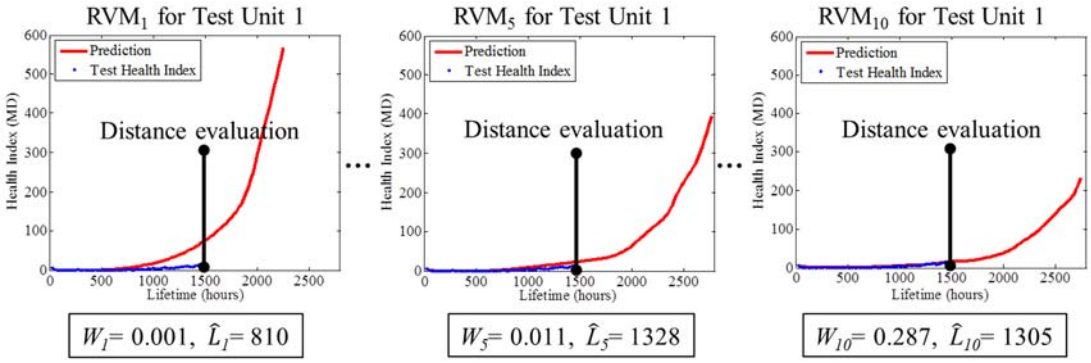


**Figure 55 Prediction process: Similarity-based statistical measure for optical health indices.**

$$RUL = \hat{L} = \frac{1}{W}(w_1\hat{L}_1 + w_2\hat{L}_2 + \cdots + w_{10}\hat{L}_{10}) \quad (43)$$

### *5.4.2 RUL Prediction in Terms of In-Situ Health Indicators*

LED prognostics with in-situ health indicators is performed in a way similar to LED prognostics with optical health indicators, using feature extraction by one-dimensional in-situ health index, a learning process using RVM regression, and a prediction process utilizing a similarity-based statistical measure. One-dimensional

in-situ health index was performed by Mahalanobis Distance (MD). Four in-situ health indicators (input current, ambient temperature, lead temperature, and forward voltage) for each LED were used to construct the health indices.

In this example, constant current was applied; however, some real applications use pulsed width modulation (PWM) mode which the current levels can change, or sometimes the input current changes based on catastrophic failures. This approach introduces the available electrical and thermal features monitored by sensors at in-situ conditions. In other cases, LED input current becomes zero due to catastrophic failures of LEDs. In the cases, input current also can be signatures representing LED performance change. For this reason, input current was also considered to construct the in-situ health indicators.

The entire data set (including failure data) of each LED was constructed based on the L70 failure criterion. Figure 56 shows how to extract features from the four optical health indicators. Ten LEDs (the same training units as used with the optical health indicators) from the 16 sample LEDs were used to perform RVM learning to construct the background health knowledge, as shown in Figure 57. The prediction process used the similarity-based statistical measure, as shown in Figure 58. The RUL was calculated using equation (17) and equation (19). The true RUL was 1,210 hours, and the similarity-based statistical measure was estimated as 1,200 hours.

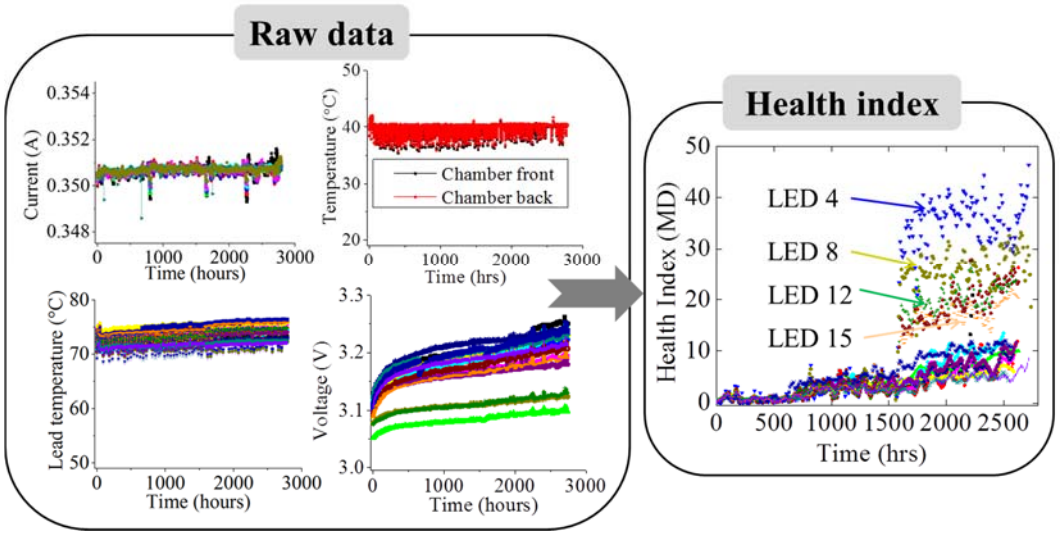


**Figure 56 Feature extraction: In-situ health index.**

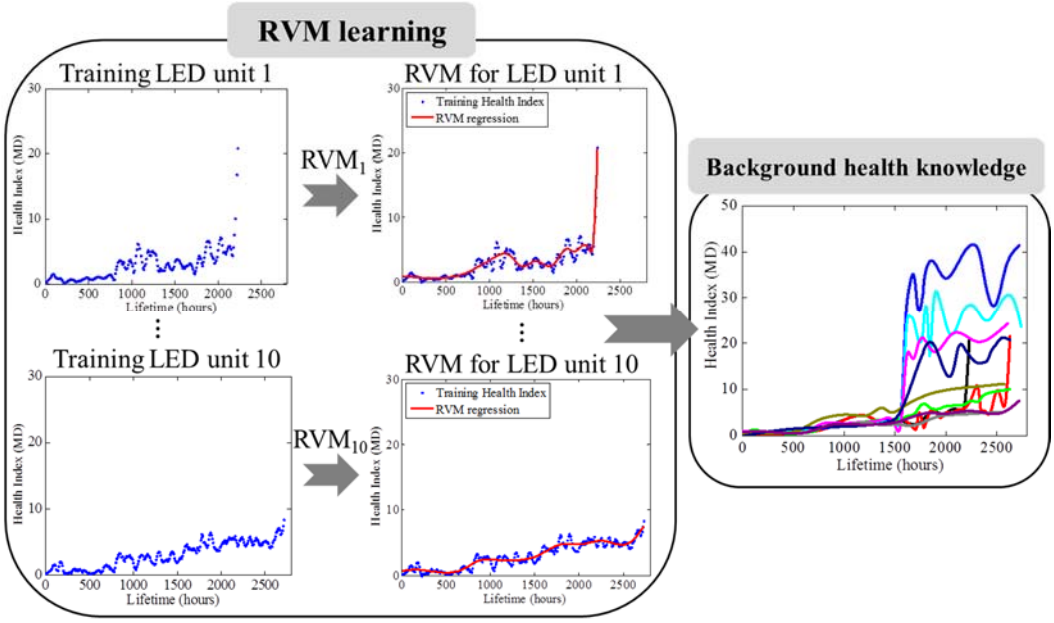


**Figure 57 Learning process: RVM regression for in-situ health indices.**

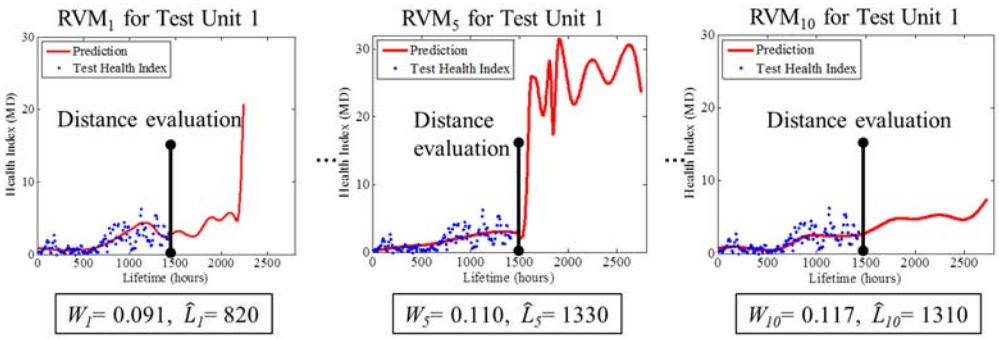


**Figure 58 Prediction process: Similarity-based statistical measure for in-situ health indices.**

As shown in Table 8 and Table 9, a comparison of the RUL prediction results based on optical health indices and in-situ health indices showed that in-situ health indices can be used to predict the RUL of LEDs with the same level of accuracy as optical health indices. For example, in Table 8, the maximum error of 6.9% was occurred at the test unit 2 though the test unit 2 in Table 9 showed -0.2% of the prediction error. But the maximum error of -6.2% in Table 9 was occurred at test unit 6. Based on the result in Table 9, in-situ health indices can be used for RUL prediction in prognostics-based qualification tests. In this test set, anomalies were detected in LEDs at 1,500 hours, as shown in Figure 57 and Figure 58. In this work, 10 LEDs were used to perform RVM regression (learning) to construct background health knowledge, but the prediction results can be made more accurate using a larger number of training samples and different training results. Prediction results at another time instant at 2,000 hrs are shown in Table 10 and Table 11. More length of data at 2,000 hrs than the length of data at 1,500 hrs gave higher accuracy to predict RUL than RUL.

**Table 8 RUL prediction using optical health indices at 1,500 hours.**

| | Test unit 1 | Test unit 2 | Test unit 3 | Test unit 4 | Test unit 5 | Test unit 6 |
|---|---|---|---|---|---|---|
| Predicted RUL | 1,201 hrs | 1,089 hrs | 1,140 hrs | 1,114 hrs | 1,155 hrs | 1,082 hrs |
| True RUL | 1,215 hrs | 1,170 hrs | 1,170 hrs | 1,170 hrs | 1,192 hrs | 1,080 hrs |
| Error (%) | 1.2 % | 6.9 % | 2.6 % | 4.8 % | 3.2 % | -0.2 % |

cf) Error (%) = (True RUL-Predicted RUL)/True RUL*100

**Table 9 RUL prediction using in-situ health indices at 1,500 hours.**

| | Test unit 1 | Test unit 2 | Test unit 3 | Test unit 4 | Test unit 5 | Test unit 6 |
|---|---|---|---|---|---|---|
| Predicted RUL | 1,200 hrs | 1,172 hrs | 1,210 hrs | 1,190 hrs | 1,183 hrs | 1,147 hrs |
| True RUL | 1,210 hrs | 1,170 hrs | 1,170 hrs | 1,170 hrs | 1,190 hrs | 1,080 hrs |
| Error (%) | 0.9 % | -0.2 % | -3.4 % | -1.7 % | 0.6 % | -6.2 % |

cf) Error (%) = (True RUL-Predicted RUL)/True RUL*100

**Table 10 RUL prediction using optical health indices at 2,000 hours.**

| | Test unit 1 | Test unit 2 | Test unit 3 | Test unit 4 | Test unit 5 | Test unit 6 |
|---|---|---|---|---|---|---|
| Predicted RUL | 684 hrs | 576 hrs | 630 hrs | 620 hrs | 658 hrs | 572 hrs |
| True RUL | 701 hrs | 589 hrs | 640 hrs | 614 hrs | 655 hrs | 582 hrs |
| Error (%) | 2.4 % | 2.2 % | 1.6 % | -0.98 % | -0.5 % | 1.7 % |

cf) Error (%) = (True RUL-Predicted RUL)/True RUL*100

**Table 11 RUL prediction using in-situ health indices at 2,000 hours.**

| | Test unit 1 | Test unit 2 | Test unit 3 | Test unit 4 | Test unit 5 | Test unit 6 |
|---|---|---|---|---|---|---|
| Predicted RUL | 716 hrs | 564 hrs | 618 hrs | 610 hrs | 668 hrs | 544 hrs |
| True RUL | 701 hrs | 586 hrs | 640 hrs | 610 hrs | 655 hrs | 582 hrs |
| Error (%) | 1.2 % | 6.9 % | 2.6 % | 4.8 % | 3.2 % | -0.2 % |

cf) Error (%) = (True RUL-Predicted RUL)/True RUL*100

### *5.5 Discussion*

Sutharssan et al. [60] predicted the remaining useful life of LEDs using MD by trending curves over time with sequential estimation between one step time ahead such as t-1 and t. They utilized voltage, current, light output, and temperature of LEDs to determine MDs. They related the maximum value of MD to the failure limit with power law approximation using (44). They assumed that the extent of deviation of MD does

not continuously increase until the LED completely failed. The degradation of MD curves exhibited decreasing trend. If the trend of MD does not decrease over time, the approach in [60] cannot be used to set up the failure limits. To validate the approach, MDs were evaluated using voltage, current, light output, and temperature of each LED. The degradation trend of LEDs increased over time. The remaining useful life of LEDs cannot be evaluated using the method presented in [60]. A similarity-based statistical measure with RVM can predict the remaining useful life of LEDs without consideration of the pattern of the data.

$$FL\ (Failure\ limit) = 2.3105 \times {MD_{max}}^{0.6746} \quad (44)$$

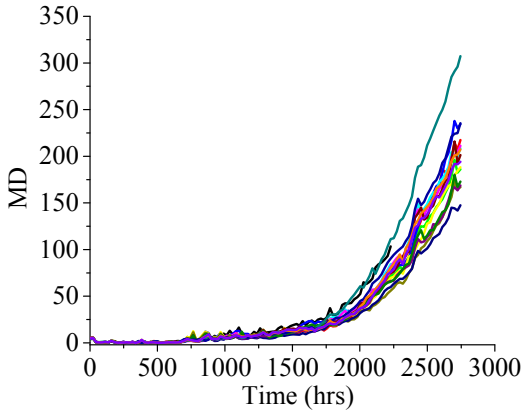


**Figure 59 Data trend using MD with the approach in [60].**

## *5.6 Conclusions*

There are many international environmental and legal trends (e.g., China's 12th Five-Year Plan for 2011 to 2015) toward the increased adoption of LEDs for general lighting. However, the LED industry cannot meet this demand if their products do not meet the quality and reliability expectations of the customer. The methodology developed and demonstrated in this paper will help the industry to evaluate LED

technologies for their lifetime goals more rapidly than the methods used as of 2013 and enable them to make better informed product introduction decisions.

In this paper, health indices were developed for rapid assessment of the remaining useful life of an LED at any point during qualification testing. An optical health index was defined based on light and color data and the in-situ health index was defined based on electrical and thermal data. Using these health indices enables the monitoring of the degradation of LEDs with one single parameter by mapping multiple dissimilar data in the experiment. Similarity-based statistical measures technique with the relevance vector machine (RVM) improved the prediction of remaining useful life compared to the technique employed by Sutharssan et al., which is only applicable to health indices with decreasing trends. Based on the similarity of the degradation trend of the test unit under test and training units having time to failure (TTF) data in prior qualification testing, the RUL of the test unit under test was predicted by calculating the linear combination of RULs of training units.

LED manufacturers and developers have TTF data available and degradation trends from their product design qualification tests. The LED manufacturers collect light output, correlated color temperature, color rendering index, chromaticity coordinates, current, voltage, and temperatures. Even though the data collection time varies from 1,000 hours to 6,000 hours, LED manufacturers have collected data, including the TTF from previous product lines. There have been improvements in quality and performance in terms of LED materials and design. For this reason, in many cases, a new LED package has been modified from an existing LED package to meet customers' needs. As a result, the historical data trend from existing LED

packages can be used to predict the RUL of a new LED package. This can be accomplished through the use of a similarity-based statistical measure accompanied by RVM regression.

We have shown that since color and light degradation patterns are different, using color or light to correlate the other degradation can lead to misleading and incorrect results. In the aging test, it was observed that the time step to reach each color distance from 0.001 to 0.007 had a nonlinear relationship with the time step to reach each percentage increment of light output from 100% (i.e., initial light output) to 70%. This was because degradation dynamics of color are different than the degradation dynamics of light output, and the standard deviation of the time to reach each step of color distance was 4 times larger than the standard deviation of the time to reach each percent increment of light output. For this reason, color degradation has to be considered as well as light output degradation for RUL prediction. In this paper, a health index was developed to represent different degradation dynamics of both light and color degradation. The health index improved the prediction of the remaining useful life of LEDs.

The average of all light output from the test units for RUL prediction as recommended by the industry standard IES TM-21-11 does not consider the variation of each test unit. As a result, the method in this standard does not offer a mean time to failure, confidence interval, or reliability function. However, this information is important for determining the failure distribution of test units. A new industrial standard has to be developed to improve the quality of products in the development stage by considering the variation of degradation of all test units. To this end, this paper

provides guidelines that industry can follow to standardize LED qualification tests by utilizing all TTF data in prior qualification testing and giving higher priority to similar data trends of training units. In addition to conducting new predictions for units under test using prognostics techniques, TTF data must be used to predict the remaining useful life of LEDs.

Unlike IES TM-21-11, by using the method presented in this paper it is possible to perform prognostics using only in-situ measured data if there is sufficient degradation data from similar LED product lines. If it is not possible to access enough degradation data, the accuracy of the prognostic results will be limited. In-situ measured data, including thermal and electrical data, can be collected more frequently and are more readily measurable using a data logger system instead of using optical measurement. By using in-situ measured data from each LED, the similarity-based statistical measure can predict the remaining useful life of individual LEDs under the test conditions. The experimental results from the electrical and thermal aging tests demonstrated the effectiveness and accuracy of the developed prognostic algorithms. The algorithms can be implemented not only in field operations to provide real-time LED remaining useful life, but also employed in LED qualification to significantly reduce testing time, since only the early period of testing is needed to generate data for remaining useful life prediction. Initial increase of light output due to the short term aging effect was solved with the more clear trending data with the health index approach. This can help the users to link the health indicators to the long term performance of the LEDs.

# CHAPTER 6 Contributions and Future Work

## *6.1 Contributions*

- Developed anomaly detection method for LEDs with test data on current devices by using new features extracted from SPD.
- Developed diagnostic and prognostic technique of LEDs by predicting SPD to determine potential degradation of die, phosphor, and encapsulant in product qualification.
- Developed RUL prediction method with statistical measure accompanied with RVM regression to capture degradation trends and predict the RUL of individual LEDs using prior electrical and thermal failure data on other devices.

## *6.2 Future Work*

- Further research can be performed on an accelerated life test profile for conducting accelerated life tests; research off-the-shelf hardware and software packages to analyze precursor parameter signals; conduct life tests on special LED

samples; verify that test stations can detect LED life degradation; develop test methods and analysis procedures that will enable suppliers and test labs to conduct LED life tests; and present research in a final report with a defined test plan.

- Further research can be performed to do and identify dominant failure modes expected from manufacturing process variations; conduct tests on a large set of special samples to detect sources of manufacturing variation; develop algorithms and methods to predict each source of variation; and present research in a final report with recommended approach for conducting on-going reliability testing program of LEDs.

# Appendix A: Test Results

1. Test results under the condition with 350mA drive current and chamber temperature 40°C

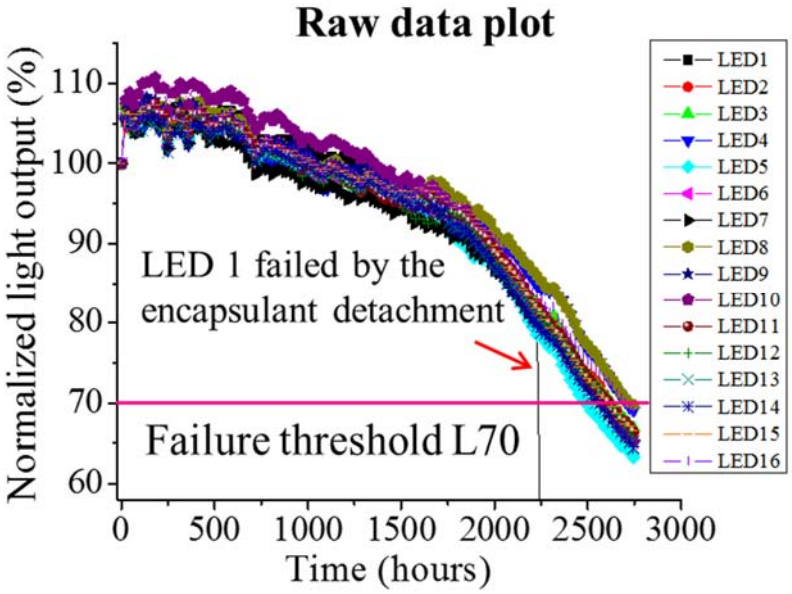


**Light output failure (L70) summary**

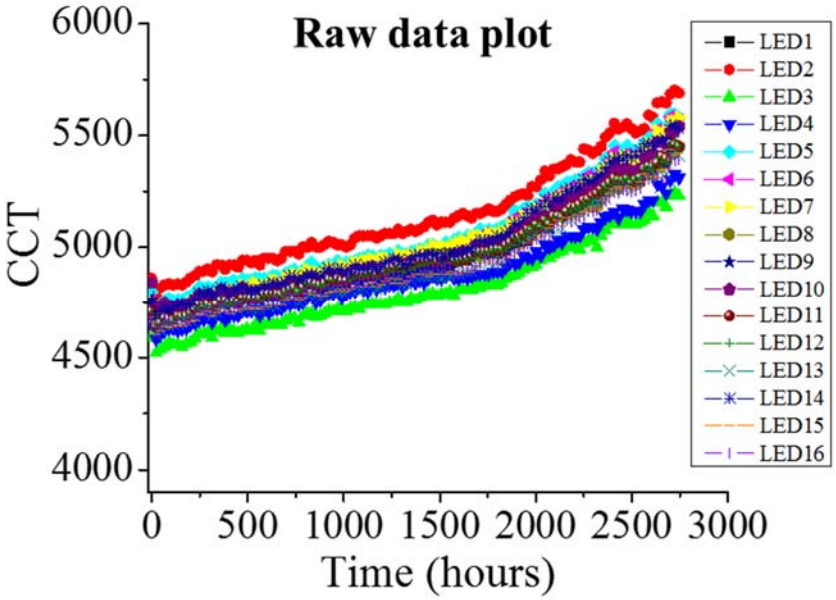


**Color temperature degradation summary**

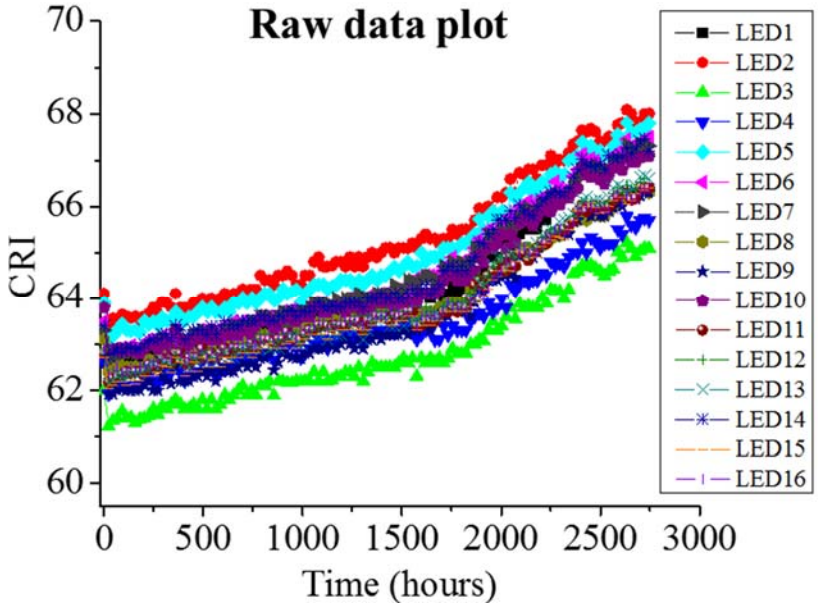


**CRI degradation summary**

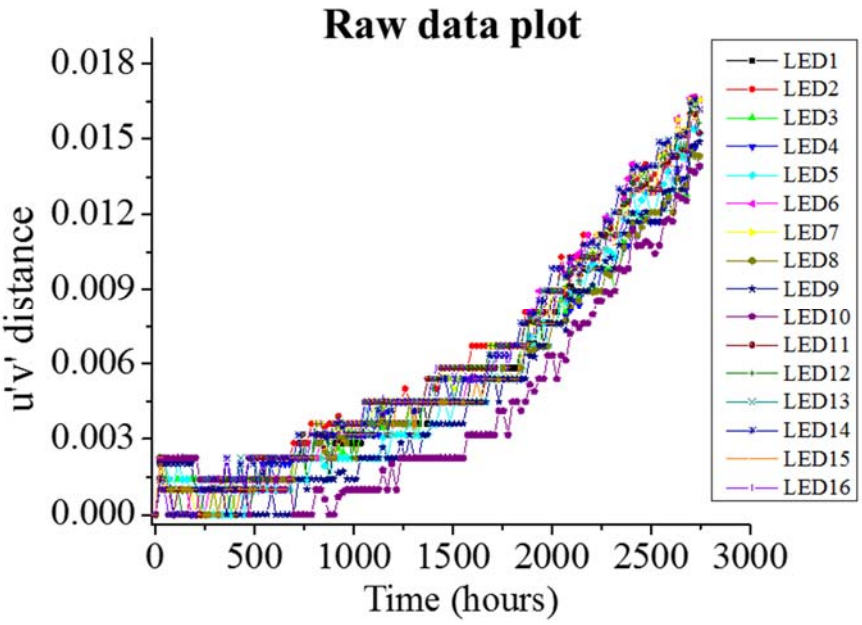


**Color (u′v′ Distance Shift) degradation summary**

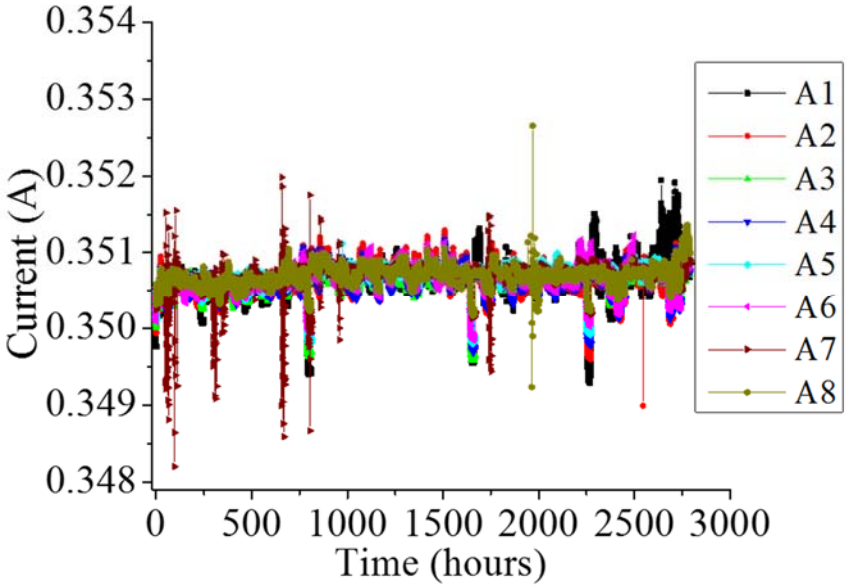


**Input current variation summary**

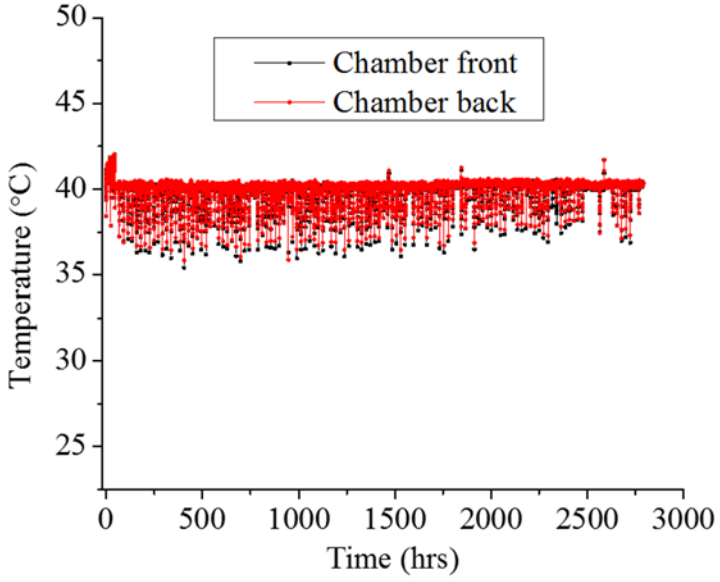


**Ambient temperature change summary**

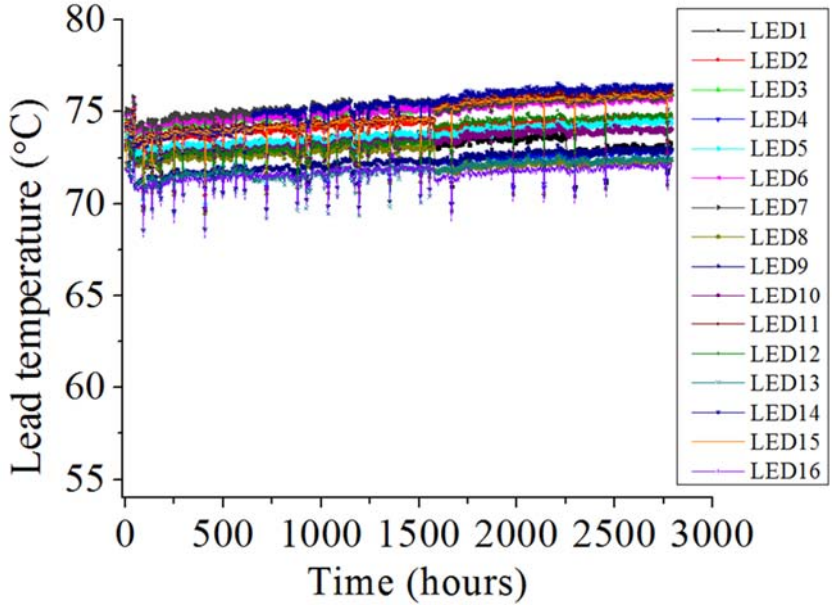


**Lead temperature change summary**

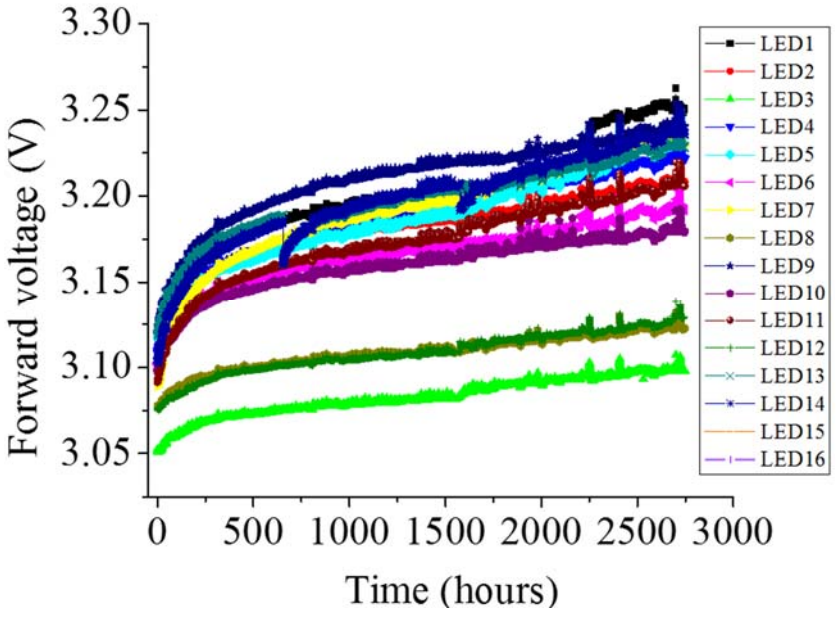


**Forward voltage change summary**

2. Test results under the condition with 350mA drive current and chamber temperature 40°C

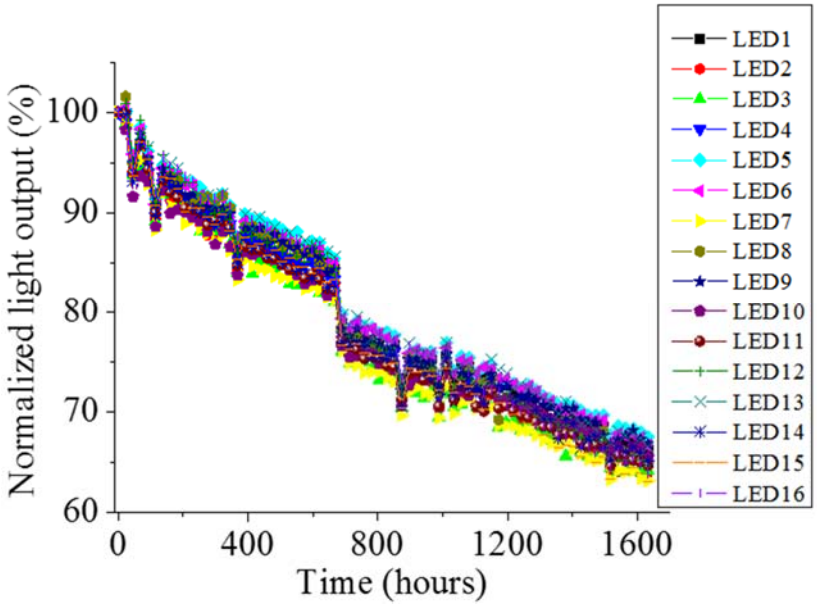


**Light output failure (L70) summary**

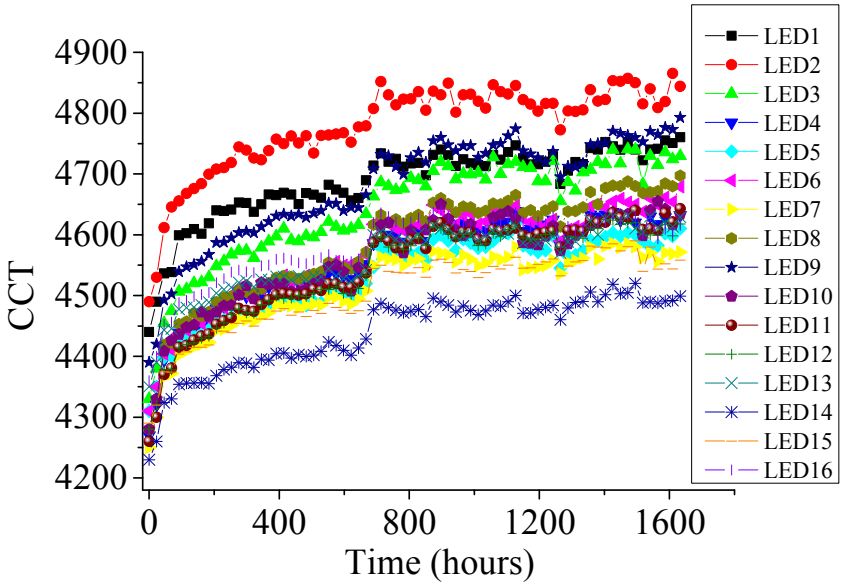


**Correlated color temperature degradation summary**

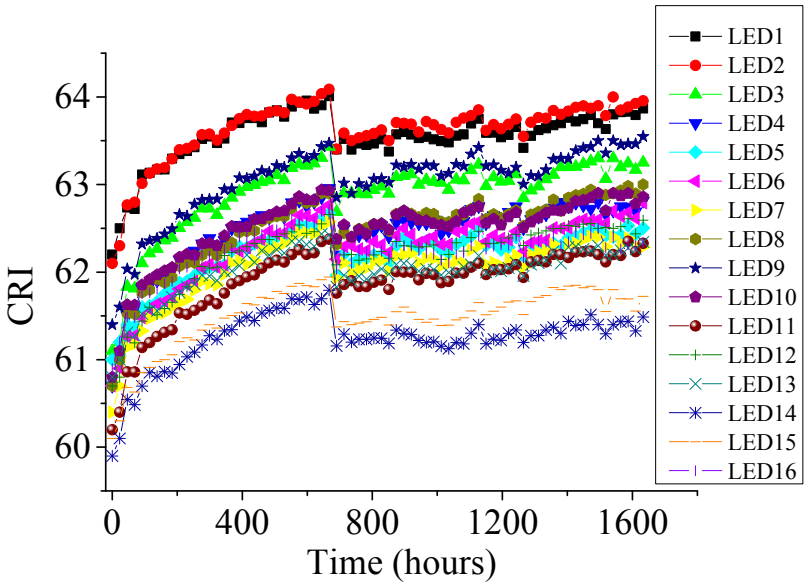


**CRI degradation summary**

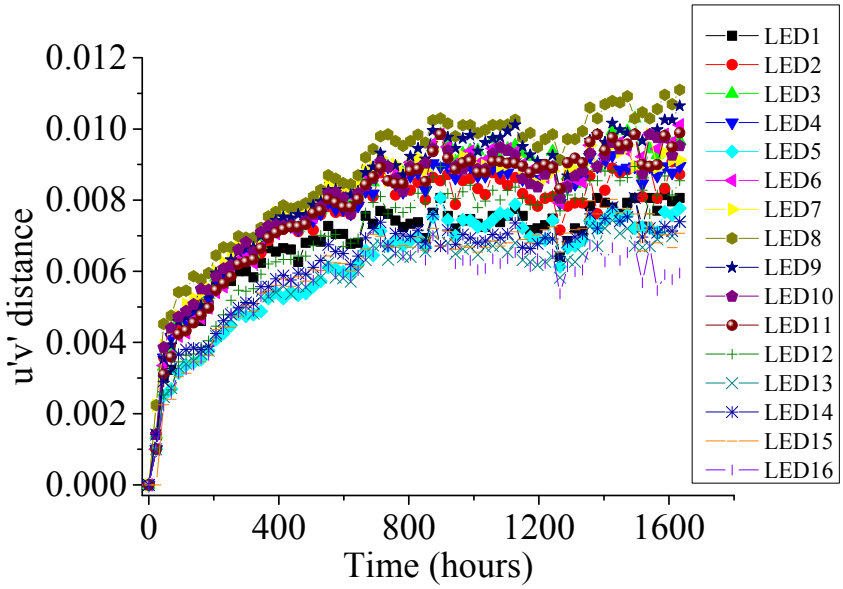


**Color (u′v′ distance shift) degradation summary**

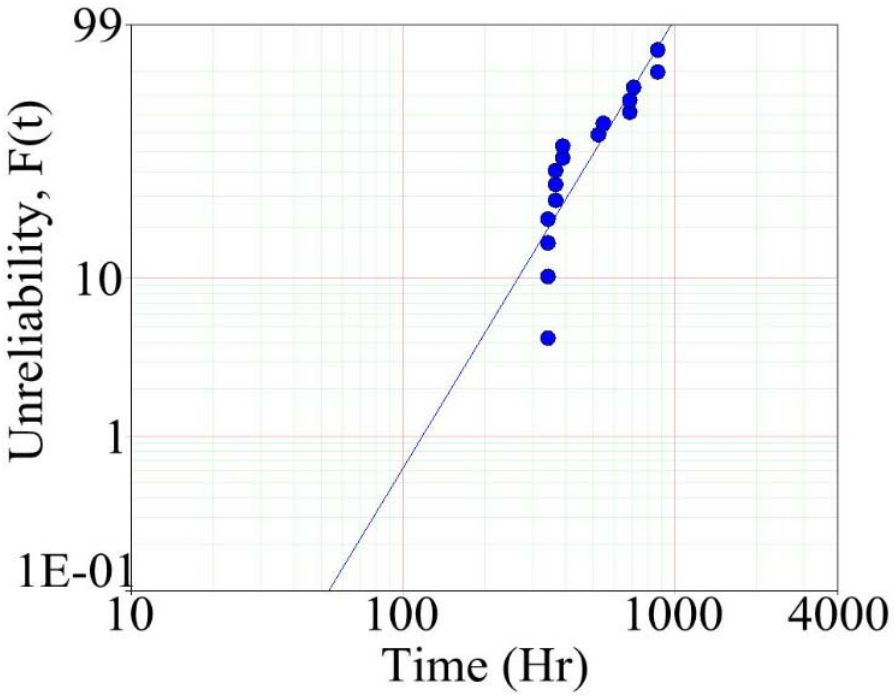


**Time to failure for color failures (based on 0.007 u′v′ distance color shift)**

# Appendix B: Anomaly Detection Results under the Condition of 350mA Drive Current and Chamber Temperature 40°C

1. Anomaly detection results for LED die peak under the condition with 350mA drive current and chamber temperature 40°C

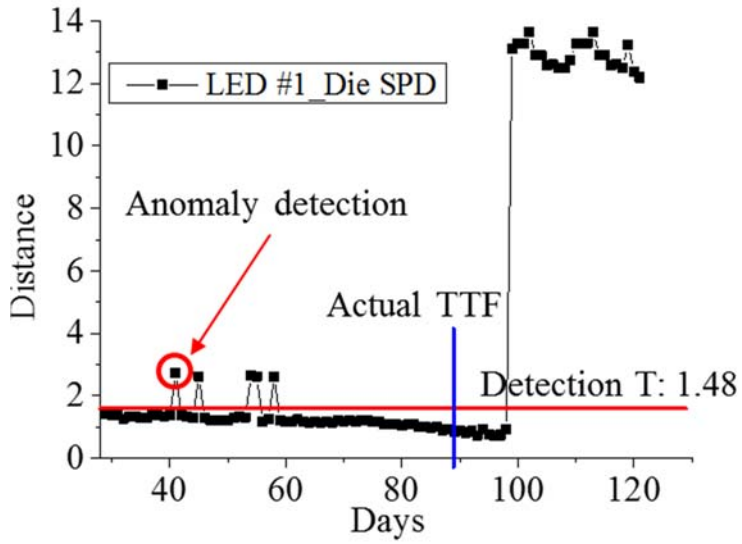


**Distance measure of cluster 1 from LED 1 for die peak.**

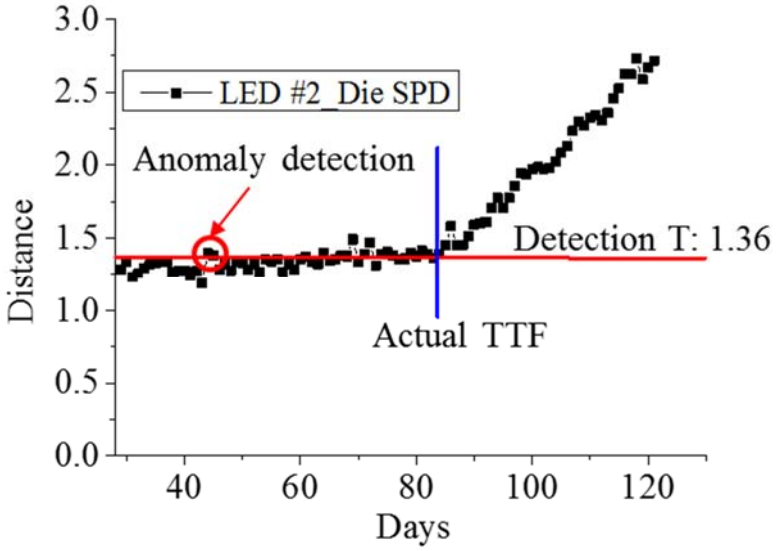


**Distance measure of cluster 2 from LED 2 for die peak.**

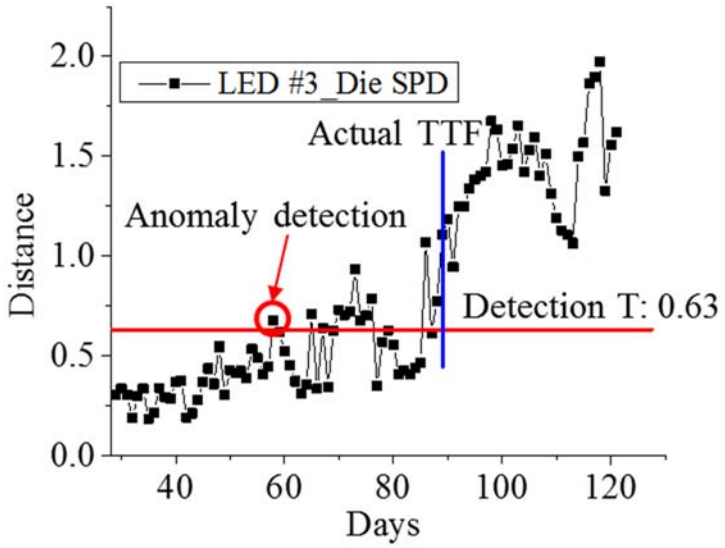


**Distance measure of cluster 4 from LED 3 for die peak.**

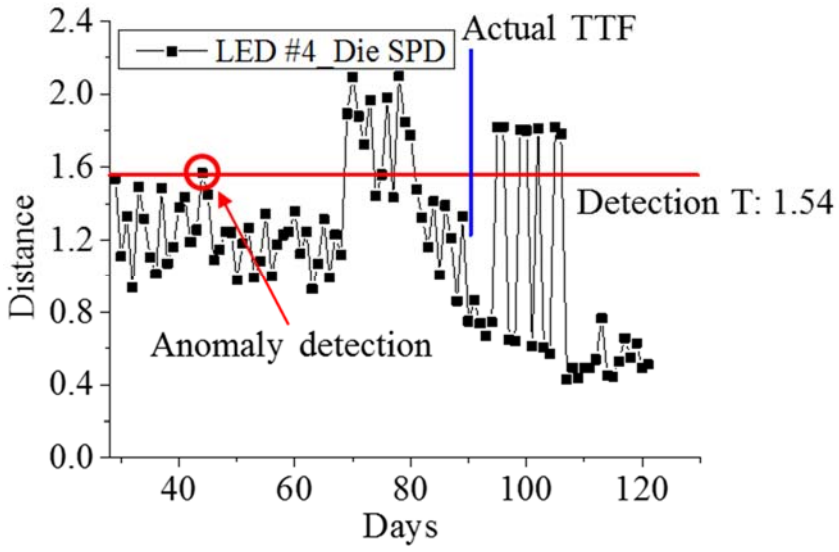


**Distance measure of cluster 7 from LED 4 for die peak.**

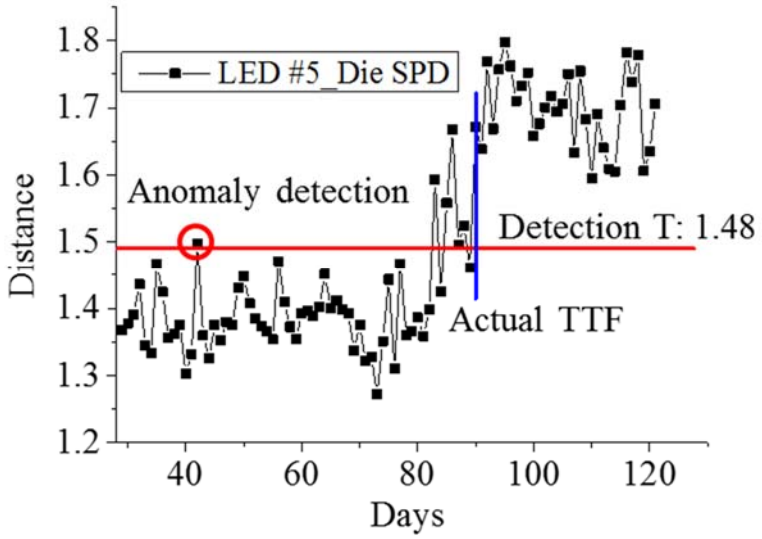


**Distance measure of cluster 1 from LED 5 for die peak.**

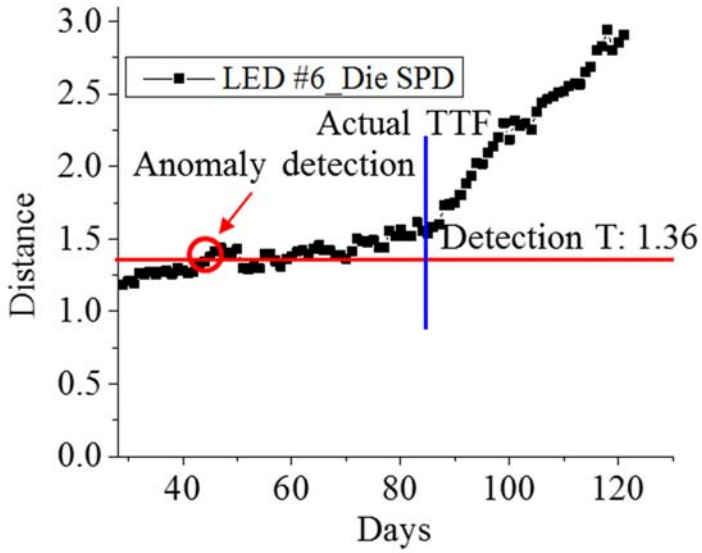


**Distance measure of cluster 2 from LED 6 for die peak.**

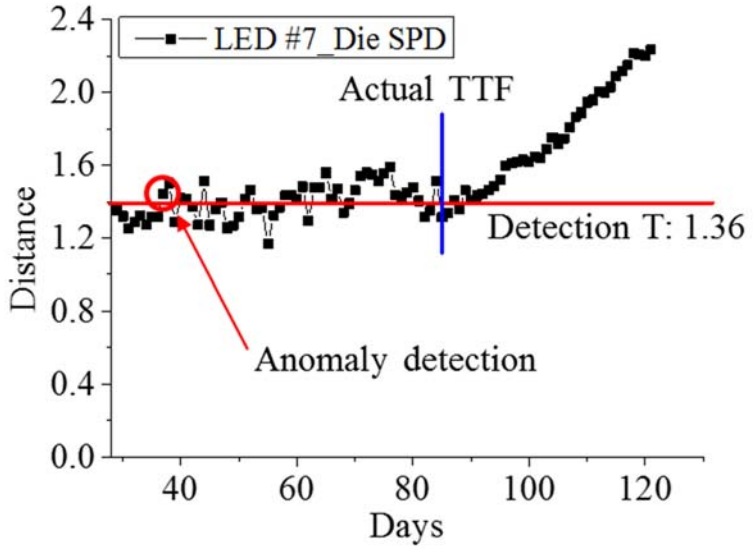


**Distance measure of cluster 2 from LED 7 for die peak.**

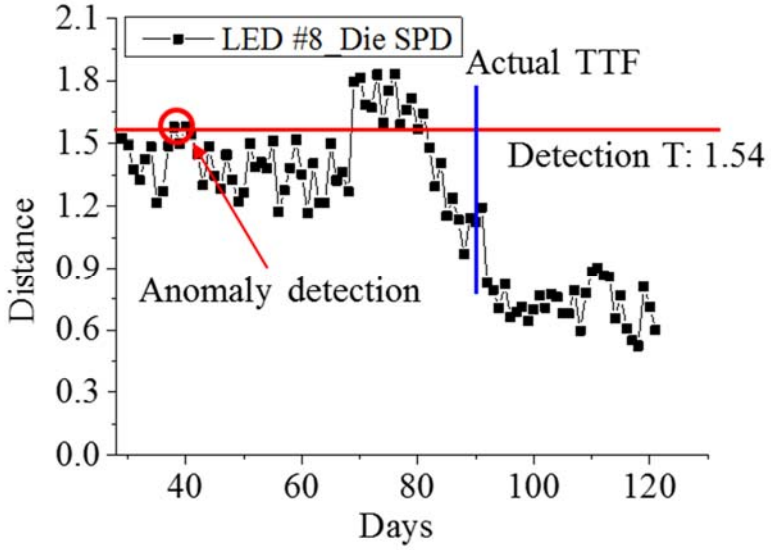


**Distance measure of cluster 7 from LED 7 for die peak.**

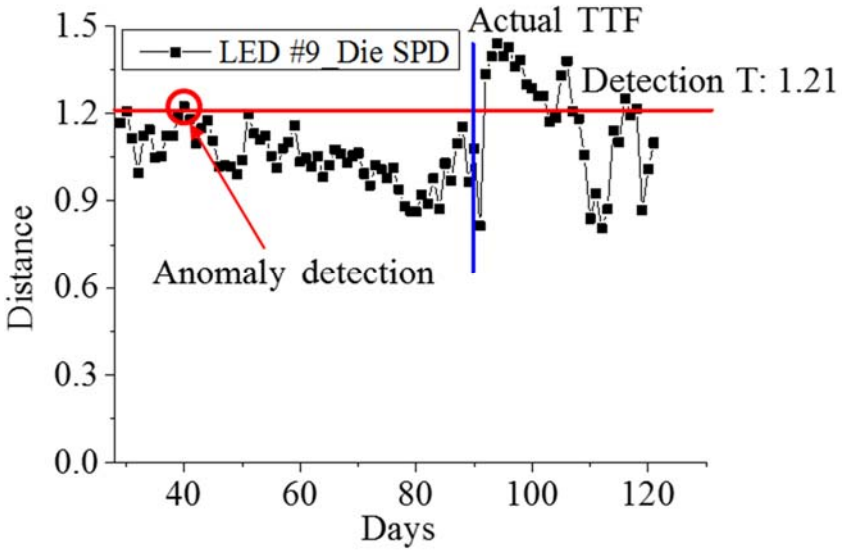


**Distance measure of cluster 3 from LED 9 for die peak.**

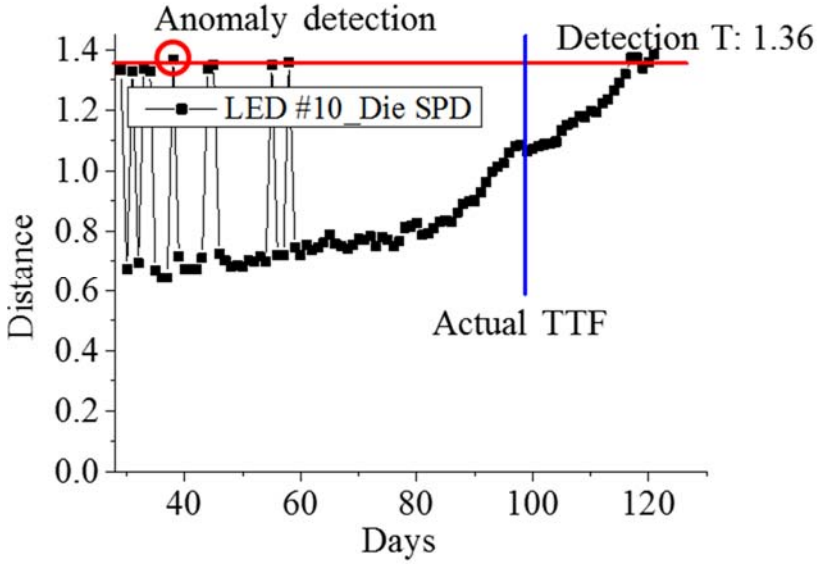


**Distance measure of cluster 2 from LED 10 for die peak.**

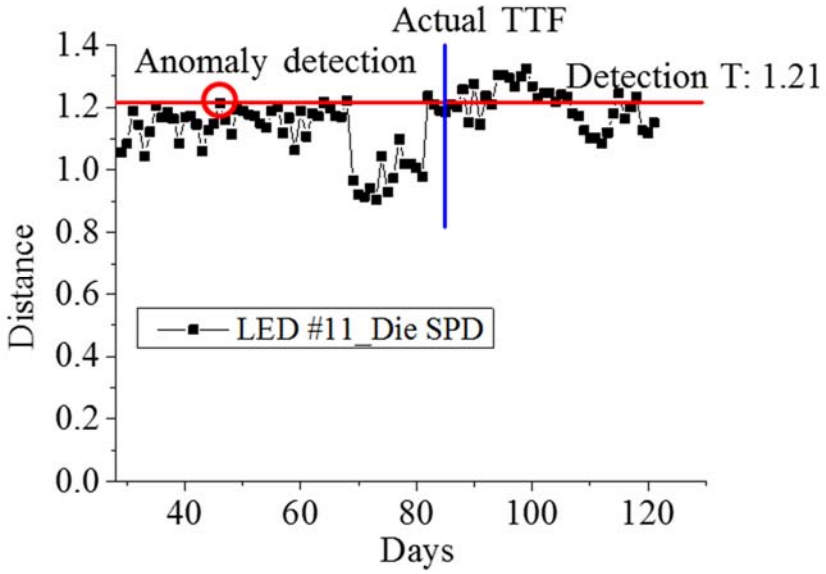


**Distance measure of cluster 3 from LED 11 for die peak.**

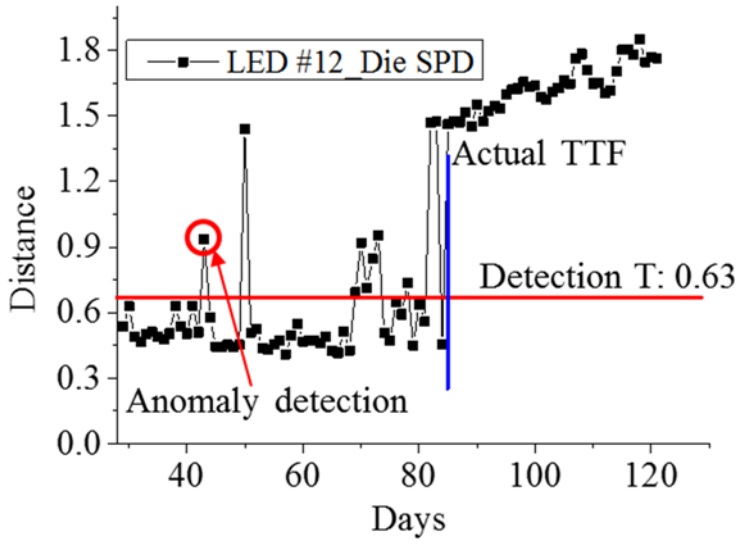


**Distance measure of cluster 4 from LED 12 for die peak.**

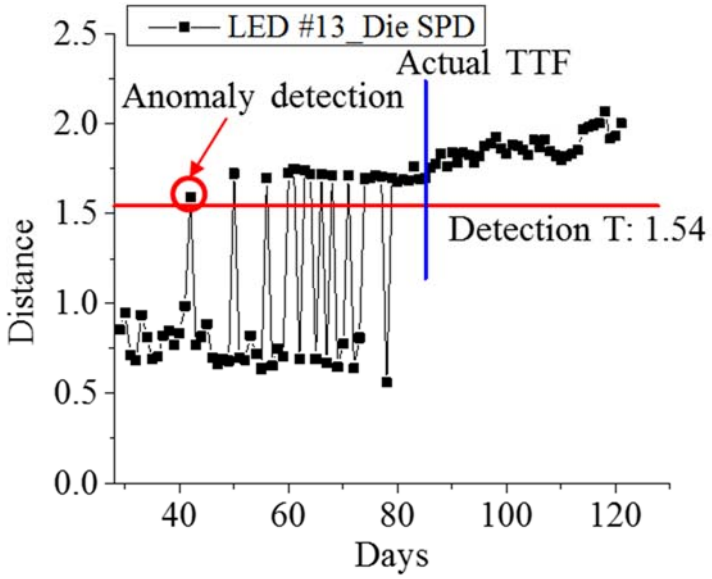


**Distance measure of cluster 7 from LED 13 for die peak.**

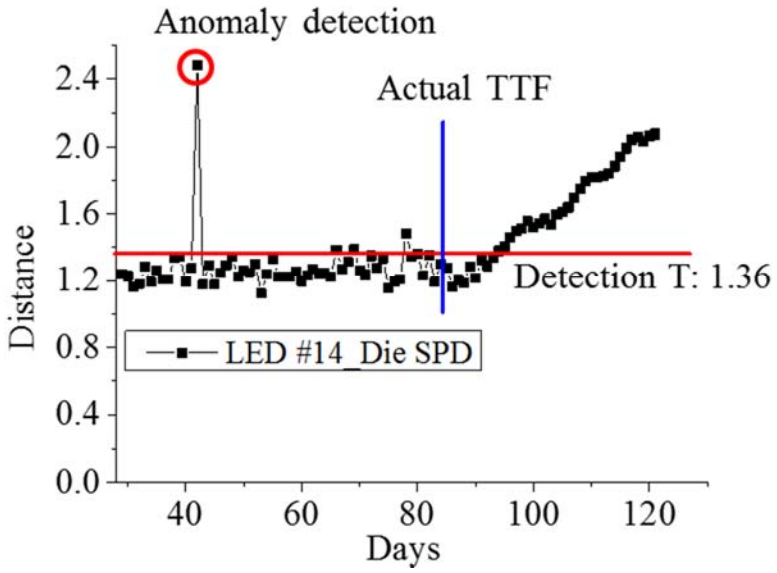


**Distance measure of cluster 2 from LED 14 for die peak.**

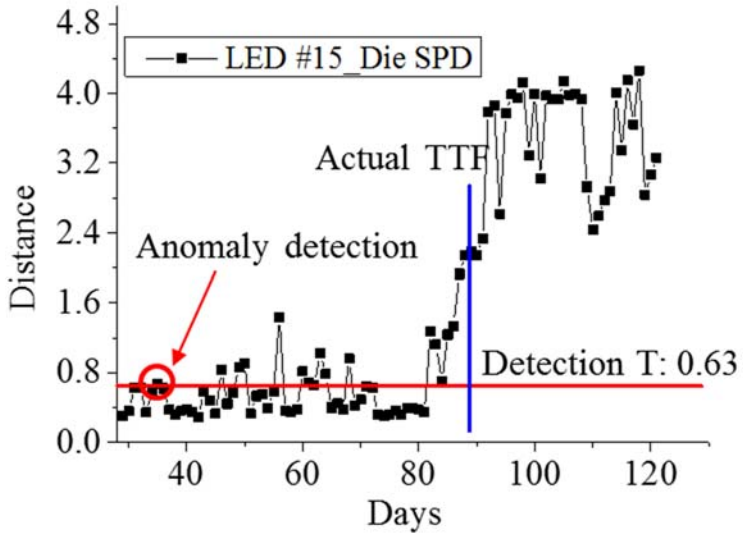


**Distance measure of cluster 4 from LED 15 for die peak.**

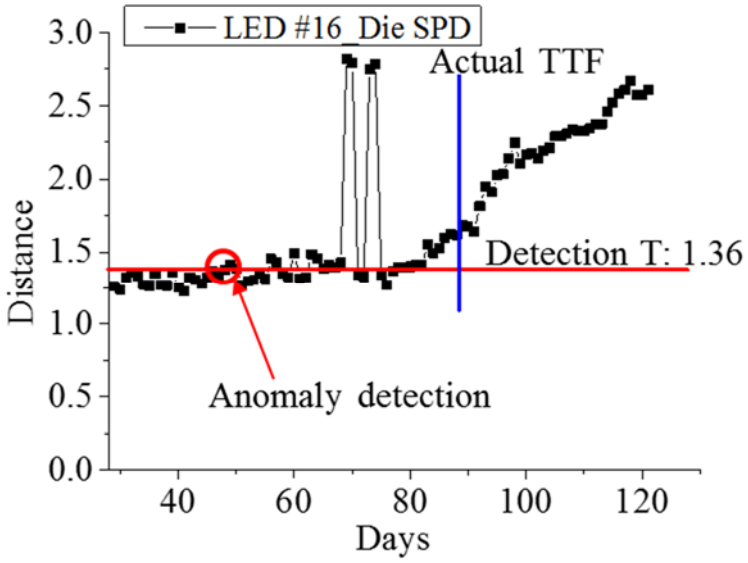


**Distance measure of cluster 2 from LED 16 for die peak.**

2. Anomaly detection results for phosphor peak under the condition with 350mA drive current and chamber temperature 40°C

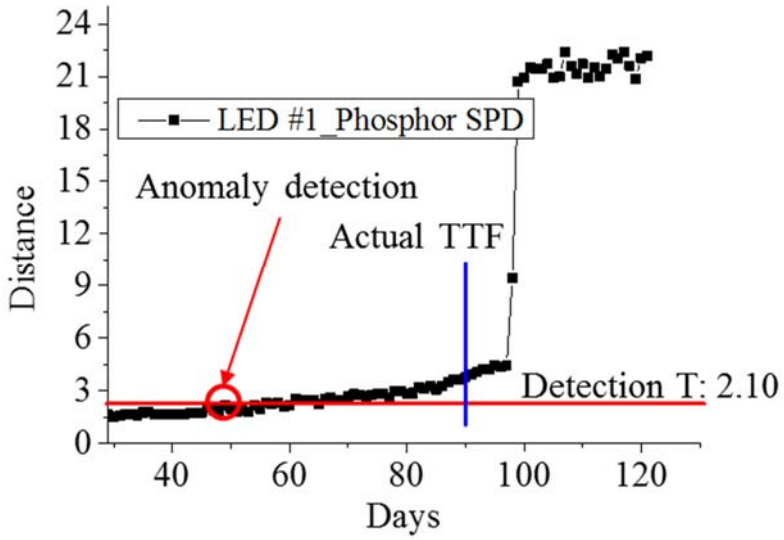


**Distance measure of cluster 2 from LED 1 for phosphor peak.**

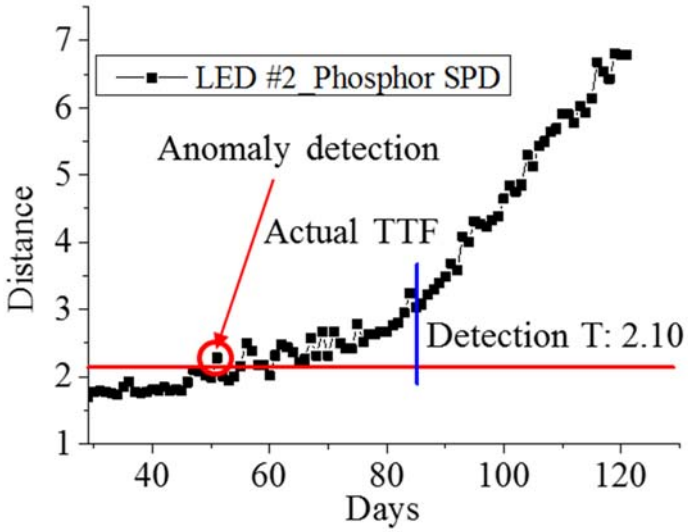


**Distance measure of cluster 2 from LED 2 for phosphor peak.**

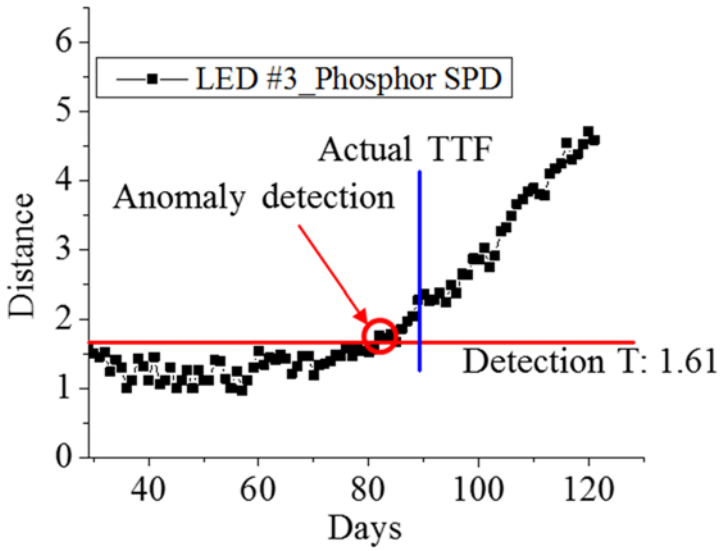


**Distance measure of cluster 1 from LED 3 for phosphor peak.**

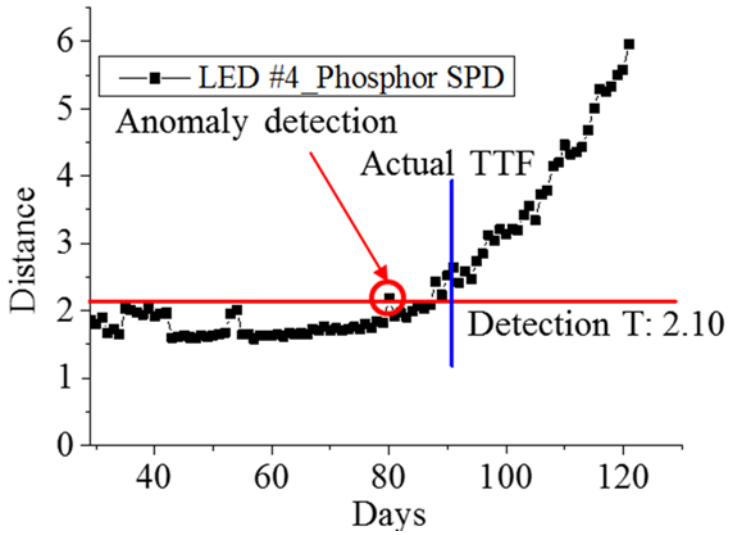


**Distance measure of cluster 2 from LED 4 for phosphor peak.**

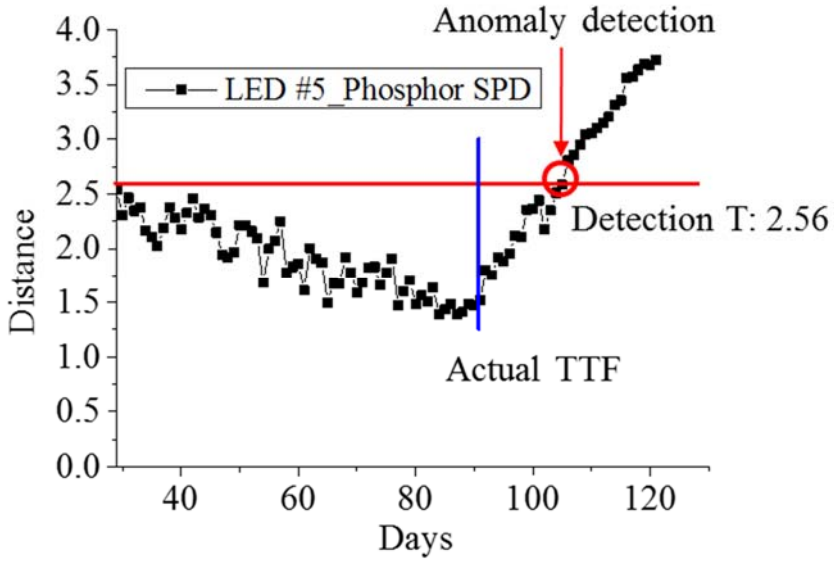


**Distance measure of cluster 6 from LED 5 for phosphor peak.**

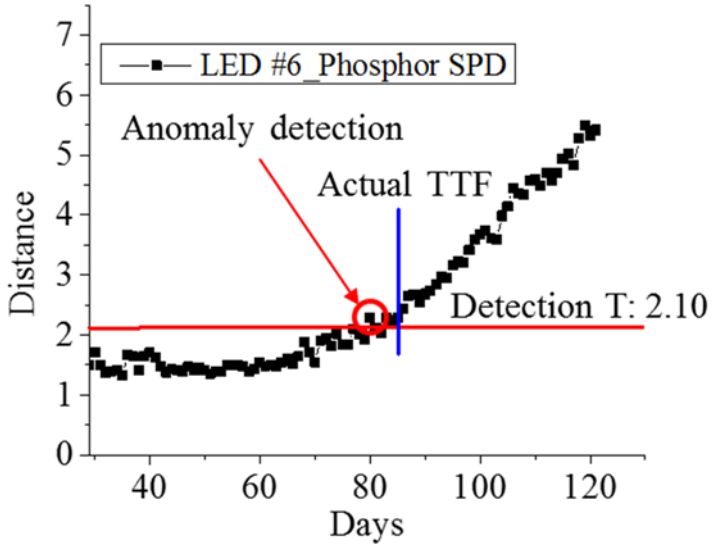


**Distance measure of cluster 2 from LED 6 for phosphor peak.**

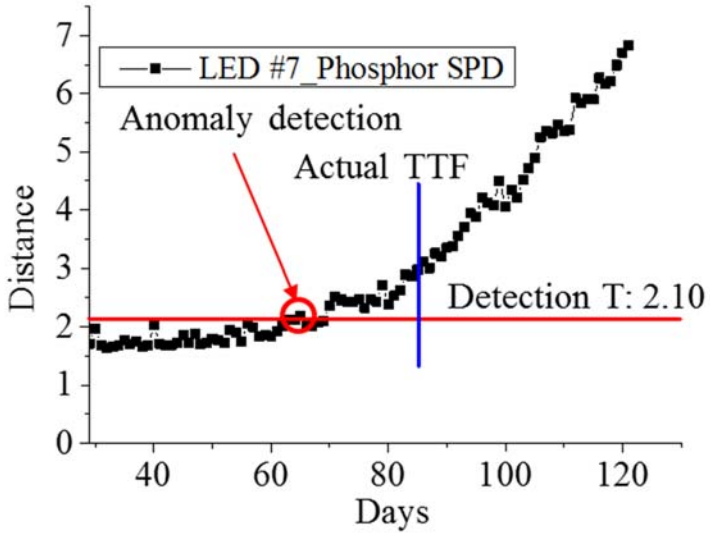


**Distance measure of cluster 2 from LED 7 for phosphor peak.**

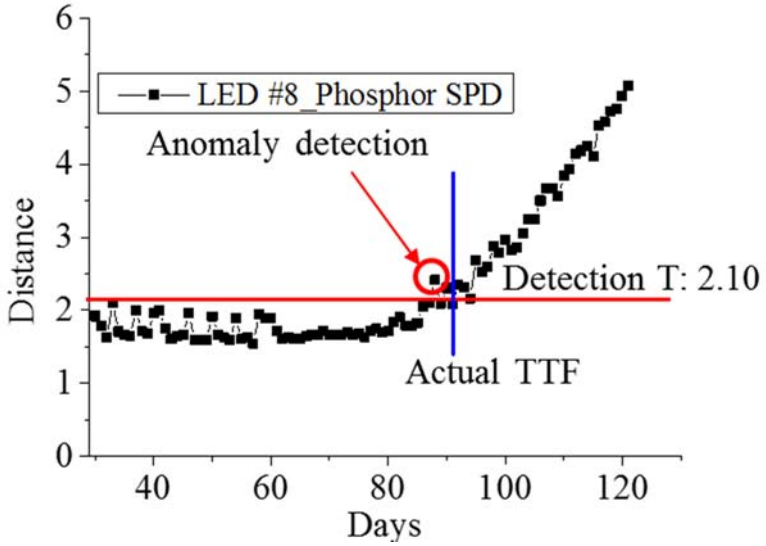


**Distance measure of cluster 2 from LED 8 for phosphor peak.**

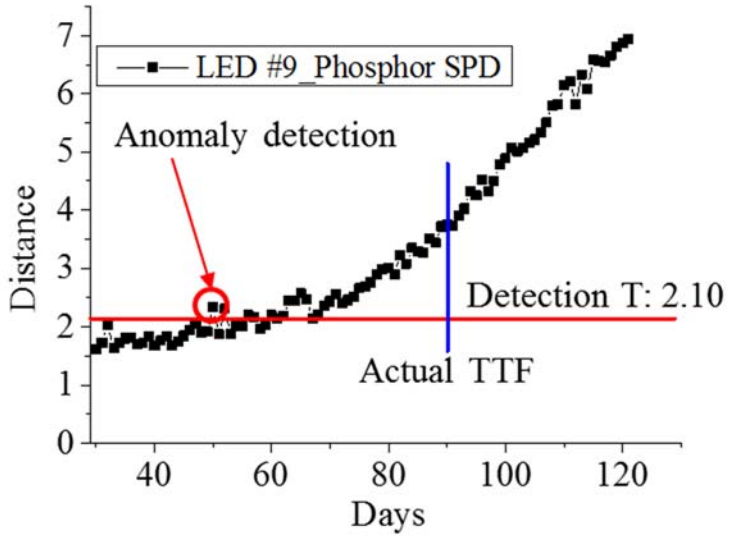


**Distance measure of cluster 2 from LED 9 for phosphor peak.**

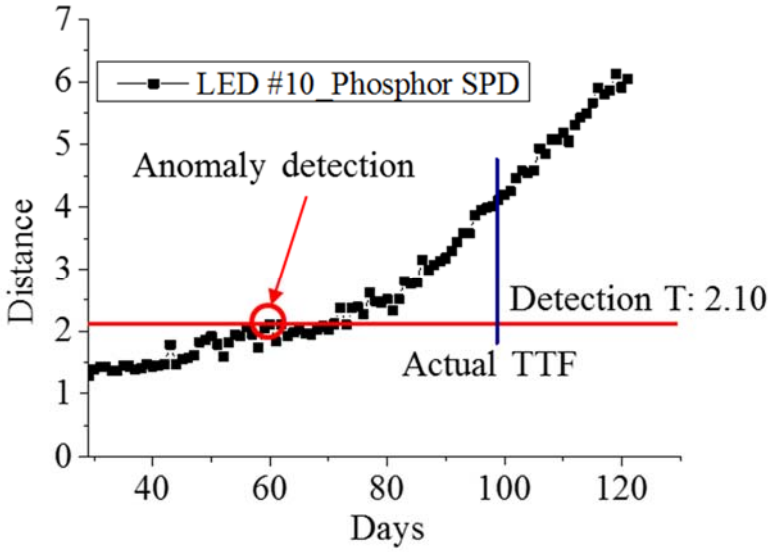


**Distance measure of cluster 2 from LED 10 for phosphor peak.**

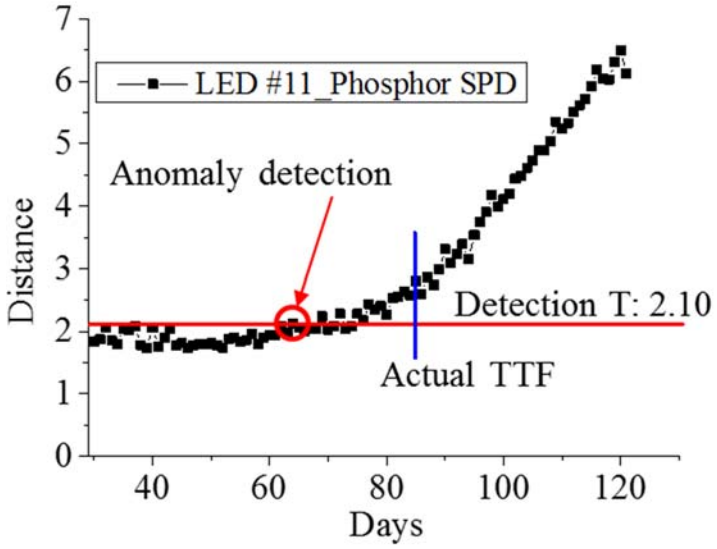


**Distance measure of cluster 2 from LED 11 for phosphor peak.**

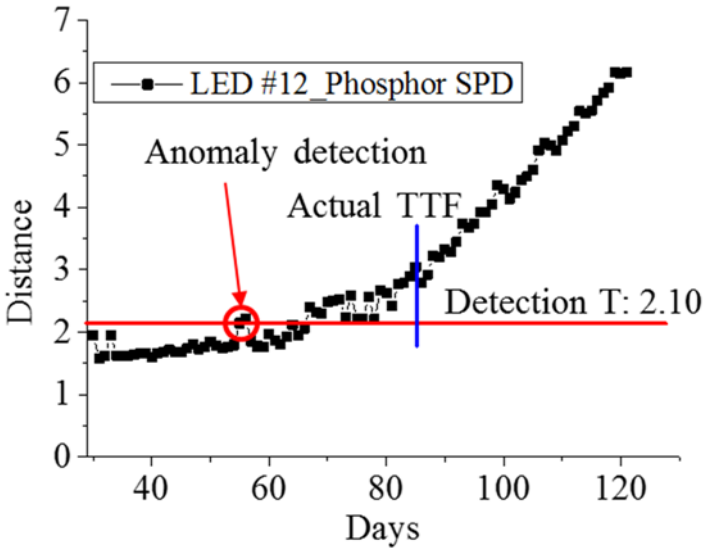


**Distance measure of cluster 2 from LED 12 for phosphor peak.**

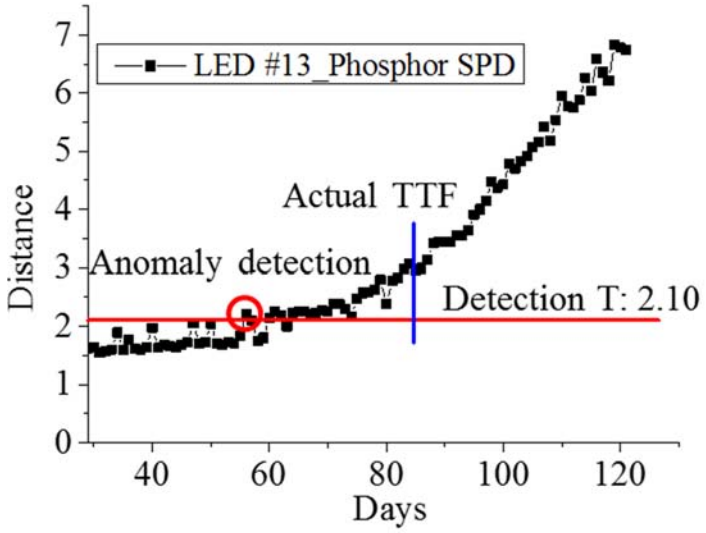


**Distance measure of cluster 2 from LED 13 for phosphor peak.**

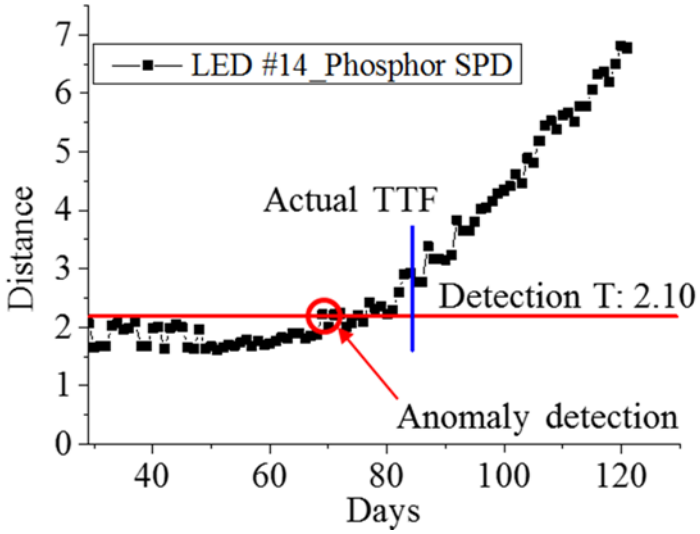


**Distance measure of cluster 2 from LED 14 for phosphor peak.**

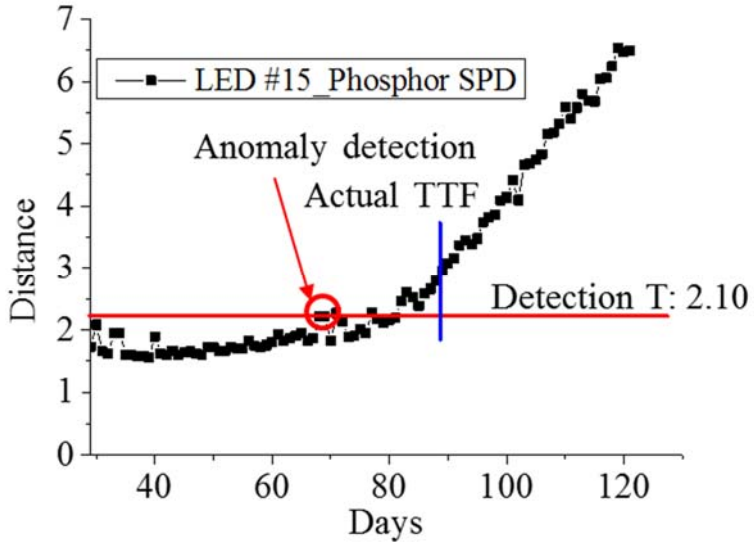


**Distance measure of cluster 2 from LED 15 for phosphor peak.**

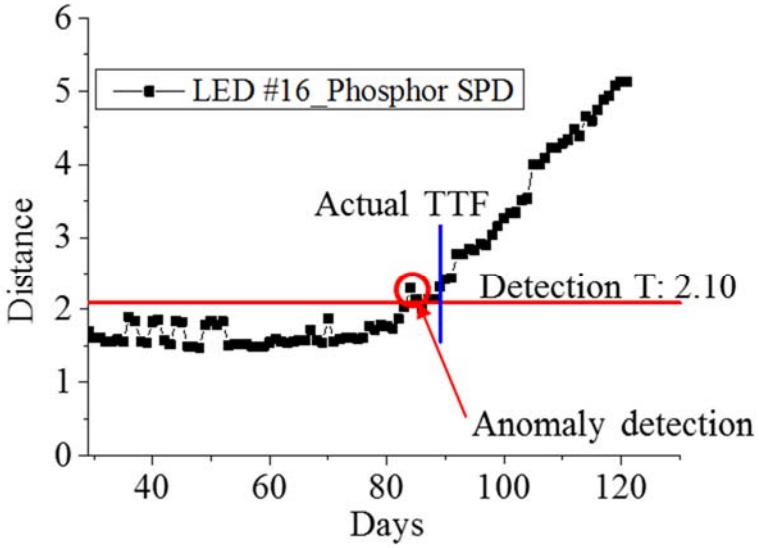


**Distance measure of cluster 2 from LED 16 for phosphor peak.**

3. Anomaly detection results for LED die peak based on five points adjacent moving averaging of distance measures under the condition with 350mA drive current and chamber temperature 40°C

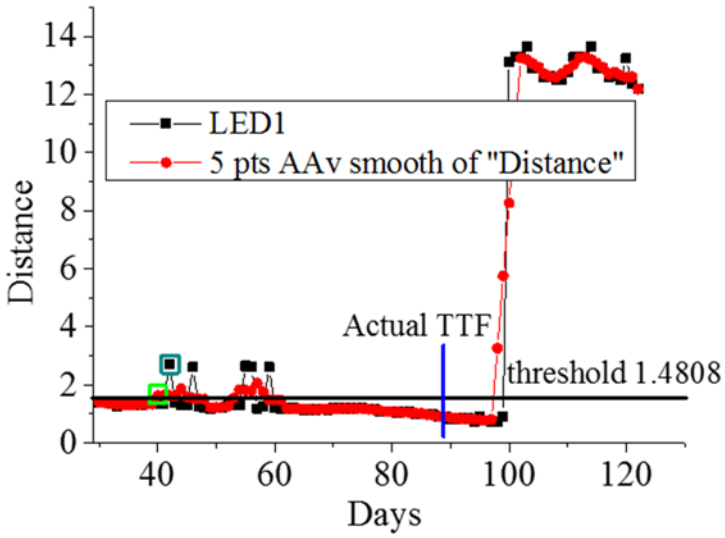


**Comparison of anomaly detection results for the die peak of LED 1.**

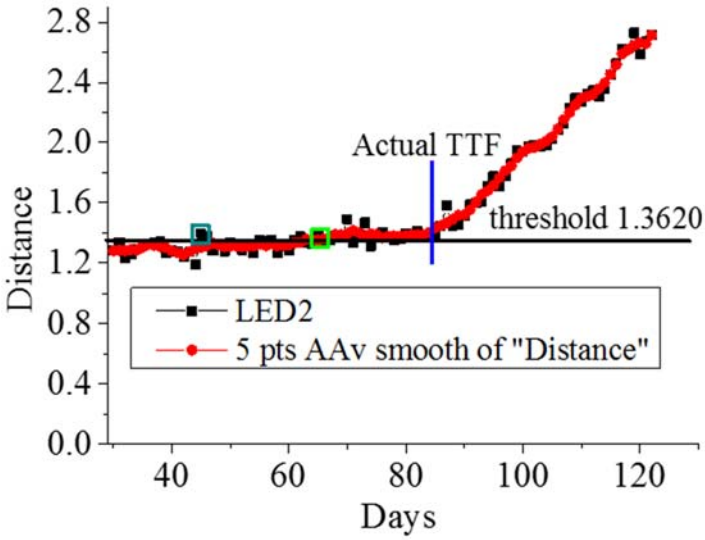


**Comparison of anomaly detection results for the die peak of LED 2.**

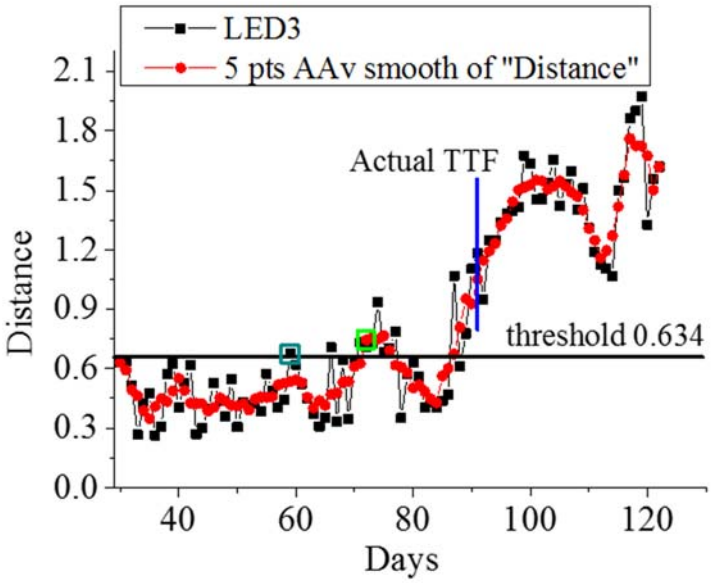


**Comparison of anomaly detection results for the die peak of LED 3.**

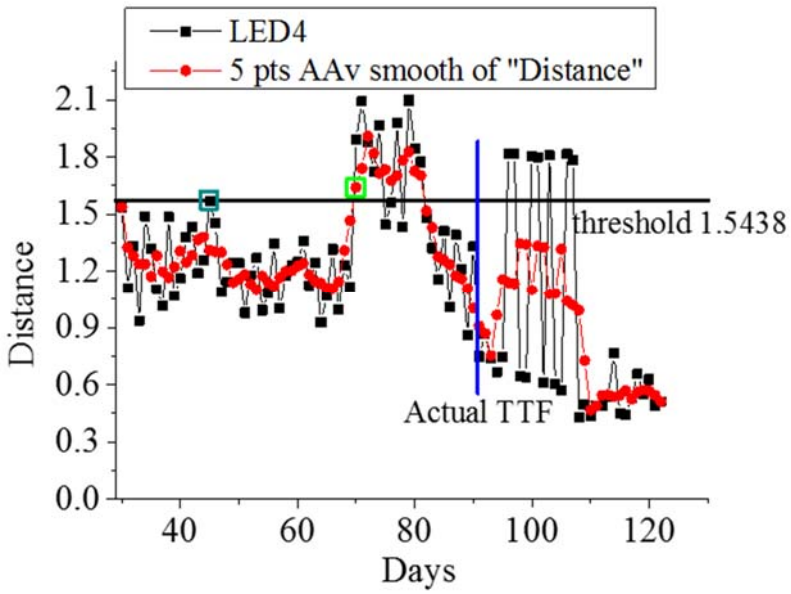


**Comparison of anomaly detection results for the die peak of LED 4.**

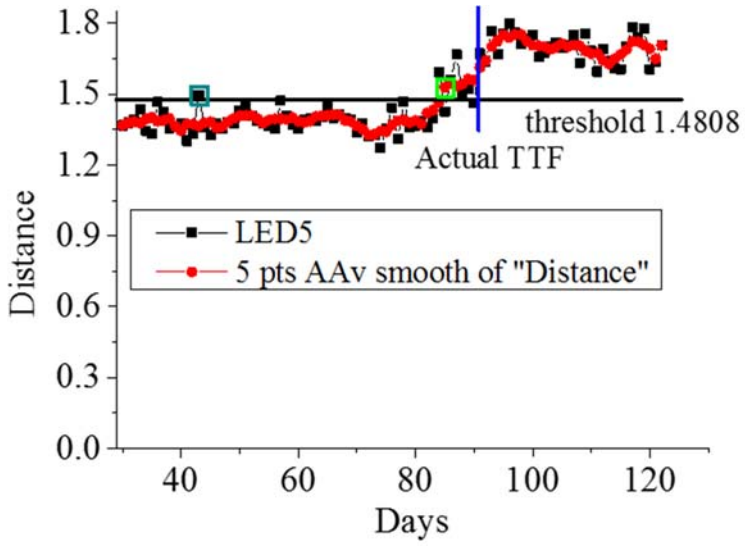


**Comparison of anomaly detection results for the die peak of LED 5.**

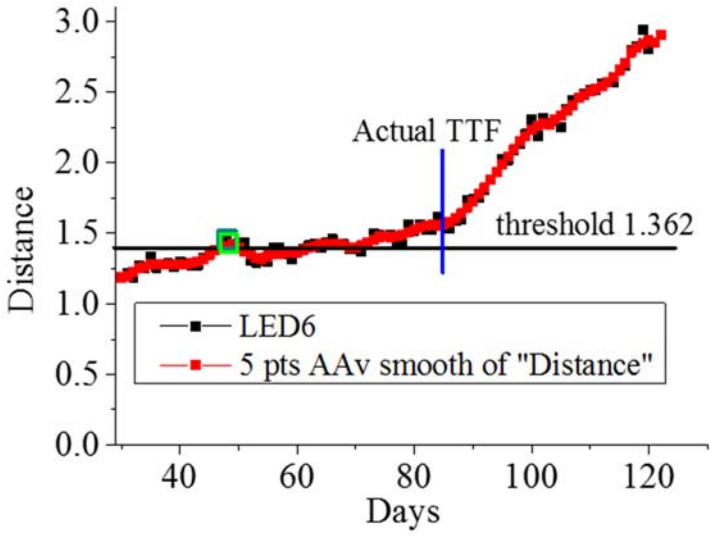


**Comparison of anomaly detection results for the die peak of LED 6.**

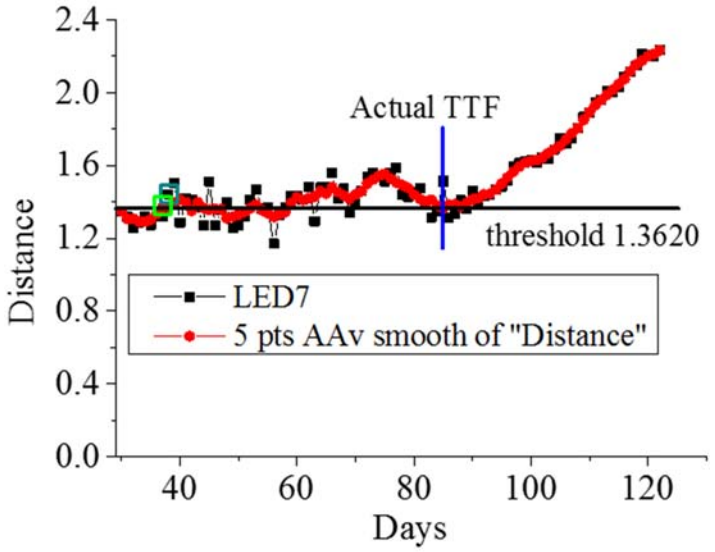


**Comparison of anomaly detection results for the die peak of LED 7.**

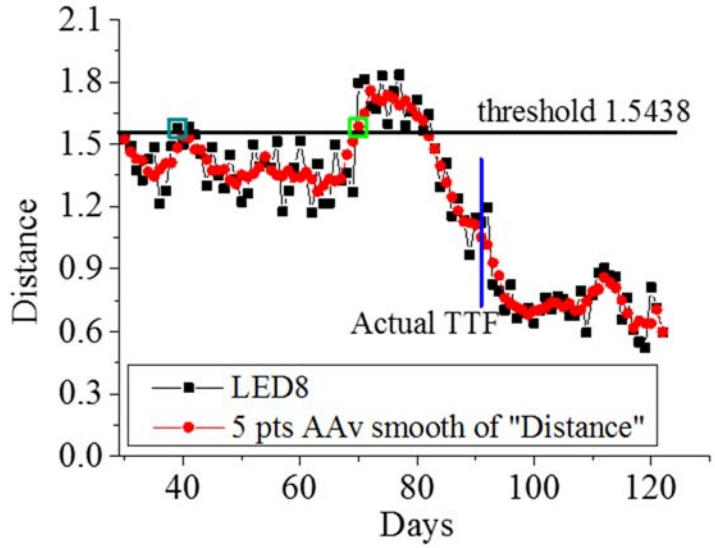


**Comparison of anomaly detection results for the die peak of LED 8.**

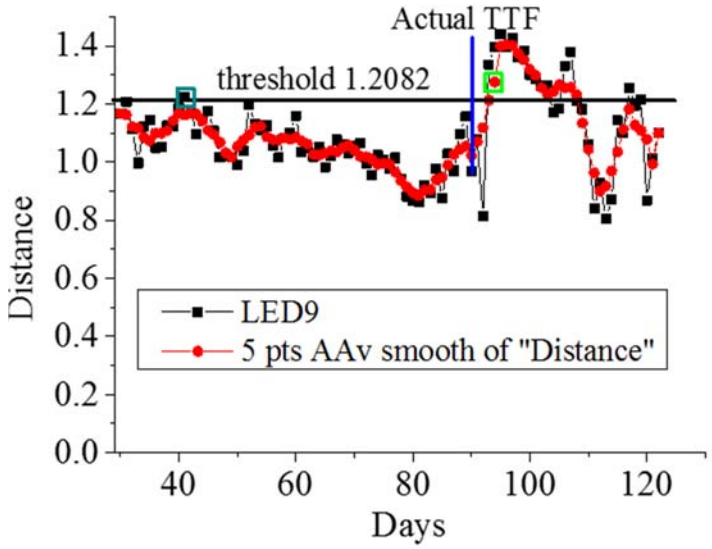


**Comparison of anomaly detection results for the die peak of LED 9.**

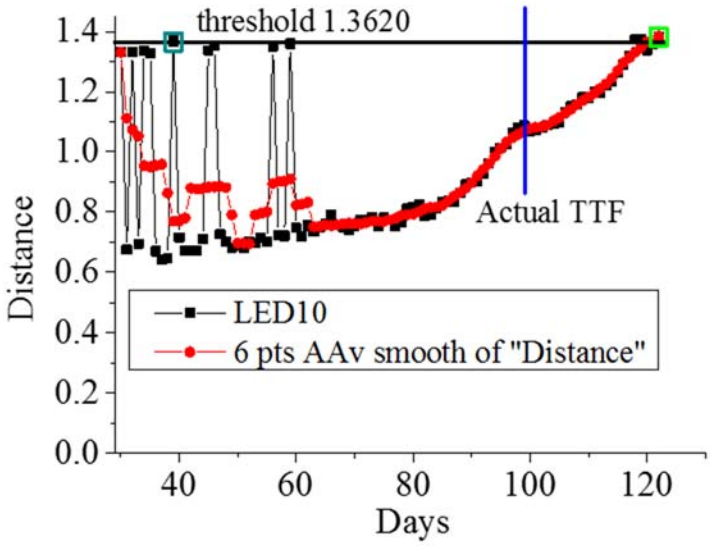


**Comparison of anomaly detection results for the die peak of LED 10.**

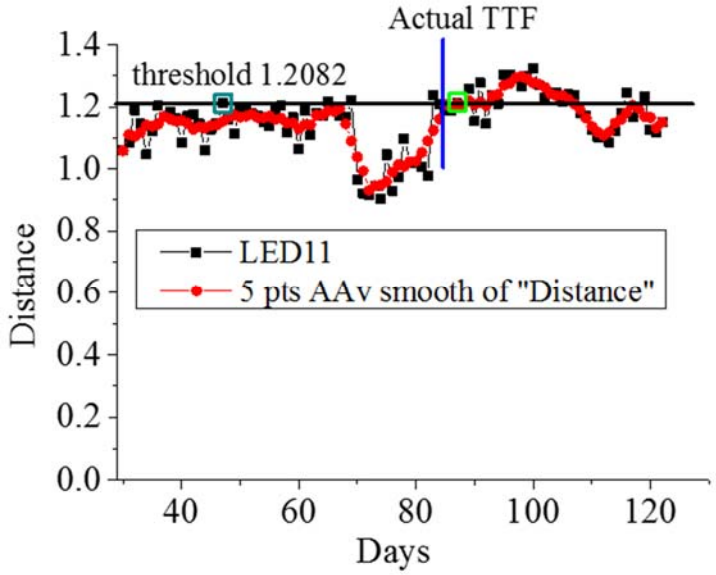


**Comparison of anomaly detection results for the die peak of LED 11.**

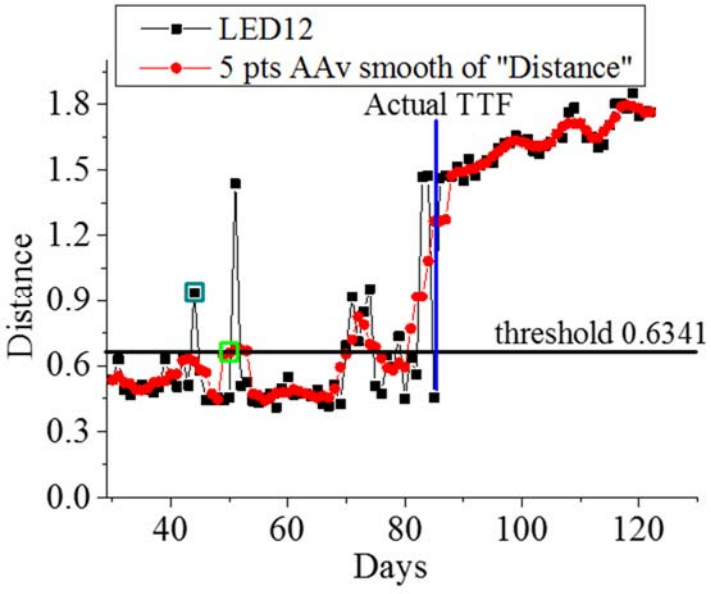


**Comparison of anomaly detection results for the die peak of LED 12.**

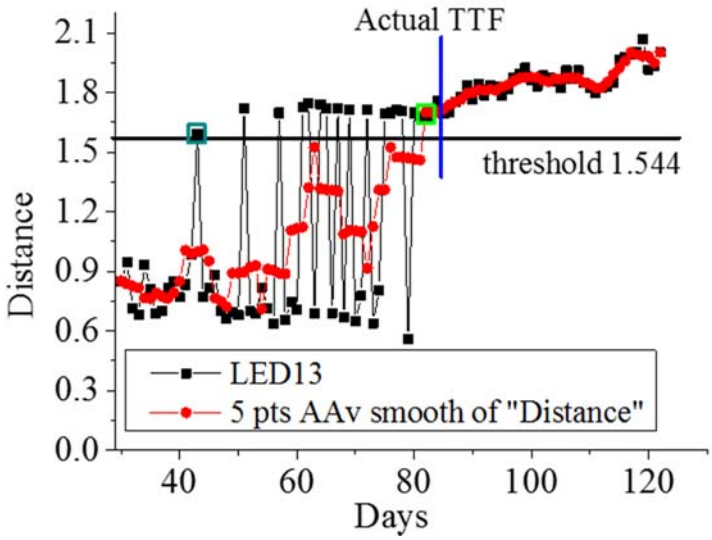


**Comparison of anomaly detection results for the die peak of LED 13.**

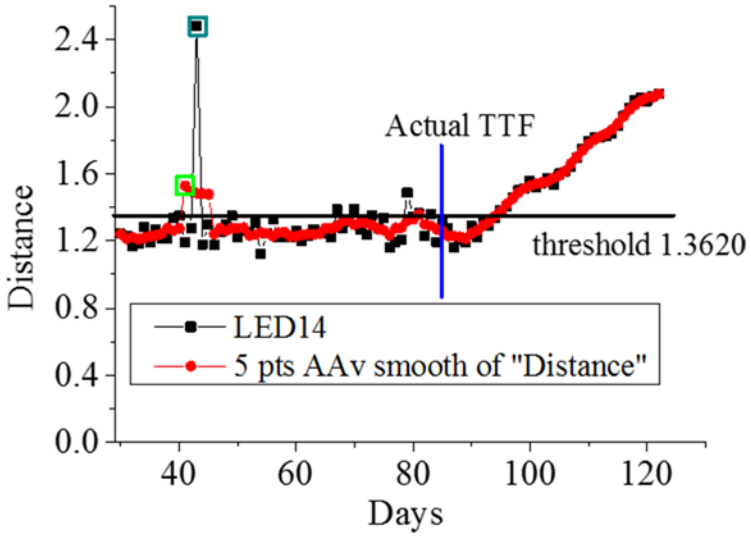


**Comparison of anomaly detection results for the die peak of LED 14.**

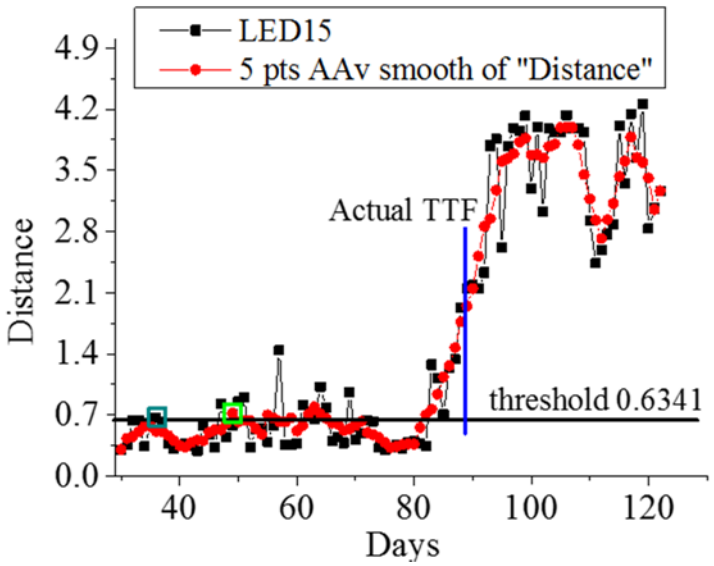


**Comparison of anomaly detection results for the die peak of LED 15.**

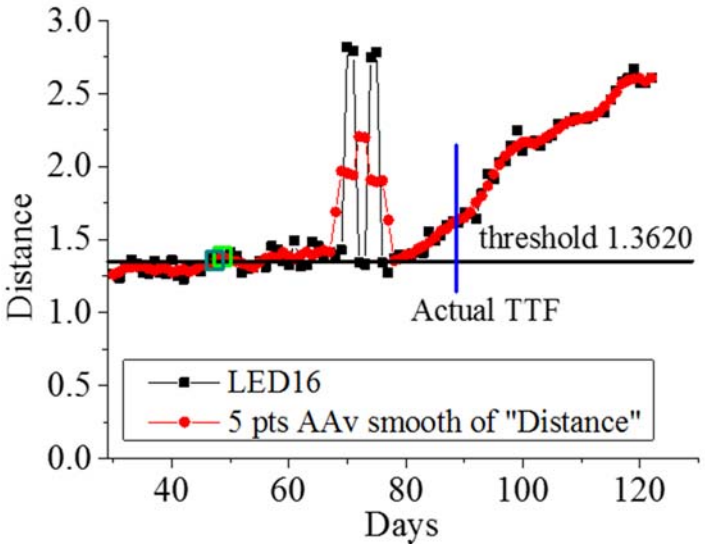


**Comparison of anomaly detection results for the die peak of LED 16.**

4. Anomaly detection results for LED phosphor peak based on five points adjacent moving averaging of distance measures under the condition with 350mA drive current and chamber temperature 40°C

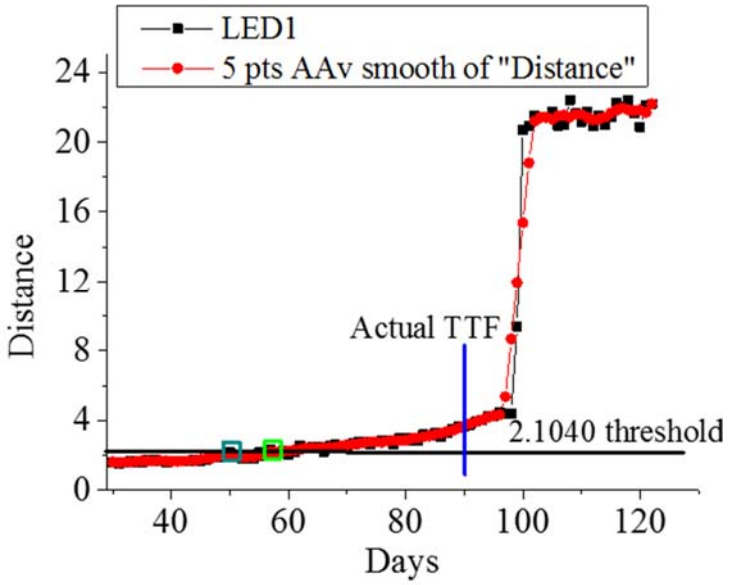


**Comparison of anomaly detection results for the phosphor peak of LED 1.**

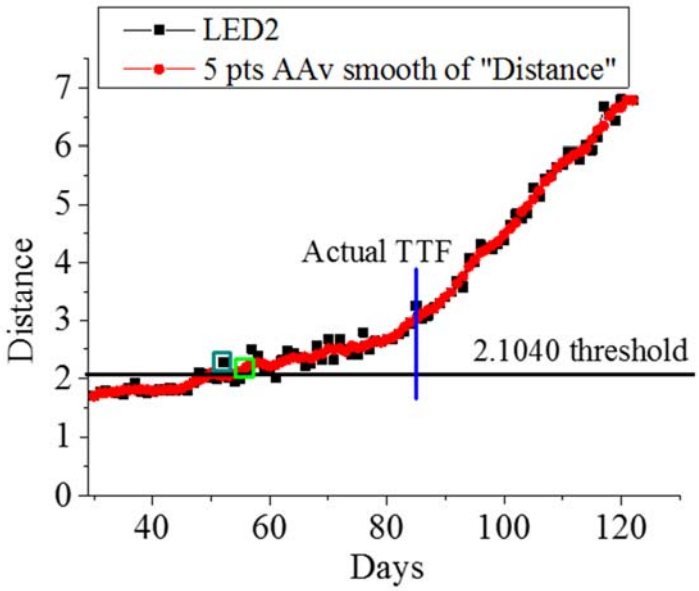


**Comparison of anomaly detection results for the phosphor peak of LED 2.**

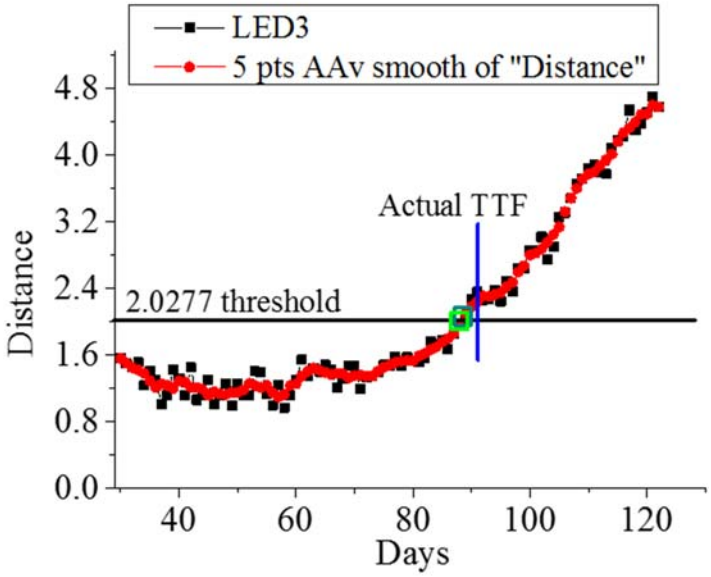


**Comparison of anomaly detection results for the phosphor peak of LED 3.**

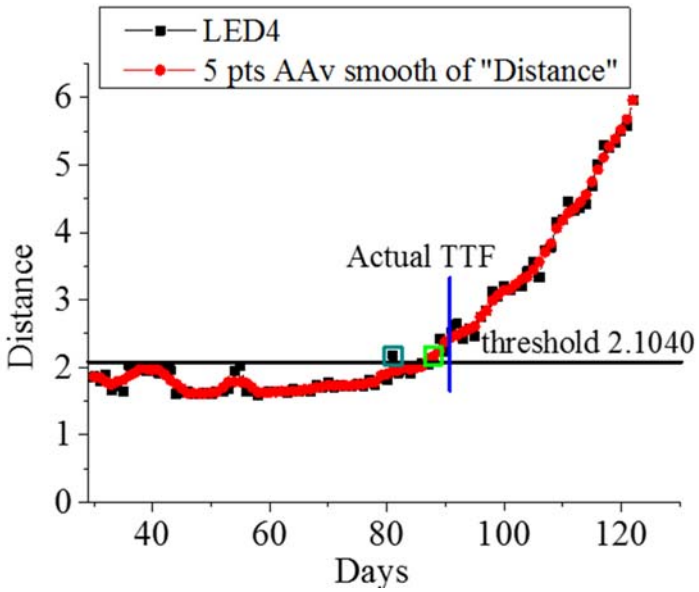


**Comparison of anomaly detection results for the phosphor peak of LED 4.**

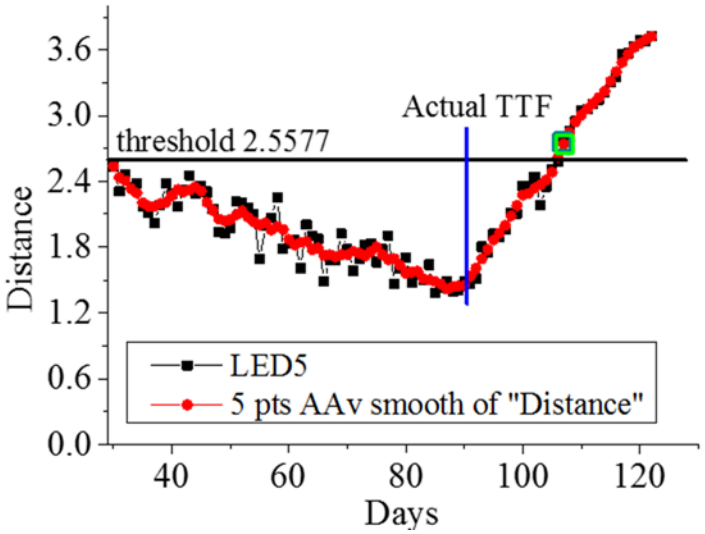


**Comparison of anomaly detection results for the phosphor peak of LED 5.**

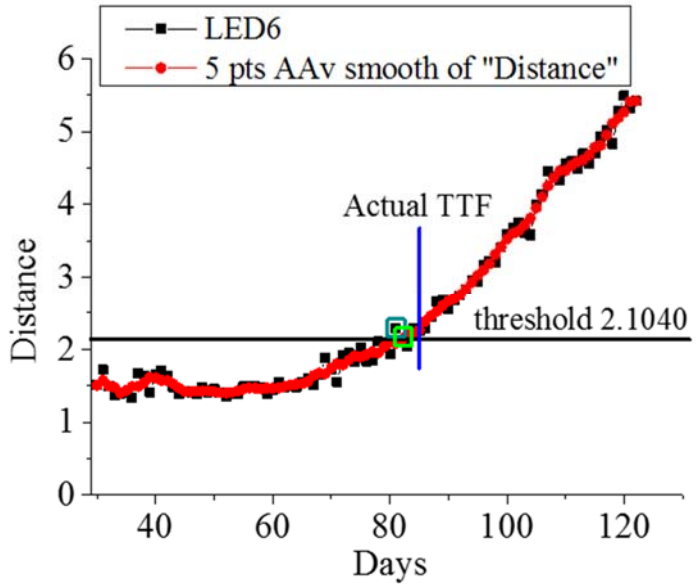


**Comparison of anomaly detection results for the phosphor peak of LED 6.**

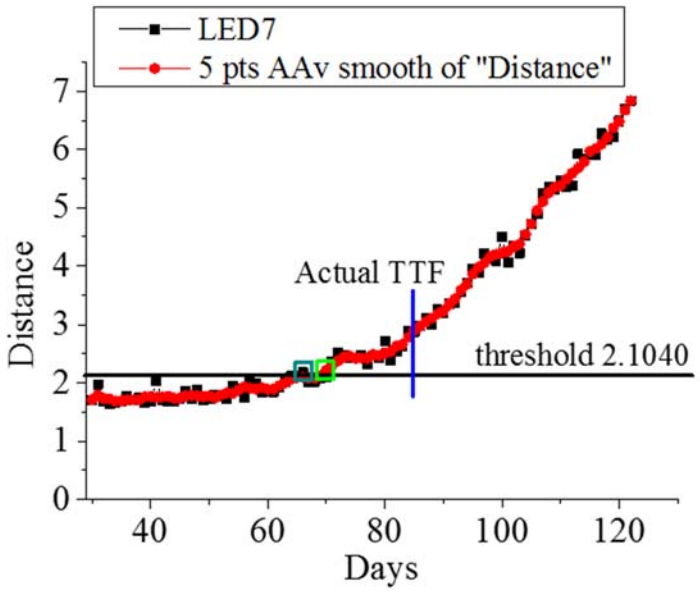


**Comparison of anomaly detection results for the phosphor peak of LED 7.**

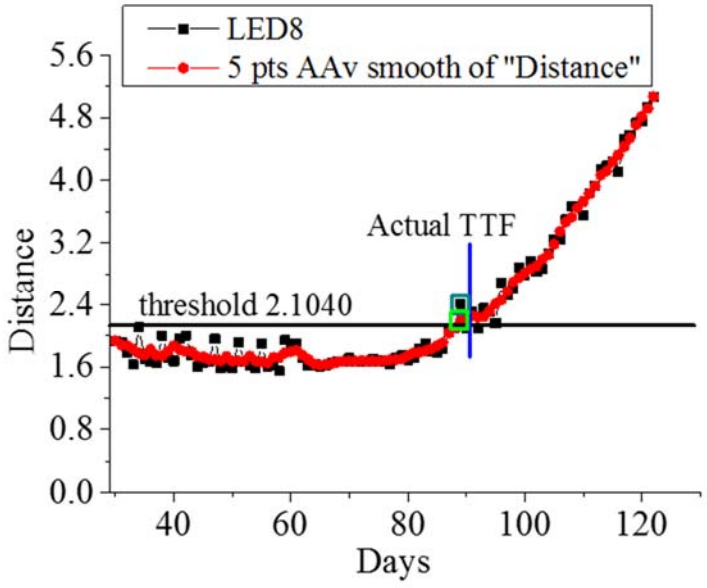


**Comparison of anomaly detection results for the phosphor peak of LED 8.**

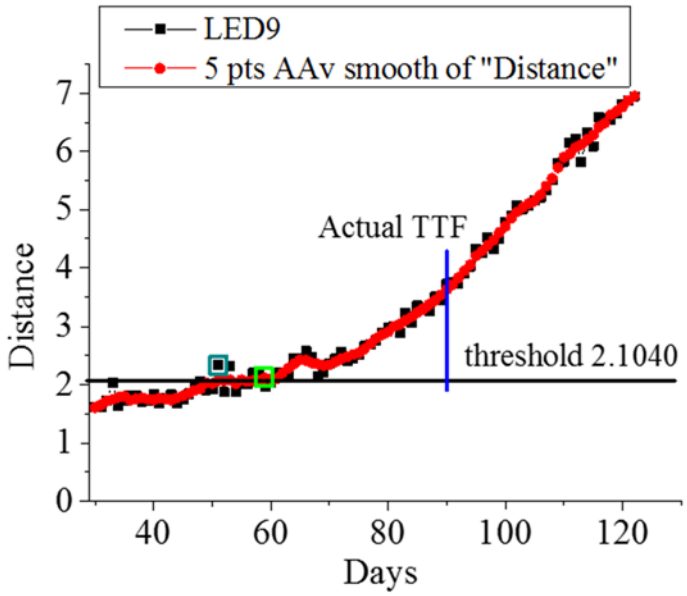


**Comparison of anomaly detection results for the phosphor peak of LED 9.**

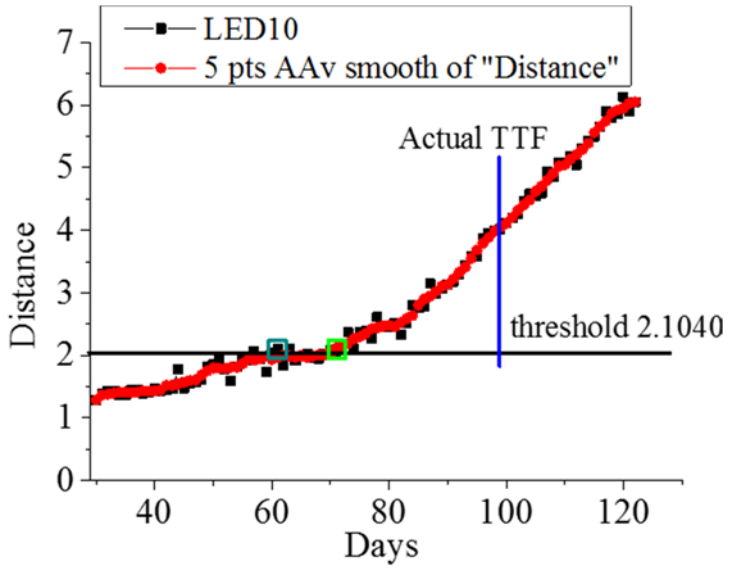


**Comparison of anomaly detection results for the phosphor peak of LED 10.**

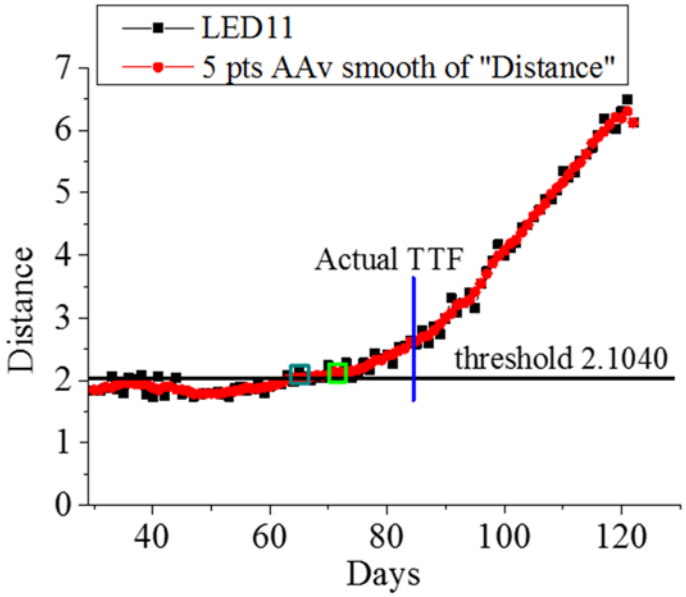


**Comparison of anomaly detection results for the phosphor peak of LED 11.**

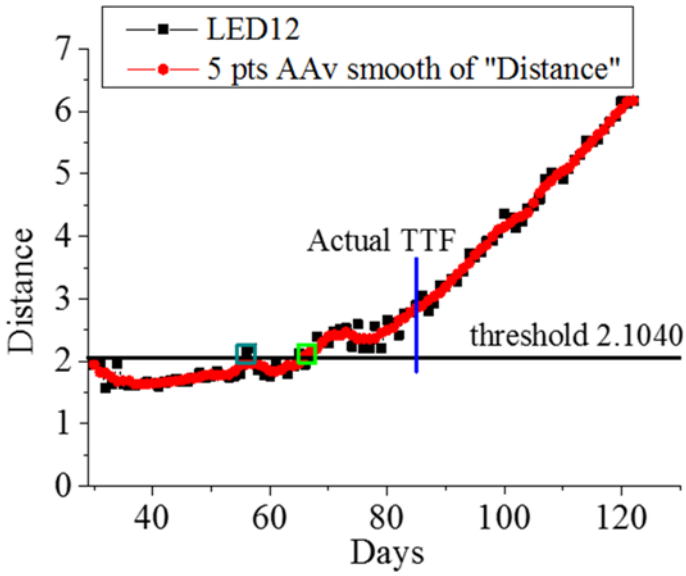


**Comparison of anomaly detection results for the phosphor peak of LED 12.**

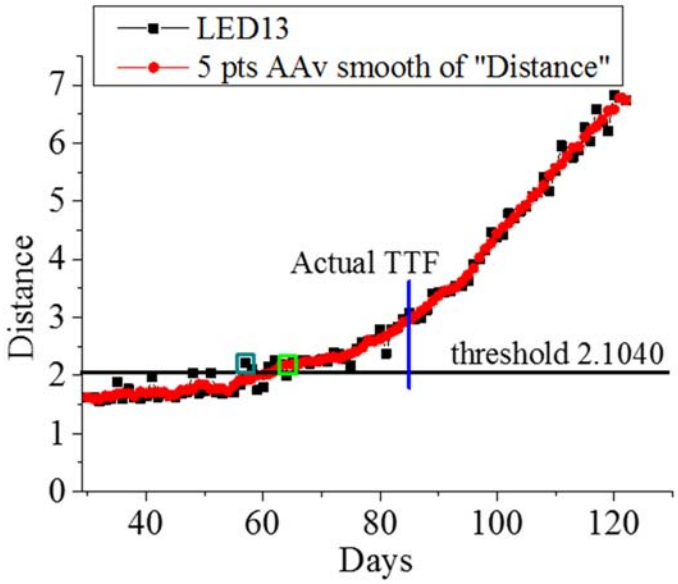


**Comparison of anomaly detection results for the phosphor peak of LED 13.**

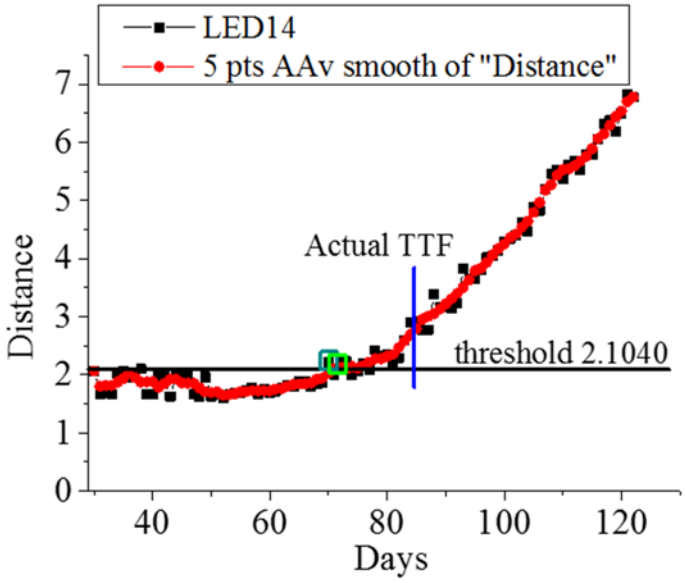


**Comparison of anomaly detection results for the phosphor peak of LED 14.**

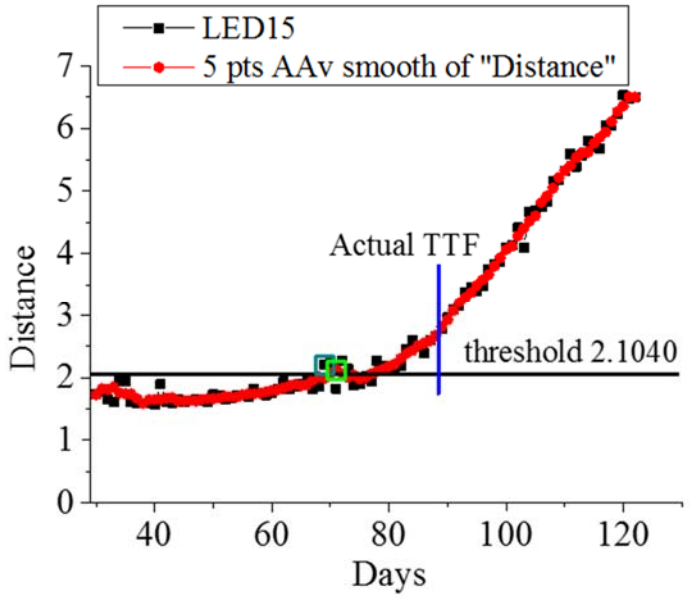


**Comparison of anomaly detection results for the phosphor peak of LED 15.**

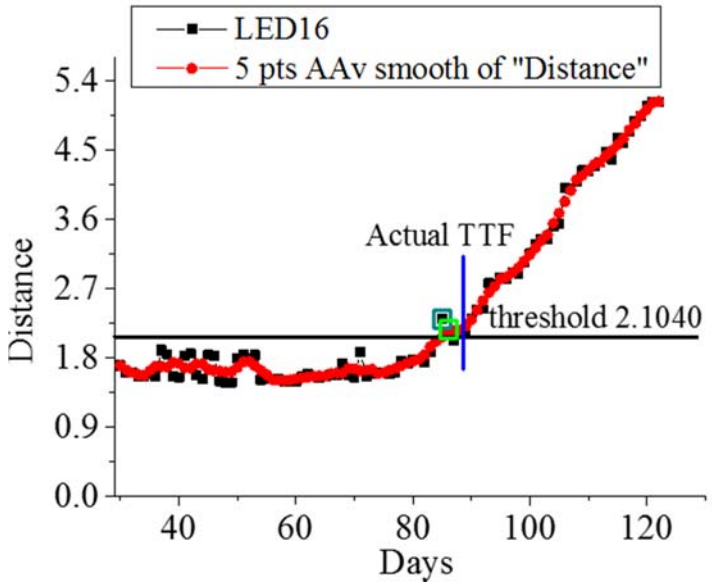


**Comparison of anomaly detection results for the phosphor peak of LED 16.**

# Appendix C: Anomaly Detection Results under the Condition of 200mA Drive Current and Chamber Temperature 90°C

1. Anomaly detection results for LED die peak under the condition of 200mA drive current and chamber temperature 90°C

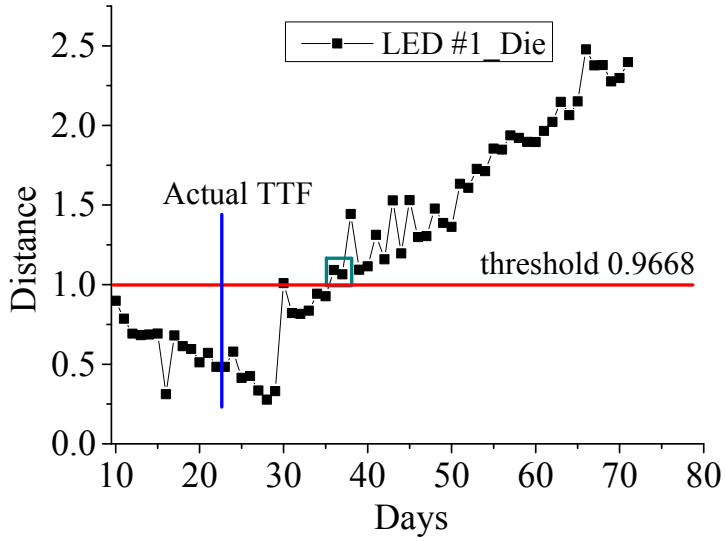


**Distance measure of cluster 1 from LED 1 for die peak.**

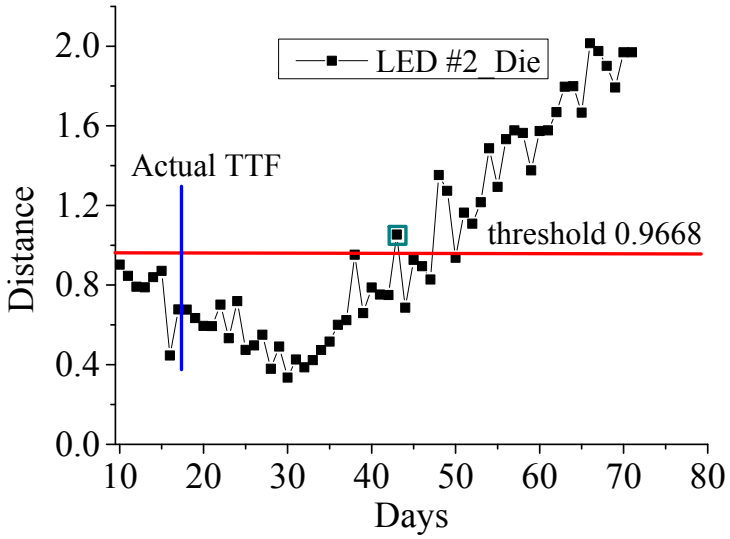


**Distance measure of cluster 2 from LED 2 for die peak.**

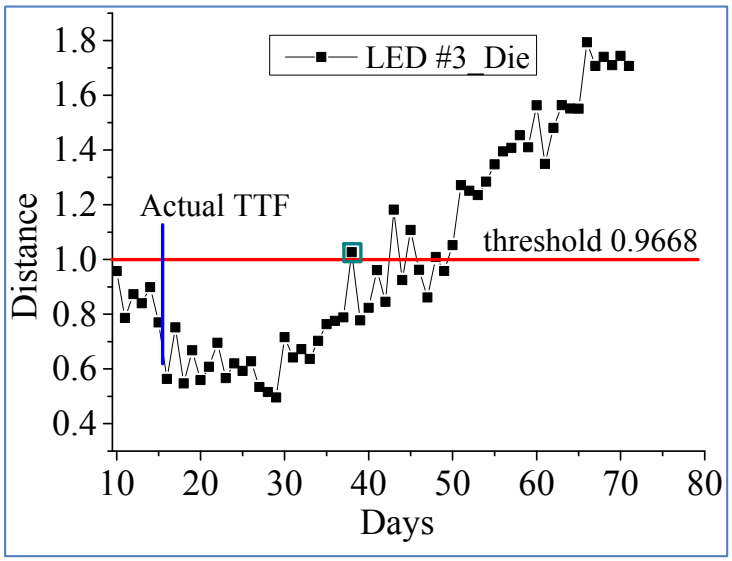


**Distance measure of cluster 2 from LED 3 for die peak.**

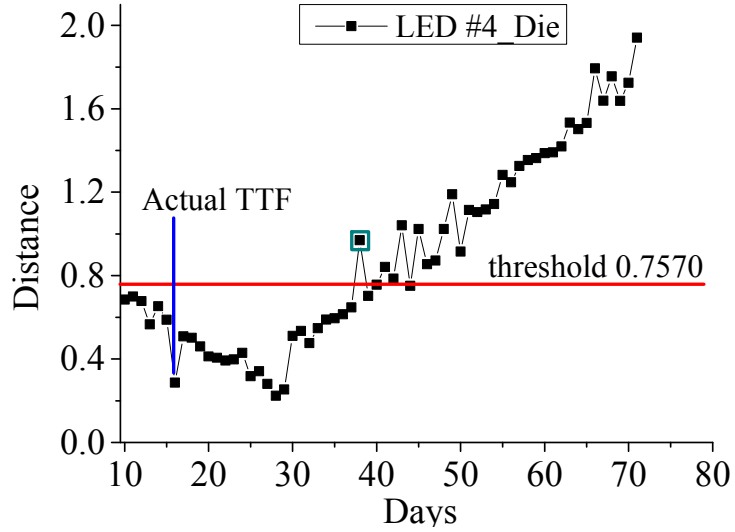


**Distance measure of cluster 3 from LED 4 for die peak.**

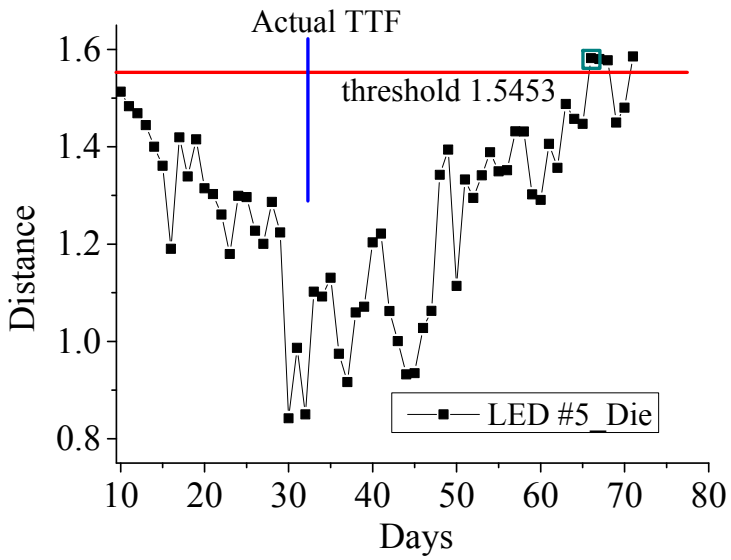


**Distance measure of cluster 5 from LED 5 for die peak.**

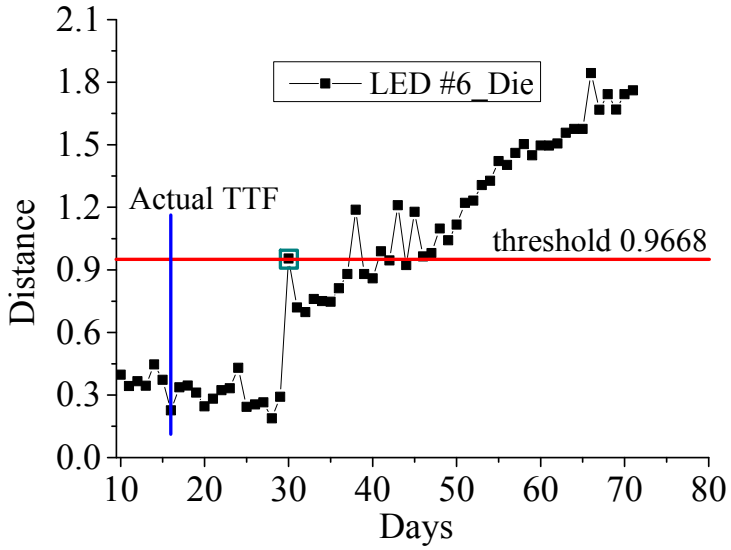


**Distance measure of cluster 2 from LED 6 for die peak.**

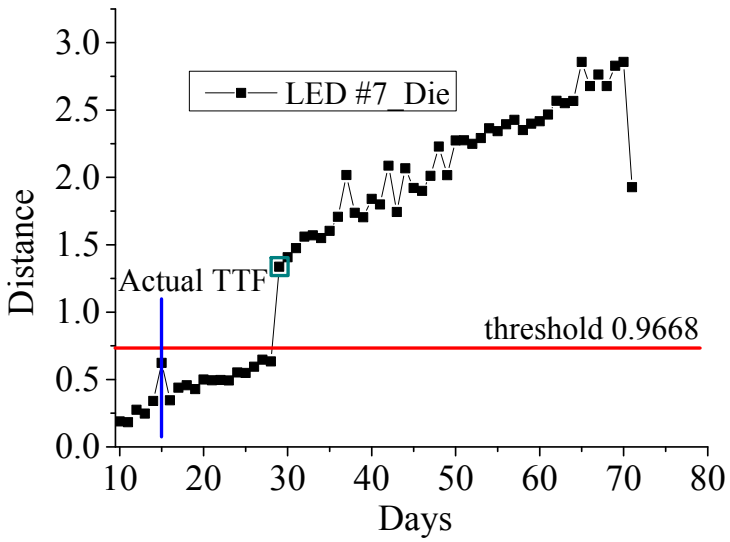


**Distance measure of cluster 3 from LED 7 for die peak.**

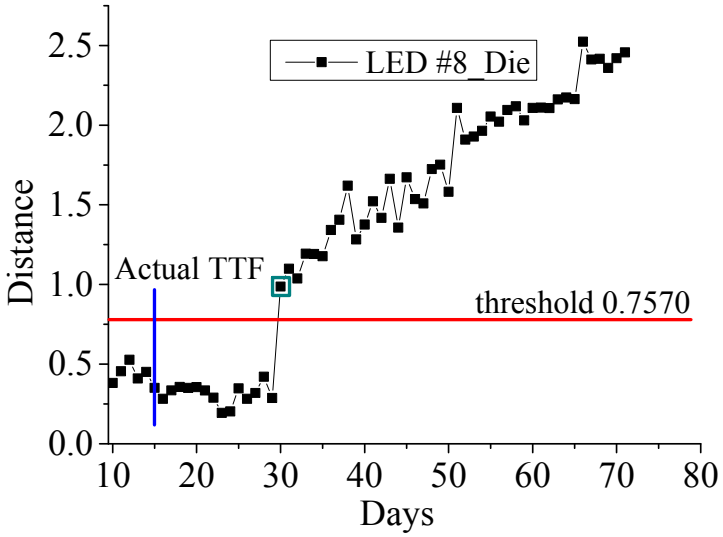


**Distance measure of cluster 3 from LED 8 for die peak.**

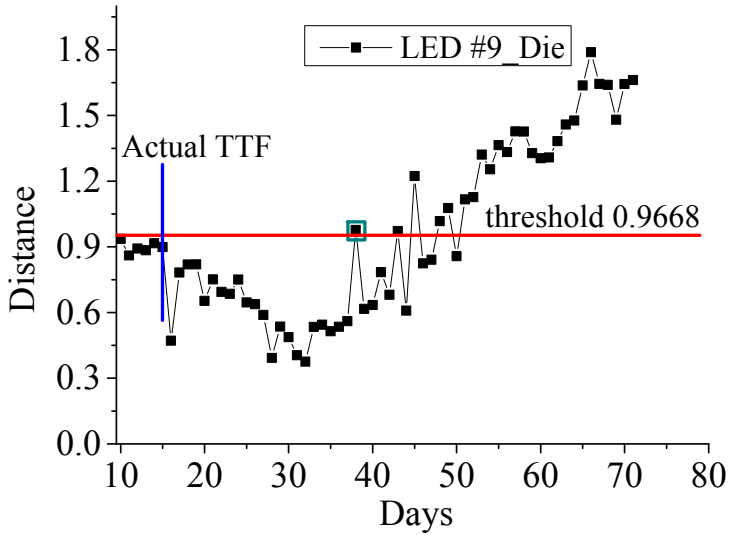


**Distance measure of cluster 2 from LED 9 for die peak.**

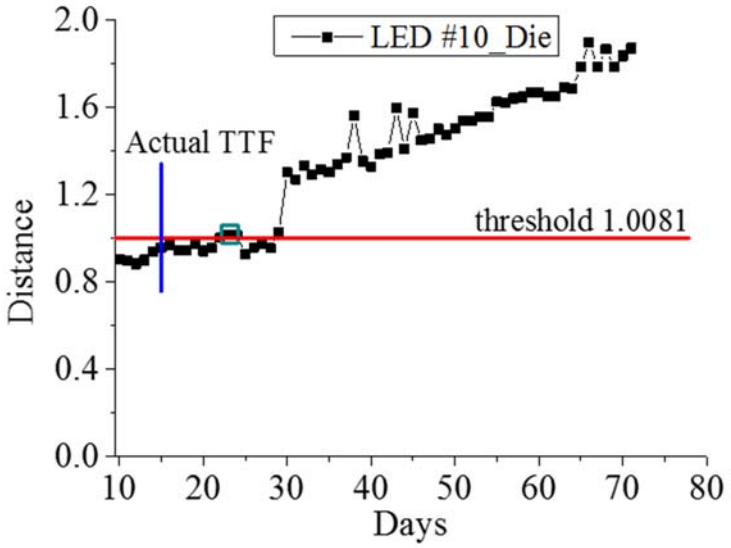


**Distance measure of cluster 1 from LED 10 for die peak.**

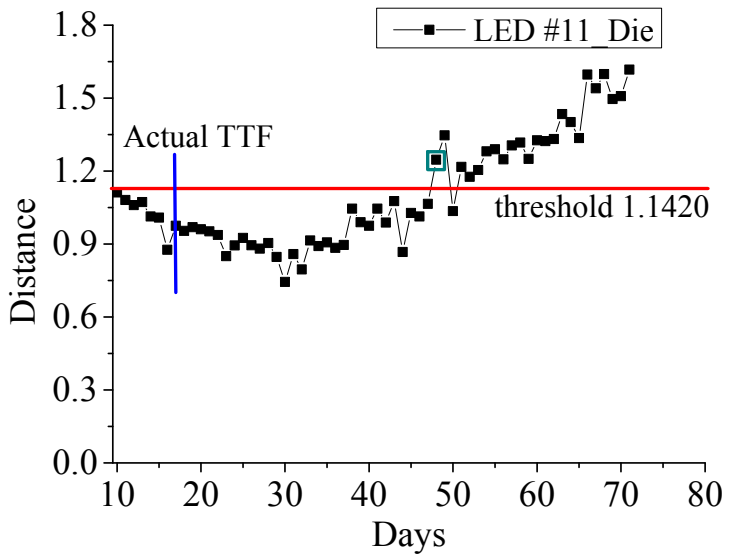


**Distance measure of cluster 7 from LED 11 for die peak.**

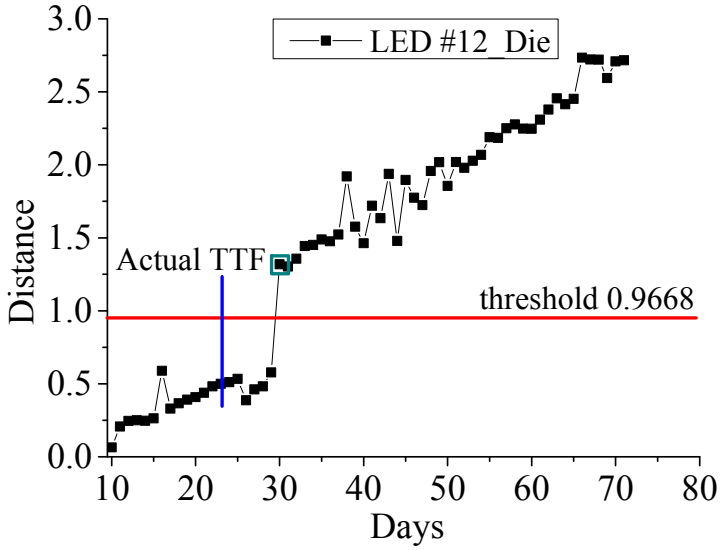


**Distance measure of cluster 2 from LED 12 for die peak.**

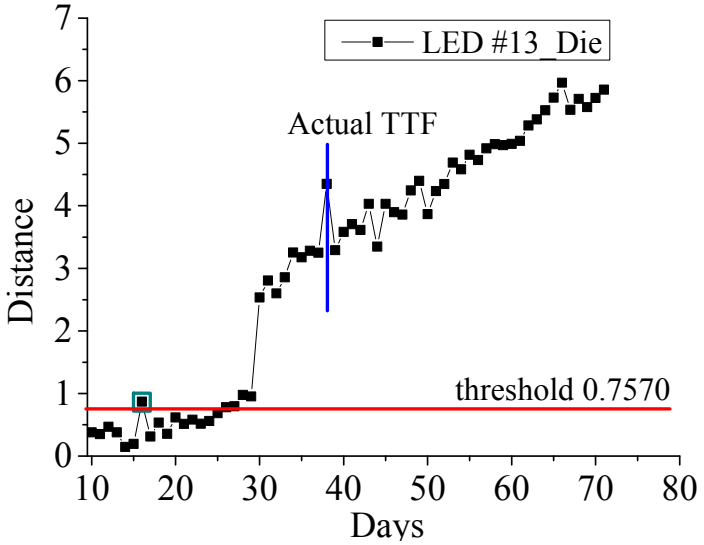


**Distance measure of cluster 3 from LED 13 for die peak.**

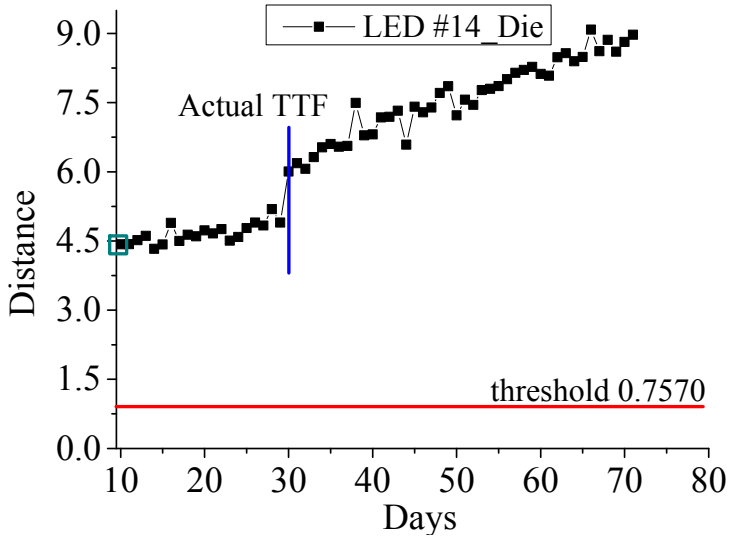


**Distance measure of cluster 3 from LED 14 for die peak.**

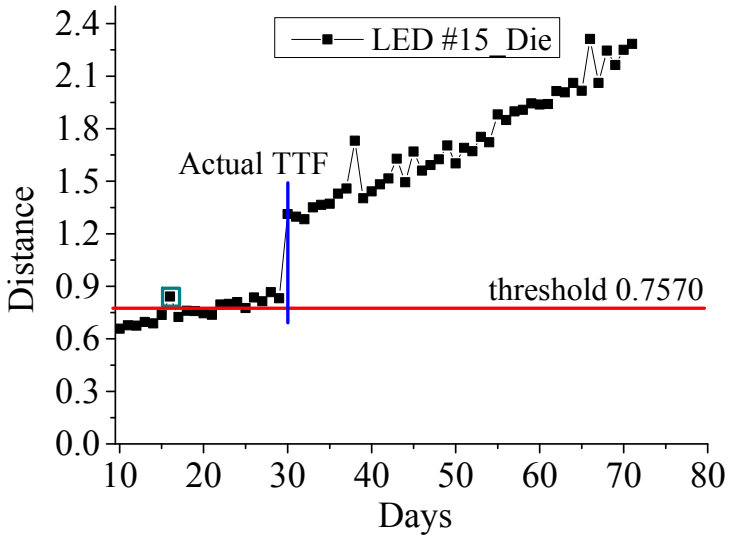


**Distance measure of cluster 3 from LED 15 for die peak.**

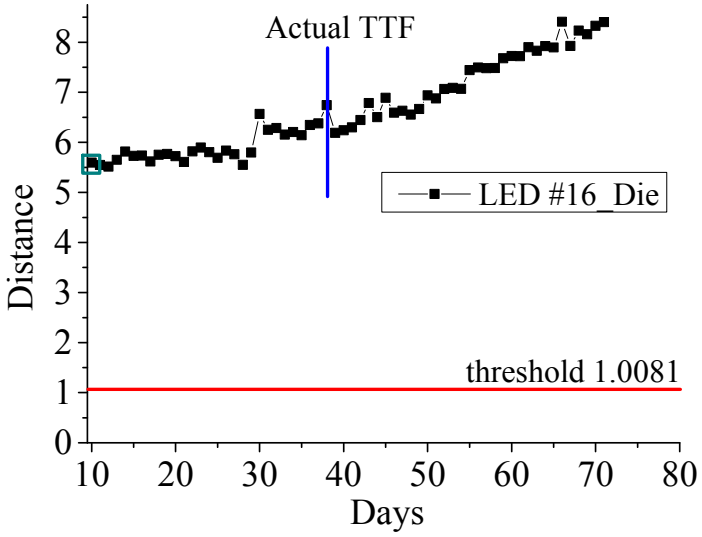


**Distance measure of cluster 1 from LED 16 for die peak.**

2. Anomaly detection results for LED phosphor peak under the condition of 200mA drive current and chamber temperature 90°C

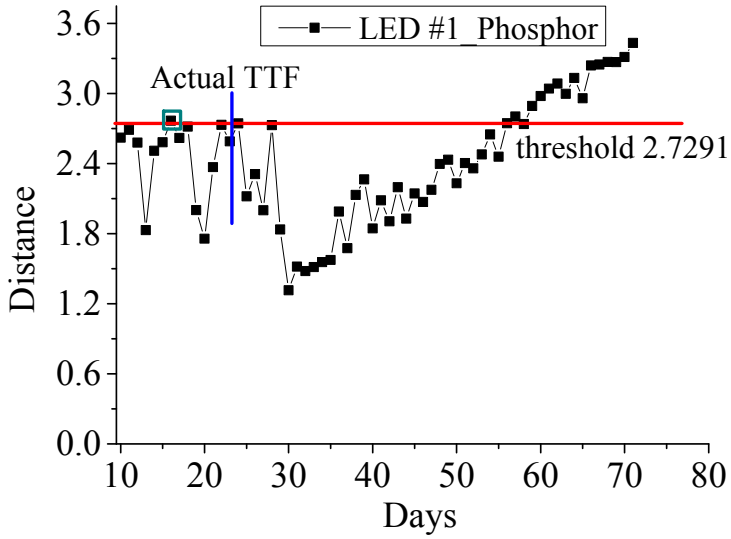


**Distance measure of cluster 6 from LED 1 for phosphor peak.**

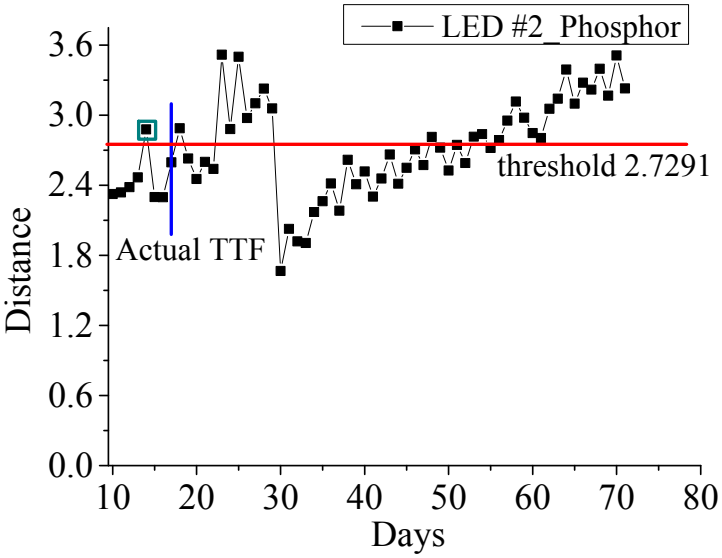


**Distance measure of cluster 6 from LED 2 for phosphor peak.**

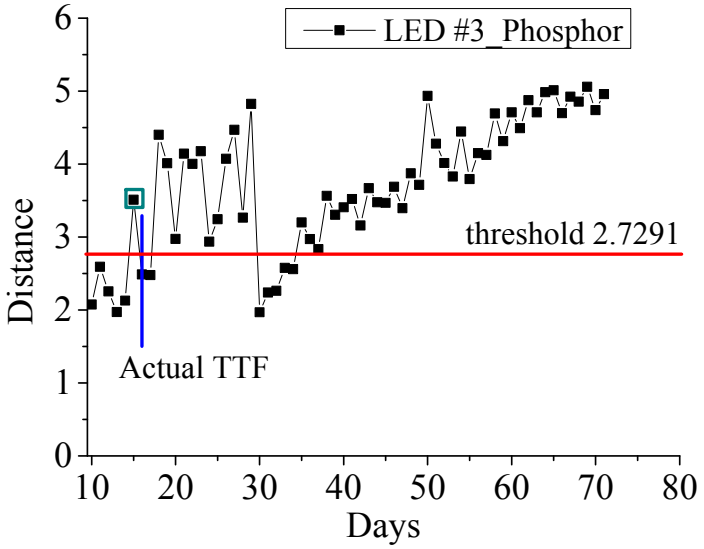


**Distance measure of cluster 6 from LED 3 for phosphor peak.**

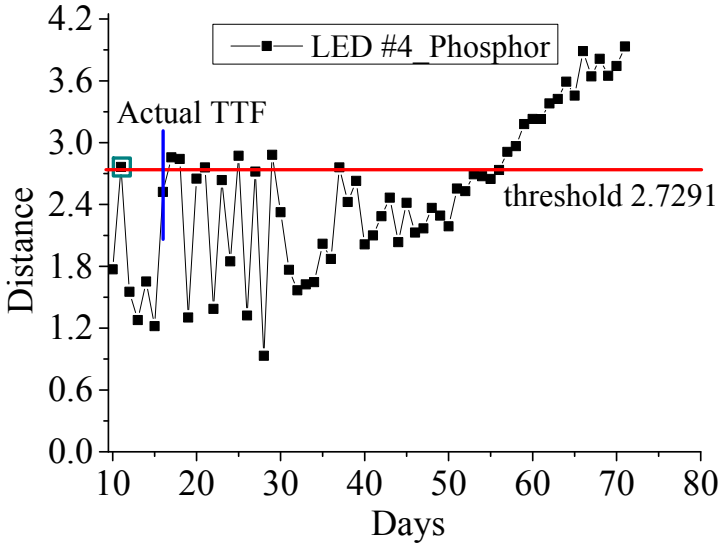


**Distance measure of cluster 6 from LED 4 for phosphor peak.**

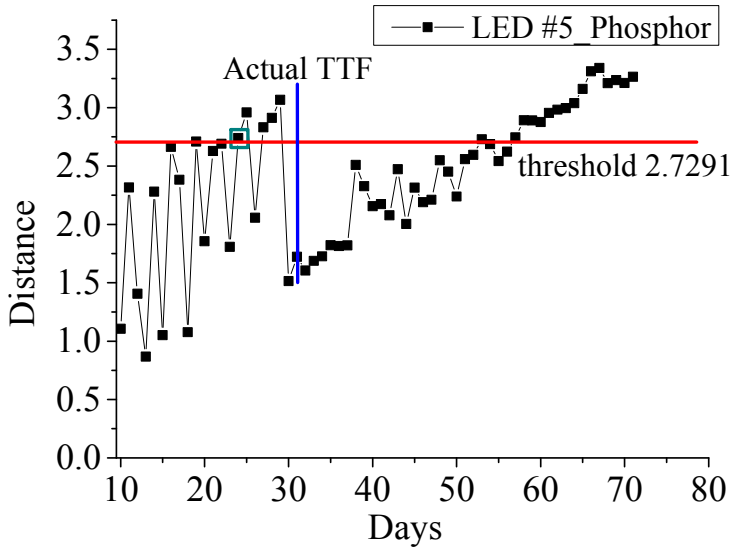


**Distance measure of cluster 6 from LED 5 for phosphor peak.**

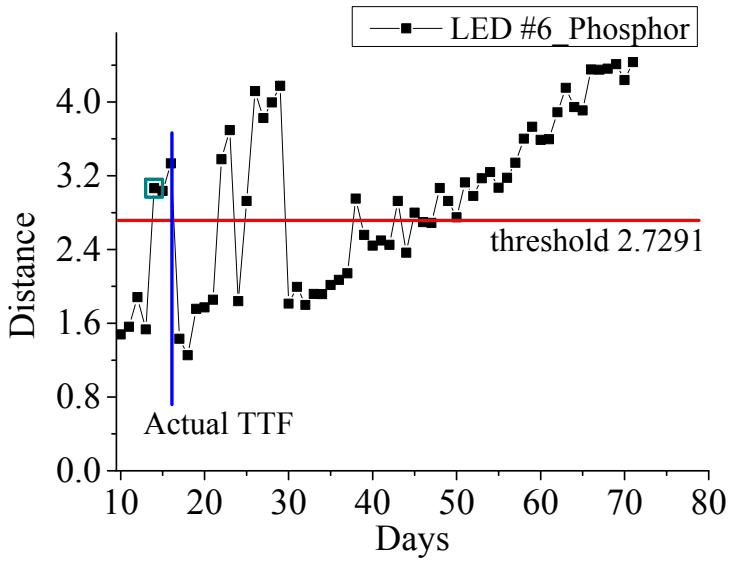


**Distance measure of cluster 6 from LED 6 for phosphor peak.**

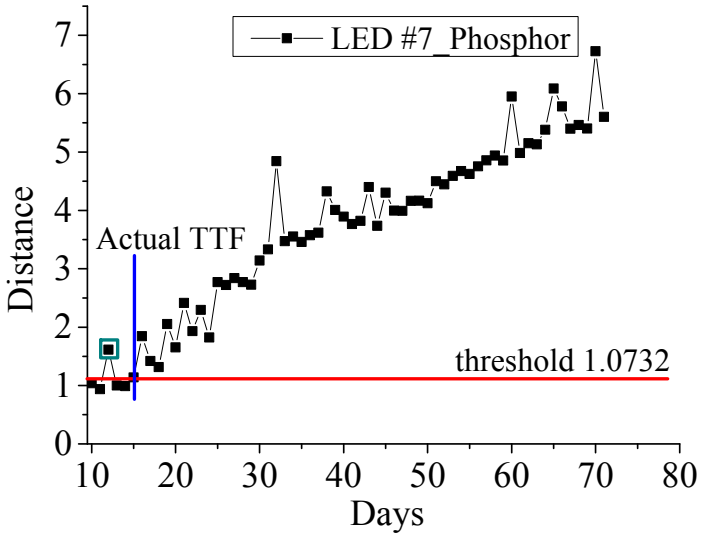


**Distance measure of cluster 4 from LED 7 for phosphor peak.**

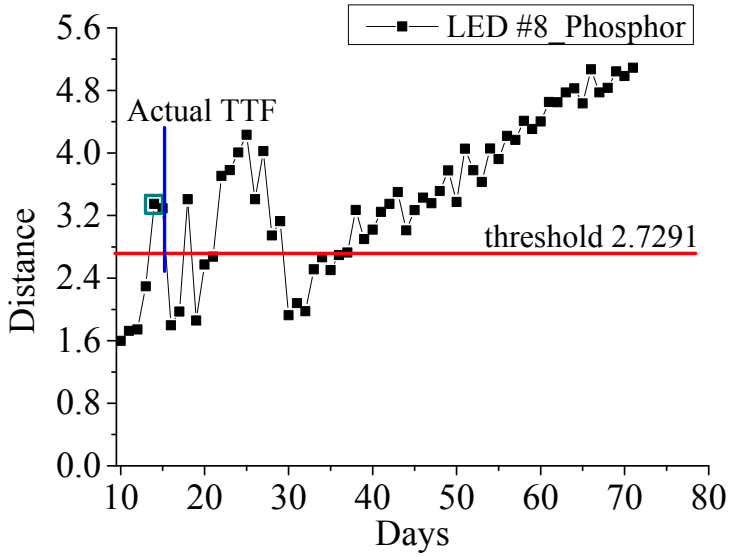


**Distance measure of cluster 6 from LED 8 for phosphor peak.**

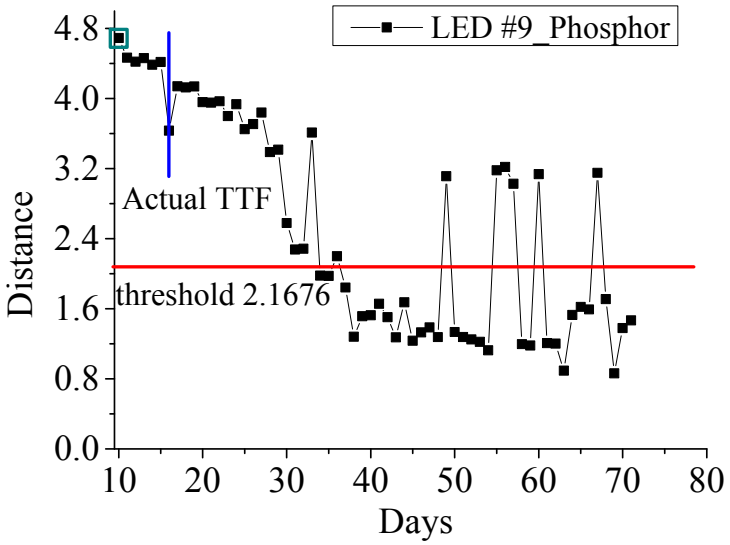


**Distance measure of cluster 1 from LED 9 for phosphor peak.**

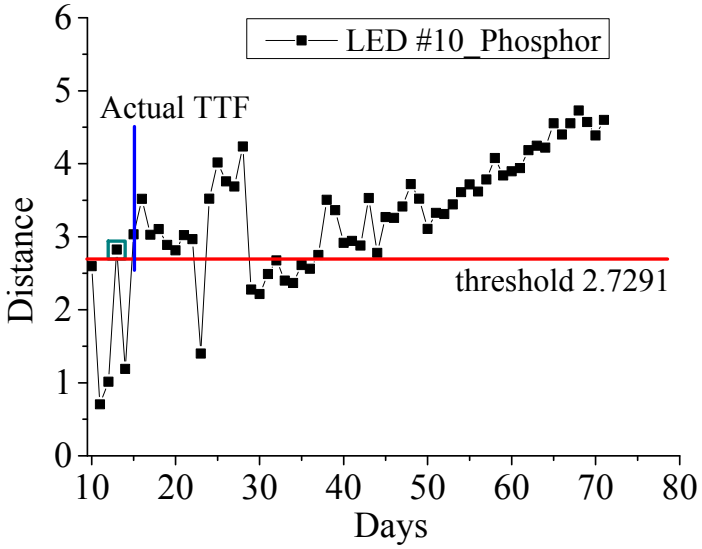


**Distance measure of cluster 6 from LED 10 for phosphor peak.**

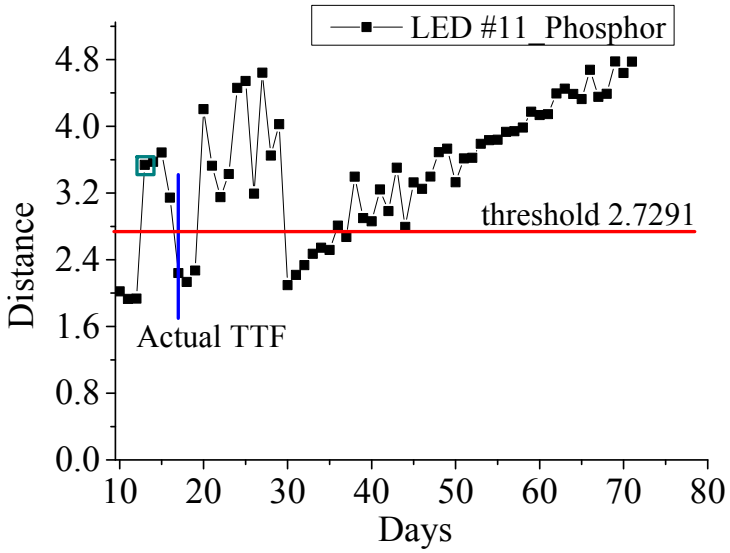


**Distance measure of cluster 6 from LED 11 for phosphor peak.**

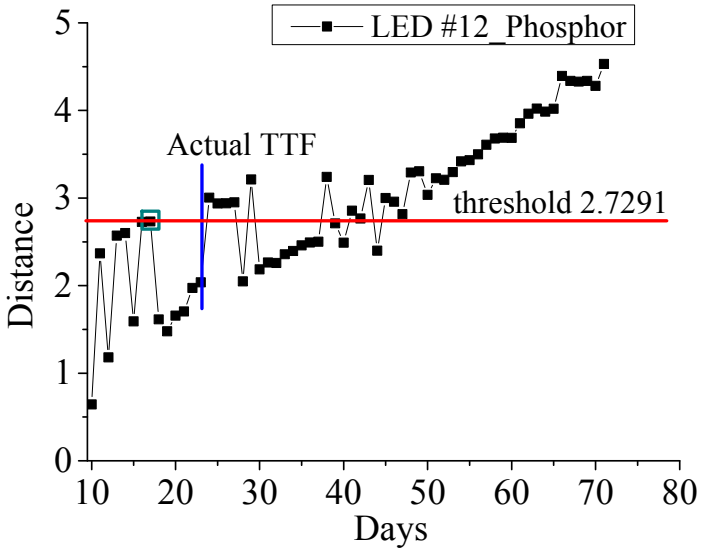


**Distance measure of cluster 6 from LED 12 for phosphor peak.**

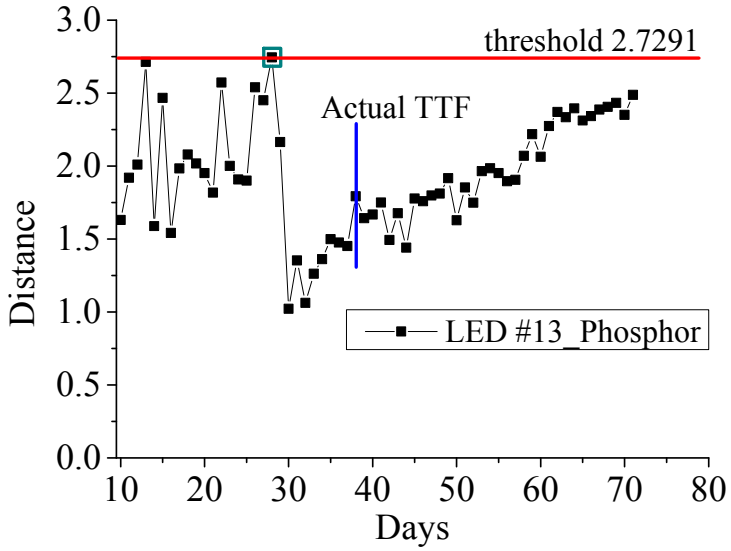


**Distance measure of cluster 6 from LED 13 for phosphor peak.**

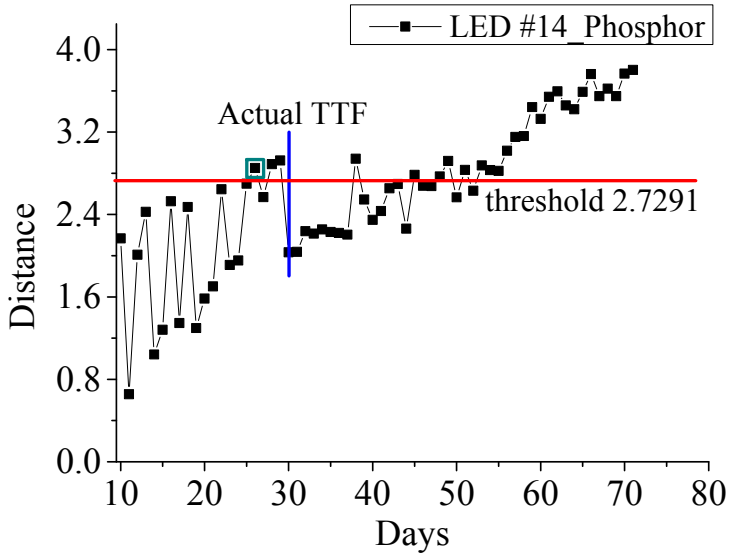


**Distance measure of cluster 6 from LED 14 for phosphor peak.**

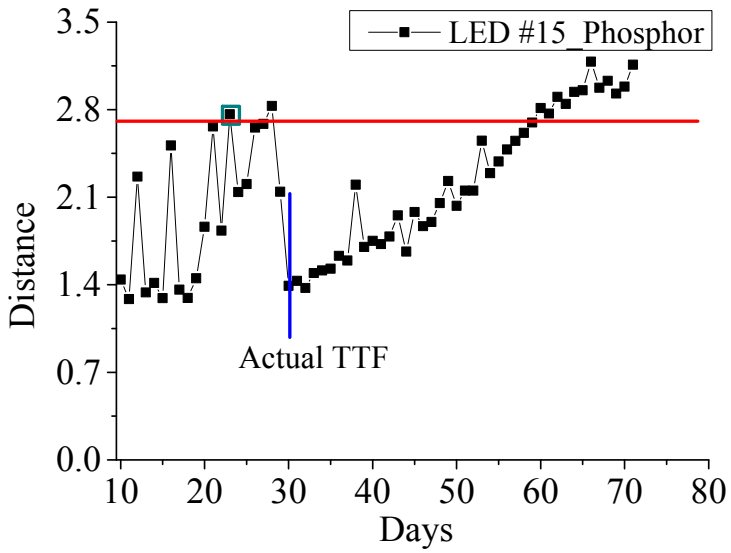


**Distance measure of cluster 6 from LED 15 for phosphor peak.**

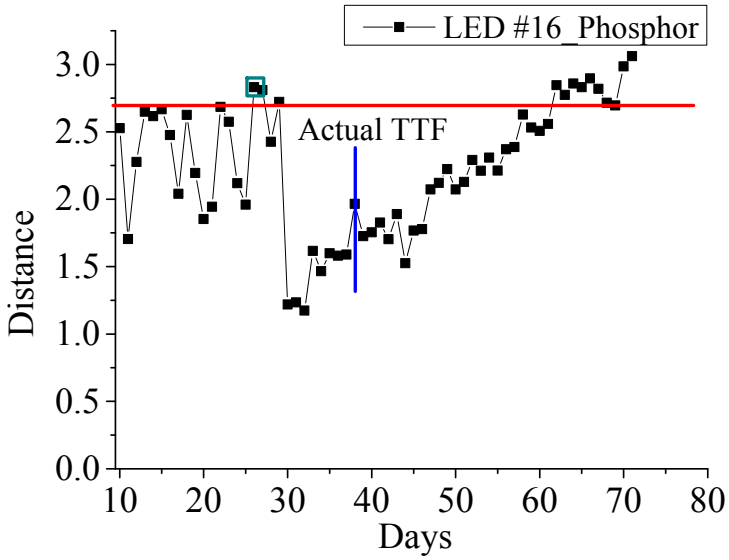


**Distance measure of cluster 6 from LED 16 for phosphor peak.**

## References


[1] M. -H. Chang, D. Das, P. V. Varde, and M. Pecht, "Light Emitting Diodes Rel iability Review", Journal of Microelectronics Reliability, vol. 52, pp. 762-782, 2012.

[2] M. Meneghini, A. Tazzoli, G. Mura, G. Meneghesso, and E. Zanoni, "A Revie w on the Physical mechanisms That Limit the Reliability of GaN-Based LEDs ", IEEE Transactions on Electron Devices, vol. 57, pp. 108-118, 2010.

[3] N. Narendran, L. Deng, R. M. Pysar, Y. Gu, and H. Yu, "Performance Charact eristics of High-power Light-emitting Diodes", Third International Conference on Solid State Lighting, Proceedings of SPIE. 5187, pp. 267-275, 2004.

[4] Y. Deshayes, L. Bechou, F. Verdier, and Y. Danto, "Long-term Reliability Pre diction of 935nm LEDs Using Failure Laws and Low Acceleration Factor Age ing Tests", Quality and Reliability Engineering International, vol. 21, no. 6, pp . 571-594, 2005.

[5] J. -S. Jeong, J. -K. Jung, and S. -D. Park, "Reliability Improvement of InGaN LED Backlight Module by Accelerated Life Test (ALT) and Screen Policy of Potential Leakage LED", Microelectronics Reliability. vol. 48, no. 8-9, pp. 121 6-1220, 2008.

[6] I. Polavarapu and G. Okogbaa, "An Interval Estimate of Mean-time-to-failure for a Product with Reciprocal Weibull Degradation Failure Rate", Proceedings of Reliability and Maintainability Symposium. pp. 261-265, 2005.

[7] C. -Y. Peng and S. -T. Tseng, "Mis-specification Analysis of Linear Degradati on Models", IEEE Transactions on Reliability, vol. 58, no. 3, pp. 444-455, 200 9.

[8] M. Vazquez, N. Nunez, E. Nogueira, and A. Borreguero, "Degradation of AlIn GaP Red LEDs under Drive Current and Temperature Accelerated Life Tests", Microelectronics Reliability, vol. 50, no. 9-11, pp. 1559-1562, 2010.

[9] Cree, "Cree Xlamp XR Family LED Reliability", CLD-AP26 Rev. 2, Cree, Inc ., 2011.

[10] Samsung LED, "Specification for White LED Model: SPHWHTL3D305E6W 0F5", Rev. 2, pp. 1-18, 2011.

[11] Nichia, "Specifications for White LED Model: NS6W183BT", Nichia STS-DA 1-1992A, Cat. No. 120524, Nichia Corporation, pp. 1-18, 2012.

[12] IES (Illuminating Engineering Society), IES LM-80-08, "Approved Method:

Measuring Lumen Maintenance of LED Light Sources", pp. 1-4, 2008.
[13] N. Narendran, J. D. Bullough, N. Maliyagoda, and A. Bierman, "What is Useful Life for White Light LEDs?", Journal of the Illumination Engineering Society vol. 30, no.1, pp. 57-68, 2001.
[14] T. Yanagisawa and T. Kojima, "Long-term Accelerated Current Operation of White Light-Emitting Diodes", Journal of Luminescence, vol. 114, no. 1, pp. 39-42, 2005.
[15] M. Bürmen, F. Pernuš, and B. Likar, "Accelerated Estimation of Spectral Degradation of White GaN-Based LEDs", Measurement Science and Technology, vol. 18, no. 1, pp. 230-238, 2007.
[16] M. R. Krames, O. B. Shchekin, R. Mueller-Mach, G. O. Mueller, L. Zhou, G. Harbers, and M. G. Craford, "Status and Future of High-power Light-emitting Diodes for Solid-state Lighting", Journal of Display Technology, vol. 3, no. 2, pp. 160-175, 2007.
[17] D. A. Steigerwald, J. C. Bhat, D. Collins, R. M. Fletcher, M. O. Holcomb, M. J. Ludowise, P. S. Martin, and S. L. Rudaz, "Illumination with Solid State Lighting Technology", IEEE Journal of Selected Topics in Quantum Electronics, vol. 8, no. 2, pp. 310-320, 2002.
[18] F. M. Steranka, J. Bhat, D. Collins, L. Cook, M. G. Craford, R. Fletcher, N. Gardner, P. Grillot, W. Goetz, M. Keuper, R. Khare, A. Kim, M. Krames, G. Harbers, M. Ludowise, P. S. Martin, M. Misra, G. Mueller, R. Mueller-Mach, S. Rudaz, Y. C. Shen, D. Steigerwald, S. Stockman, S. Subramanya, T. Trottier, and J. J. Wierer, "High Power LEDs - Technology Status and Market Applications", Physica Status Solidi (a), vol. 194, no. 2, pp. 380-388, 2002.
[19] E. F. Schubert, J. K. Kim, H. Luo, and J. -Q. Xi, "Solid-State Lighting-A Benevolent Technology", Reports on Progress in Physics, vol. 69, pp. 3069-3099, 2006.
[20] Y. Aoyama and T. Yachi, "An LED Module Array System Designed for Street light Use", IEEE Energy 2030 Conference, Atlanta, GA, Nov. 17-19, pp. 1-5, 2008.
[21] R. Vittori and A. Scaburri, "New Solid State Technologies and Light Emission Diodes as a Mean of Control and Lighting Source Applicable to Explosion Proof Equipment, with the Scope to Reduce Maintenance, to Limit the Risk of Bad Maintenance and to Expand the Plants' Life", PCIC Europe '09, pp. 193-198, 2009.
[22] D. G. Moore, Sierra Products Inc., "Request for Legal Interpretations on FMVSS #108 Subjects", July 14, 2006, "http://www.sierraproductsinc.com/filebox/108Fed/Heat%20Degradation%20LED.htm".
[23] R. Easterling, "LED Street Lighting – No Longer King of the Road", Jan. 17, 2011, Ezinearticles, "http://ezinearticles.com/?LED-Street-Lighting---No-Longer-King-of-the-Road&id=5722801".
[24] MadeinAsia, "Taiwan Market: LED Street Lamp Failure Rates about 8%", Feb. 18, 2011, "http://lighting.madeinasia.com/news/Taiwan-Market-LED-Street-Lamp-Failure-Rates-About-8-6305.html".
[25] M. –S. Huang, C. –C. Hung, Y. –C. Fang, W. –C. Lai, and Y. –L. Chen, "Optical Design and Optimization of Light Emitting Diode Automotive Head Light

with Digital Micromirror Device Light Emitting Diode", Optik, International J ournal for Light and Electron Optics, pp. 1-9, 2009.
[26] S. W. R. Lee, C. H. Lau, S. P. Chan, K. Y. Ma, M. H. NG, Y. W. NG, K. H. L EE, and J. C. C. Lo, "Development and Prototyping of a HB-LED Array Modu le for Indoor Solid State Lighting", High Density Microsystem Design and Pa ckaging and Component Failure Analysis, 2006. HDP´06. Conference, pp. 141 -145, 2006.
[27] R. Peon, G. Doluweera, I. Platonova, D. Irvine-Halliday, and G. Irvine-Hallida y, "Solid State Lighting For The Developing World – The Only Solution", Opt ics & Photonics 2005, Proceedings of SPIE, vol. 5941, pp. 109-123, San Diego , 2005.
[28] R. A. Pinto, M. R. Cosetin, M. F. da Silva, G. W. Denardin, J. Fraytag, A. Ca mpos, and R. N. do Prado, "Compact Emergency Lamp Using Power LEDs", I ndustrial Electronics, 2009. IECON ´09. 35th Annual Conference of IEEE, pp. 3494-3499, 2009.
[29] S. –I. Shibata, T. Oyabu, and Haruhiko Kimura, "Bioelectric Potential Charact eristic of Pothos under Light Emitting Diode", ICCAS-SICE, pp. 4663-4668, 2 009.
[30] T. Wipiejewski, T. Moriarty, V. Hung, P. Doyle, G. Duggan, D. Barrow, B. Mc Garvey, M. O'Gorman, T. Calvert, M. Maute, V. Gerhardt, J. D. Lambkin, "Gi gabits in the Home with Plugless Plastic Optical Fiber (POF) Interconnects", E lectronics System-Integration Technology Conference, 2008. ESTC 2008. 2nd, pp. 1263-1266, 2008.
[31] Lumileds, "Luxeon Reliability", Reliability Datasheet RD25, Philips Lumileds , 2006.
[32] Y. N. Chang, C. C. Hung, and S. C. Tung, "Auto Mixed Light for RGB LED Backlight Module", Industrial Electronics, 2009. ISIE 2009. IEEE Internationa l Symposium, pp. 864-869, 2009.
[33] S. W. Chang, "LED Lighting: High Efficiency and Environmental Benefit" Sa msung Economic Research Institute Economic Focus, vol. 206, pp. 1-10, 2008.
[34] L. Trevisanello, M. Meneghini, G. Mura, M. Vanzi, M. Pavesi, G. Meneghess o, and E. Zanoni, "Accelerated Life Test of High Brightness Light Emitting Di odes", IEEE Transactions on Device and Materials Reliability, vol. 8, no. 2, pp . 304-311, 2008.
[35] Y. Deshayes, I. Bord, G. Barreau, M. Aiche, P. H. Moretto, L. Bechou, A.C. R oehrig, and Y. Ousten, "Selective Activation of Failure Mechanisms in Packag ed Double-Heterostructure Light Emitting Diodes Using Controlled Neutron E nergy Irradiation", Microelectronics Reliability, vol. 48, pp. 1354-1360, 2008.
[36] Nichia, "Specifications for Nichia Chip Type White LED Model: NCSW119T-H3", Nichia STS-DA1-0990A, Nichia Corporation, 2009.
[37] C. J. M. Lasance, "Recent Progress in Compact Thermal Models", 19th IEEE SEMI-THERM Symposium, pp. 290-299, 2003.
[38] N. Hwang, "Failure Analysis Matrix of Light Emitting diodes for General Ligh ting Applications", Physical and Failure Analysis of Integrated Circuits, 2008. IPFA 2008. 15th International Symposium, pp. 1-4, 2008.
[39] Q. Hu and R. Zane, "LED Drive Circuit with Series Input Connected Converte

r Cells Operating in Continuous Conduction Mode", Applied Power Electronic s Conference and Exposition, 2009. APEC 2009. Twenty-Fourth Annual IEEE, pp. 1511-1517, 2009.

[40] A. Christensen and S. Graham, "Thermal Effects in Packaging High Power Li ght Emitting Diode Arrays", Applied Thermal Engineering, vol. 29, pp. 364-37 1, 2009.

[41] Q. Li and D. B. Kececioglu, "Design of an Optimal Plan for an Accelerated De gradation Test: A Case Study", International Journal of Quality & Reliability Management", vol. 23, no. 4, pp. 426-440, 2006.

[42] E. Nogueira, M. Vazquez, and N. Nunez, "Evaluation of AlGaInP LEDs Relia bility Based on Accelerated Tests", Microelectronics Reliability, vol. 49, pp. 1 240-1243, 2009.

[43] J. -M. Kang, J. -W. Kim, J. -H. Choi, D. -H. Kim, and H. -K. Kwon, "Life-Ti me Estimation of High-Power Blue Light-Emitting Diode Chips", Microelectr onics Reliability, vol. 49, pp. 1231-1235, 2009.

[44] T. Cheng, X. Luo, S. Huang, and S. Liu, "Thermal Analysis and Optimization of Multiple LED Packaging Based on a General Analytical Solution", Internati onal Journal of Thermal Sciences, vol. 49, pp. 196-201, 2010.

[45] G. Molnar, G. Nagy, and Z. Szucs, "A Novel Procedure and Device to Allow Comprehensive Characterization of Power LEDs over a Wide Range of Tempe rature", TERMINIC 2008, Rome, Italy, pp. 89-92, Sep. 2008.

[46] V. Szekely, G. Somlay, P. G. Szabo, and M. Rencz, "Design of a Static TIM T ester", THERMINIC 2008, Rome, Italy, pp. 132-136, Sep. 2008.

[47] R. Linderman, T. Brunschwiler, B. Smith, and B. Michel, "High-Performance Thermal Interface Technology Overviews", THERMINIC 2007, 13th Internati onal Workshop on, Budapest, Hungary, pp. 129-134, Sep. 2007.

[48] R. -H. Horng, H. -Y. Hsiao, C. -C. Chiang, D. -S. Wuu, Y. -L. Tsai, and H. -I. Lin, "Novel Device Design for High-Power InGaN/Sapphire LEDs using Copp er Heat Spreader With Reflector", IEEE Journal of Selected Topics in Quantu m Electronics, vol. 15, no. 4, 2009.

[49] J. H. Yu, W. Oepts, and H. Konijn, "PC Board Thermal Management of High Power LEDs", Semiconductor Thermal Measurement and Management Sympo sium, 2008. Semi-Therm 2008. Twenty-fourth Annual IEEE, pp. 63-67, 2008.

[50] M. Pecht and M. –H. Chang, "Chapter 3: Failure Mechanisms and Reliability I ssues in LEDs", Solid State Lighting Reliability: Components to Systems: Soli d State Lighting Technology and Application Series, vol. 1, Springer Science+ Business Media, (ISBN 978-1-4614-3066-7), pp. 43-110, 2013.

[51] J. Liu, W. S. Tam, H. Wong, and V. Filip, "Temperature-Dependent Light-Emi tting Characteristics of InGaN/GaN Diodes", Microelectronics Reliability, vol. 49, pp. 38-41, 2009.

[52] S. Chhajed, Y. Xi, Th. Gessmann, J. –Q. Xi, J. M. Shah, J. K. Kim, and E. F. S chubert, "Junction Temperature in Light-Emitting Diodes Assessed by Differe nt Methods", Progress in Biomedical Optics and Imaging – Proceedings of SPI E, vol. 5739, pp. 16-24, 2005.

[53] M. -H. Chang, D. Das, S.W. Lee, and M. Pecht, "Concerns with Interconnect Reliability Assessment of High Power Light Emitting Diodes (LEDs)", SMTA

China South Technical Conference 2010, Shenzhen, China, pp. 63-69, 2010.
[54] M. –H. Chang, D. Das, and M. Pecht, “Interconnect Reliability Assessment of High Power Light Emitting Diodes (LEDs) through Simulation”, ICHRESH 2 010, pp. 418-424, 2010.
[55] U. S. Department of Energy, “Energy Star® Program Requirements for Solid State Lighting Luminaires”, Eligibility Criteria – Version 1.1, pp. 1-23, Decem ber 19, 2008.
[56] U. S. Department of Energy, “Energy Star® Program Requirements: Product S pecification for Luminaires (Lighting Fixtures)”, Eligibility Criteria Version 1. 2, pp. 1-36, December 21, 2012.
[57] S. Cheng, M. H. Azarian, and M. G. Pecht, “Sensor Systems for Prognostics a nd Health Management”, Sensors, Vol. 10, pp. 5774-5797, 2010.
[58] M. G. Pecht, “Chapter 1. Introduction”, Prognostics and Health Management o f Electronics, 1st ed., Hoboken, New Jersey, John Wiley & Sons, pp. 1-24, 200 8.
[59] S. Cheng, K. Tom, and M. Pecht, “Anomaly Detection of Polymer Resettable Circuit Protection Devices”, IEEE Transactions on Device and Materials Relia bility, Vol. 12, No. 2, pp. 420-427, 2012.
[60] T. Sutharssan, S. Stoynanov, C. Bailey, and Y. Rosunally, “Prognostics and He alth Monitoring of High Power LED”, Micromachines, Vol. 3, pp. 78-100, 201 2.
[61] J. –J. M. Avenel, “Technique for Identifying At Least One Faulty Light Emitti ng Diode in a String of Light Emitting Diodes”, U. S. Patent Application No. 1 3/369,949, pp. 1-8, 2012.
[62] J. Fan, K. C. Yung, and M. Pecht, “Anomaly Detection for Chromaticity Shift of High Power White LED with Mahalanobis Distance Approach”, Proceeding of the 14th International Conference on Electronics Materials and Packaging ( EMAP2012, Hong Kong), pp. 13-26, 2012.
[63] S. B. Kotsiantis and P. E. Pintelas, “Recent Advances in Clustering: A Brief Su rvey”, WSEAS Transactions on Information Science and Applications, vol. 1, pp. 73-81, 2004.
[64] P. Berkhin, “Survey of Clustering Data Mining Techniques, Technical Report” , Accrue Software, San Jose, CA, pp. 1-56, 2002.
[65] A. K. Jain, M. N. Murty, and P. J. Flyn, “Data Clustering: A Review”, ACM C omputing Surveys, vol. 31, no. 3, pp. 264-323, 1999.
[66] L. Talavera, “Dependency-Based Dimensionality Reduction for Clustering Sy mbolic Data”, In Proceedings of the Workshop on Pre- and Post-Processing in machine Learning and Data Mining (ACAI ’99), Advanced Course on Artifici al Intelligence, pp.1-8, 1999.
[67] R. Xu and D. Wunsch II, “Survey of Clustering Algorithms”, IEEE Transactio ns on Neural Networks, vol. 16, no. 3, pp. 645-678, 2005.
[68] Z. Huang, “Extensions to the k-Means Algorithms for Clustering Large Data S ets with Categorical Values”, Data Mining and Knowledge Discovery, vol. 2, pp. 283-304, 1998.
[69] L. Ertőz, M. Steinbach, and V. Kumar, “Finding Clusters of Different Sizes, S hapes, and Densities in Noisy, High Dimensional Data”, Proceedings of Secon

d SIAM International Conference on Data Mining, pp. 1-12, 2003.
[70] M. Ester, H. –P. Kriegel, J. Sander, and X. Xu, "A Density-Based Algorithm f or Discovering Clusters in Large Spatial Data Sets with Noise", Proceedings of 2nd International Conference on KDD, pp. 226-231, 1996.
[71] R. Agrawal, J. Gehrke, D. Gunopulos, and P. Raghavan, "Automatic Subspace Clustering of High Dimensional Data for Data Mining Applications", Proceedi ngs of the 1998 ACM-SIGMOD Conference on the Management of Data, pp. 94-105, 1998.
[72] T. N. Tran, R. Wehrens, and L. M. C. Buydens, "Clustering Multispectral Ima ges: A Tutorial", Chemometrics and Intelligent Laboratory Systems, vol. 77, n o. 1-2, pp. 3-17, 2005.
[73] T. N. Tan, R. Wehrens, and L. M. C. Buydens, "KNN-Kernel Density-Based Clustering for High-Dimensional Multivariate Data", Computational Statistics & Data Analysis, vol. 51, no. 2, pp. 513-525, 2006.
[74] A. Webb, "Statistical Pattern Recognition", Wiley, Malvern, UK, pp. 81-122, 2002.
[75] S. Zhong and J. Ghosh, "A Unified Framework for Model-based Clustering", J ournal of Machine Learning Research, vol. 4, pp. 1001-1037, 2003.
[76] Illuminating Engineering Society of North America, "TM-21-11: Projecting Lo ng Term Lumen Maintenance of LED Light Sources", IES, pp. 1-25, 2011.
[77] CIE (Commission Internationale de l'Eclairage), "Technical Reports and Guid es", October 13, 2013, "http://www.cie.co.at/index.php/Publications/ Technical+Reports+and+Guides".
[78] A. Albertini, M. G. Masi, G. Mazzanti, L. Peretto, and R. Tinarelli, "A Test Se t for LEDs Life Model Estimation", Instrumentation and Measurement Techno logy Conference (2010 IEEE), pp. 424-431, 2010.
[79] N. Narendran, Y. Gu, J. P. Freyssinier, H. Yu, and L. Deng, "Solid-State Light ing: Failure Analysis of White LEDs", Journal of Crystal Growth, vol. 268, pp. 449-456, 2004.
[80] J. Beringer, K. Borer, C. B. Brooks, A. Fox-Murphy, R. B. Nickerson, and A. R. Weidberg, "A Life Time Test of Neutron Irradiated Light Emitting Diodes", Nuclear Instruments and Methods in Physics Research A, vol. 373, pp. 320-32 4, 1996.
[81] J. F. Fan, K. C. Yung, and M. Pecht, "Physics-of-Failure-Based Prognostics an d Health Management for High-Power White Light-Emitting Diode Lighting", IEEE Transactions on Device and Materials Reliability, vol. 11, pp. 407-416, 2011.
[82] B. –M. Song, B. Han, A. Bar-Cohen, R. Sharma, and M. Arik, "Hierarchical Li fe Prediction Model for Actively Cooled LED-Based Luminaire", IEEE Trans actions on Components and Packaging Technologies, vol. 33, no. 4, pp. 728-73 7, 2010.
[83] T. Yanagisawa, "Estimation of the Degradation of InGaN/AlGaN Blue Light-Emitting Diodes", Microelectronics Reliability, vol. 37, pp. 1239-1241, 1997.
[84] S. Levada, M. Meneghini, G. Meneghesso, and E. Zanoni, "Analysis of DC Cu rrent Accelerated Life Tests of GaN LEDs Using a Weibull-based Statistical Model", IEEE Transaction Device Material Reliability, vol. 5, pp. 688-693, 20

05.
[85] S. –L. Chuang, A. Ishibashi, S. Kijima, N. Nakayama, M. Ukita, and S. Tanigu chi, “Kinetic Model for Degradation of Light-Emitting Diodes”, IEEE Journal of Quantum Electronics, vol. 33, pp. 970-979, 1997.
[86] J. Fan, K. –C. Yung, and M. Pecht, “Lifetime Estimation of High-Power Whit e LED Using Degradation-Data-Driven Method”, IEEE Transactions on Devic e and Materials Reliability, vol. 12, no. 2, pp. 470-477, 2012.
[87] M. Bürmen, F. Pernuš, and B. Likar, “Prediction of Intensity and Color Degrad ation of LEDs”, Proceedings of SPIE, vol. 6486, pp. 64860M-1-10, 2007.
[88] O. Pursiainen, N. Linder, A. Jaeger, R. Oberschmid, and K. Streubel, “Identifi cation of Aging Mechanisms in the Optical and Electrical Characteristics of Li ght-Emitting Diodes”, Applied Physics Letter, vol. 79, pp. 2895-2897, 2001.
[89] X. A. Cao, P. M. Sandvik, S. F. LeBoeuf, and S. D. Arthur, “Defect Generatio n in InGaN/GaN Light-Emitting Diodes Under Forward and Reverse Electrical Stresses”, Microelectronics Reliability, vol. 43, pp. 1987-1991, 2003.
[90] F. Rossi, M. Pavesi, M. Meneghini, G. Salviati, and M. Manfredi, “Influence o f Short-term Low Current DC Aging on the Electrical and Optical Properties o f InGaN Blue Light-Emitting Diodes”, Journal of Applied Physics, vol. 99, pp. 053104-1-7, 2006.
[91] M. Meneghini, S. Podda, A. Morelli, R. Pintus, L. Trevisanello, G. Meneghess o, M. Vanzi, and E. Zanoni, “High Brightness GaN LEDs Degradation During DC-aged GaN LEDs”, Microelectronics Reliability, vol. 46, pp. 1720-1724, 20 06.
[92] Z. –Q. Fang, D. C. Reynolds, and D. C. Look, “Changes in Electrical Characte ristics Associated with Degradation of InGaN Blue Light-Emitting Diodes”, Jo urnal of Electronic materials, vol. 29, pp. 448-451, 2000.
[93] H. Chen, A. Keppens, P. Hanselaer, Y. Lu, Y. Gao, R. Zhuang, and Z. Chen, “ Failure Analysis of Electrical-Thermal-Optical Characteristics of LEDs Based on AlGaInP and InGaN/GaN”, Physics of Semiconductor Devices, vol. 46, no. 10, pp. 1310-1315, 2012.
[94] A. Keppens, H. Chen, Y. Lu, Z. Chen, Y. Gao, G. Deconinck, and P. Hanselae r, “Light-Emitting Diode Junction Temperature and Power Determination from Forward Current”, Light & Engineering, vol. 19, no. 1, pp. 34-44, 2011.
[95] M. –H. Chang, C. Chen, D. Das, and M. Pecht, “New Failure Precursors for Re liability Assessment of Light-Emitting Diodes (LEDs)”, under internal revision , pp. 1-10, submission to journal in 2014.
[96] Avago Technologies, “ASMT-Jx3x 3W Mini Power LED Light Source: Data Sheet”, AV02-1941EN, pp. 1-15, 2009.
[97] A. K. Jain, M. N. Murty, and P. J. Flyn, “Data Clustering: A Review”, ACM C omputing Surveys, Vol. 31, pp. 264-323, 1999.
[98] A. W. F. Edwards and L. L. Cavalli-Sforza, “A Method for Cluster Analysis”, Biometrics, Vol. 21, no. 2, pp. 362-375, 1965.
[99] J. A. Hartigan and M. A. Wong, “Algorithm AS 136: A K-Means Clustering A lgorithm”, Journal of the Royal Statistical Society. Series C (Applied Statistics ), Vol. 28, no. 1, pp. 100-108, 1979.
[100] T. Zhang, R. Ramakrishnan, and M. Livny, “BIRCH: An Efficient Data Cluste

ring Method for Very large Databases", SIGMOD Record 1996 ACM SIGMO D International Conference on Management of Data, Vol. 25, pp. 103-114, 199 6.
[101] K. Burbeck and S. Nadjm-Tehrani, "ADWICE – Anomaly Detection with Real -Time Incremental Clustering", Proceedings of Seventh International Conferen ce: Information Security and Cryptology (ICISC 2004), LNCS 3506, pp.407-4 24, 2005.
[102] B. –M. Song and B. Han, "Spectral Power Distribution Deconvolution Scheme for Phosphor-Converted White Light-Emitting Diode Using Multiple Gaussia n Functions", Applied Optics, vol. 52, no. 5, pp. 1016-1024, 2013.
[103] M. D. Fairchild, "Color Appearance Models", 2nd Edition, John Wiley and So ns, West Chester, England, 2005.
[104] Y. –H. Lin, J. P. You, Y. –C. Lin, N. T. Tran, and F. G. Shi, "Development of High-Performance Optical Silicone for the Packaging of High-Power LEDs", I EEE Transactions on Components and Packaging Technologies, vol. 33, no. 4, pp. 761-766, 2010.
[105] P. Jähnigen, C. Nebelung, and G. Bernhard, "Simultaneous Determination of Beta Nuclides by Liquid Scintillation Spectrometry", FZD – IRC Annual Repo rt 2007, Institute of Radiochemistry, Forschungszentrum Dresden-Rossendorf, Dresden, Germany, pp. 60, 2007.
[106] E. F. Shubert, "Chapter 17. Colorimetry", Light-Emitting Diodes, 2nd Edition, Cambridge University Press, New York, pp. 292-305, 2006.
[107] R. M. Boynton, "History and Current Status of a Physiologically Based Syste m of Photometry and Colorimetry", Journal of Optical Society of America A, vol. 13, no. 8, pp. 1609-1621, 1996.
[108] P. F. M. Stalmeier and C. M. M. de Weert, "Large Color Differences and Selec tive Attention", Journal of Optical Society of America A, vol. 8, no. 1, pp. 237 -247, 1991.
[109] D. L. Macadam, "Visual Sensitivities to Color Differences in Daylight", Journ al of the Optical Society of America, vol. 32, no. 5, pp. 247-273, 1942.
[110] M. E. Tipping, "Bayesian Inference: An Introduction to Principles and Practice in Machine Learning", Advanced Lectures on Machine Learning, Springer, pp . 41-62, 2006.
[111] V. A. Sotiris, P. W. Tse, and M. G. Pecht, "Anomaly Detection Through a Bay esian Support Vector Machine", IEEE Transactions on Reliability, vol. 59, no. 2, pp. 277-286, 2010.
[112] V. N. Vapnik, "An Overview of Statistical Learning Theory", IEEE Transactio ns on Neural Networks, vol. 10, no. 5, pp. 988-999, 1999.
[113] M. E. Tipping, "Sparse Bayesian Learning and the Relevance Vector Machine ", Journal of Machine Learning Research, vol. 1, pp. 211-244, 2001.
[114] M. E. Tipping, "The Relevance Vector machine", Advances in Neural Informa tion Processing Systems, MIT Press, vol. 12, pp. 652-658, 2000.
[115] P. Wang, B. D. Youn, and C. Hu, "A Generic Probabilistic Framework for Str uctural Health Prognostics and Uncertainty Management", Mechanical System s and Signal Processing, vol. 28, pp. 622-637, 2012.
[116] T. Wang, J .Yu, D. Siegel, and J. Lee, "A Similarity-Based Prognostics Appro

ach for Remaining Useful Life Estimation of Engineered Systems", 2008 Inter national Conference on Prognostics and Health Management, pp. 1-6, Oct 6-9, Denver, CO, 2008.

[117] N. Gebraeel, M. Lawley, R. Liu, and V. Parmeshwaran, "Residual Life Predict ion from Vibration-Based Degradation Signals: A Neural Network Approach", IEEE Transactions on Industrial Electronics, vol. 51, no. 3, pp. 694-700, 2004.

[118] M. –H. Chang, D. Das, and M. Pecht, "Junction Temperature Characterization of High Power Light Emitting Diodes", IMAPS Mid-Atlantic Microelectronics Conference 2011, Atlantic City, New Jersey, pp. 1-6, 2011.

[119] S. Kumar, T. W. S. Chow, and M. Pecht, "Approach to Fault Identification for Electronic Products Using Mahalanobis Distance", IEEE Transactions on Instr umentation and Measurement, vol. 59, no. 8, pp. 2055-2064, 2010.

[120] S. Kumar, V. Sotiris, and M. Pecht, "Health Assessment of Electronic Product s Using Mahalanobis Distance and Projection Pursuit Analysis", International Journal of Computer and Information Engineering, vol. 2, no. 4, pp. 242-250, 2008.